# MANUFACTURING AND MECHANICAL BEHAVIOR OF LIGHTWEIGHT COMPOSITES BY ACCUMULATIVE ROLL BONDING

A Thesis

by

Furqan Tahir

Submitted to the

Graduate School of Sciences and Engineering
In Partial Fulfillment of the Requirements for
the Degree of

Master of Science

in the
Department of Mechanical Engineering

Özyeğin University
August 2021

Copyright © 2021 by Furqan Tahir

# MANUFACTURING AND MECHANICAL BEHAVIOR OF LIGHTWEIGHT COMPOSITES BY ACCUMULATIVE ROLL BONDING

Approved by:

Assoc. Prof. Dr. Güney Güven Yapıcı,
Advisor,
Head of Department of Mechanical Engineering
*Özyeğin University*

Asst. Prof. Dr. Altuğ Başol,
Department of Mechanical Engineering
*Özyeğin University*

Asst. Prof. Dr. Mehmet İpekoğlu,
Department of Mechanical Engineering
*Türk-Alman University*

Date Approved: 18 August 2018

# DEDICATION

*To My Family*

# ABSTRACT

Severe plastic deformation (SPD) methods have received significant attention in fabricating a combination of similar and dissimilar metal composites. Accumulative roll bonding (ARB) is one of the SPD techniques employed to produce high strength, fine-grained, and multi-layered metal matrix composites (MMCs). The current work is characterized into two parts. The major part deals with the fabrication of different combinations between titanium and interstitial free (IF) steel interlayered with aluminum alloy (Al2024). While the second part studies the effect of post-ARB heat treatment on Al2024-IF steel composite.

Microstructural evaluation and mechanical characteristics of processed composites were examined by optical microscope (OM), scanning electron microscope (SEM), and mechanical tests. Surface and bulk properties were analyzed through microhardness, uniaxial tensile, and shear punch test (SPT). Finally, experiment results were validated using numerical analysis.

For the first case of titanium-IF steel composites, the optical micrographs indicated the reduction in layer thickness and grain size after each rolling cycle. Necking was initiated in some layers of the processed composite after the third (final) ARB cycle, suggesting the interlocking of layers and consequently stronger bonding. SEM figures from fracture surfaces revealed the delamination of layers from interfaces in early cycles, that lessened in the final cycle due to high strain exerted after each rolling cycle.

Significant improvement was noticed in hardness levels as the number of ARB cycles increased. Enhancement levels for titanium and IF steel layers were up to 1.4 and 2.6 times, respectively after the ARB process. The tensile strength of the titanium-IF steel composite rolled at 400°C exceeded over 670MPa after three cycles. Typical to SPD processes, the ductility was reduced to less than 5% in all cases after three ARB cycles. Enhancement levels in tensile strength of each layer of the final composite compared to the initial metals were similar to hardness. SPT results showed the improvement in shear strength of the sample with

the increasing number of cycles, a maximum shear strength of around 440MPa was achieved after three cycles.

For the second part of aluminum-IF steel composite, microstructure observation revealed that long aging imparted partial coarsening of the average grain size in a three-cycle ARBed sample. Furthermore, the ductility was recovered after aging without losing tensile strength due to the occurrence of precipitation hardening along with recovery in individual layers. A maximum ultimate tensile strength (UTS) and ductility of around 420MPa and 18%, respectively, was obtained after aging at 150°C for 24h. SPT results showed a similar response as the tensile test, and maximum shear strength was reached up to 270MPa at the peak-aged condition.

The ARB process, in the case of titanium-IF steel composite, was modeled by employing finite element analysis through ANSYS workbench. The effective plastic strain and effective stress (von-Mises) were calculated through the thickness of ARBed samples. A close agreement between experimental findings and numerical simulations was observed.

# ÖZET

Aşırı plastik deformasyon (APD) yöntemleri, benzer ve farklı metal kompozitlerin üretilmesinde büyük dikkat çekmiştir. Birikmeli hadde yapıştırması (ARB), yüksek mukavemetli, ince iç yapılı ve çok katmanlı metal matrisli kompozitler (MMC) üretmek için kullanılan APD tekniklerinden biridir. Mevcut çalışma iki bölümden oluşmaktadır. Ana kısım, titanyum ve alüminyum alaşımı (Al2024) ile ara tabakalı arayer atomsuz (IF) çelik arasındaki farklı kombinasyonların imalatı üzerinedir. İkinci kısım ise ARB sonrası ısıl işlemin Al2024 ve IF çelik kompozit üzerindeki etkisini inceler.

İşlenik kompozitlerin mikroyapı analizleri optik mikroskop (OM) ve taramalı elektron mikroskobu (SEM) ile; mekanik özellikleri ise yapılan mekanik testler ile incelenmiştir. Yüzey ve malzeme özellikleri mikrosertlik, tek eksenli çekme ve kayma zımba testi (SPT) ile analiz edildi. Son olarak, deney sonuçları sayısal analiz yöntemi kullanılarak doğrulanmıştır.

Titanyum-IF çelik kompozitlerde, her haddeleme döngüsünden sonra optik mikroskop aracılığı ile tabaka kalınlığında ve tane boyutunda azalma saptandı. İşlenik kompozitin bazı katmanlarında üçüncü (son) ARB döngüsünden sonra boyun verme gözlemlendi. Bu durum, katmanların birbirine geçerek daha güçlü bağlar oluşturduğunu gösterir. Kırılma yüzeylerinden alınan SEM görüntüleri yüksek gerinim uygulanan haddeleme döngüleri sebebiyle, arayüzlerde son haddeleme döngüsüne kadar azalarak devam eden katman ayrılmasını ortaya çıkardı.

ARB döngülerinin sayısı arttıkça mikro sertlik seviyelerinde önemli bir iyileşme saptandı. ARB işleminden sonra titanyum ve IF çelik katmanları için sırasıyla 1.4 ve 2.6 kata kadar mikro sertlik artışı gözlemlendi. 400°C'de haddelenmiş Ti/IF çelik kompozitinin çekme mukavemeti, üç döngüden sonra 670MPa'yı aştı. APD proseslerinde beklendiği üzere, üç ARB döngüsünden sonra tüm durumlarda süneklik %5'in altına düşürülmüştür. SPT sonuçları, artan

döngü sayısı ile numunenin kesme mukavemetininde arttığını gösterdi ve üç döngüden sonra yaklaşık 440MPa'lık bir maksimum kesme mukavemeti elde edildi.

İkinci kısımda yapılan mikroyapısal inceleme uzun yaşlanmanın, üç döngülü ARB işlenik numune iç yapısındaki tanecik boyutunda kısmi büyümeye yol açtığı belirlendi. Ayrıca, uygulanan yaşlandırma sonrası, çökelti sertleşmesi sayesinde malzemenin çekme mukavvemetini kaybetmeden süneklik kazandığı gözlemlenmiştir. 150°C'de 24 saat yaşlandırmanın ardından maksimum çekme mukavemeti (UTS) yaklaşık 420MPa seviyesine yükseldi ve %18 süneklik elde edildi. Aynı şartlarda maksimum kesme mukavemeti 270MPa seviyesine kadar yükseldi.

ARB prosesi sonlu elemanlar analizi temelinde Ansys Workbench kullanılarak modellendi. Efektif plastik gerinim ve gertime (von-Mises) değerlerinin ARB işlenik numunelerin kalınlığına göre değişim hesaplanmıştır. Deneysel bulgular ve sayısal analizlerin örtüştüğü gözlemlenmiştir.

# ACKNOWLEDGEMENTS

Firstly, I want to express my gratitude to my supervisor, Dr. Güney Güven Yapıcı, for his scholarly guidance, constructive criticism along with encouragement, and limitless support during my research work. Also, I would like to thank my committee members, Dr. Mehmet İpekoğlu and Dr. Altuğ Melik Başol for their attention and guidance to this work.

I am also grateful to Mr. Ulaş Yıldırım, technician of the manufacturing laboratory, for his continuous efforts in this study. I am grateful to my colleagues and MEMFIS group members, especially, Ali Hosseinzadeh Ghobadlou, Seyed Veghar Seyed Mohammadi, Ibrahim Orhun Tugay, Amin Radi, and Farhan Raza for their support, suggestions, and enjoyable time I have spent with them throughout my studies. Finally, I am thankful to my beloved family who supported me throughout my education.

# TABLE OF CONTENTS

**DEDICATION** ..... **III**

**ABSTRACT** ..... **IV**

**ÖZET** ..... **VI**

**ACKNOWLEDGEMENTS** ..... **VIII**

**TABLE OF CONTENTS** ..... **IX**

**LIST OF FIGURES** ..... **XII**

**LIST OF TABLES** ..... **XVII**

**1. INTRODUCTION** ..... **1**

1.1 Motivation ..... 1

1.2 Research Objectives ..... 2

1.3 Work Summary ..... 2

**2. LITERATURE REVIEW** ..... **4**

2.1 Overview ..... 4

2.2 Metal Matrix Composite (MMC) ..... 4

2.3 Severe Plastic Deformation (SPD) ..... 6

2.4 Conventional Rolling ..... 9

2.5 Accumulative Roll Bonding (ARB) ..... 12

2.5.1 Basics and Bonding Mechanism ..... 13

2.5.2 Process Parameters ..... 17

2.6 Advantages of the ARB Process ..... 26

2.7 ARB Processed Materials....27
2.7.1 Aluminum Alloys....27
2.7.2 Steel....32
2.7.3 Titanium....34
2.7.4 Dissimilar Metals....36
2.7.5 Roll Bonding of Dissimilar Alloys Using Interlayers....39
2.8 Application of Shear Punch Test in Evaluating Mechanical Behavior....41
**3. EXPERIMENTAL METHODS....43**
3.1 Materials....43
3.2 Processing of Accumulative Roll Bonding....44
3.3 Post-ARB Heat Treatment....48
3.4 Microstructural Characterizations....48
3.5 Mechanical Behavior Evaluation....49
**4. EVALUATION OF THE TITANIUM-STEEL COMPOSITE....51**
4.1 Overview....51
4.2 Microstructure....51
4.2.1 ARBed Ti-IF Steel Composite....51
4.2.1 ARBed Ti-Al2024-IF Steel Composite....57
4.3 Mechanical Response....61
4.3.1 Ti-IF Steel Composite Rolled at 480°C....61
4.3.2 Ti-Al2024-IF Steel Composite Rolled at 480°C....62

4.3.3 Ti-IF Steel Composite Rolled at 400°C ..... 66

4.3.4 Ti-Al2024-IF Steel Composite Rolled at 400°C ..... 71

4.4 Interfacial Strength ..... 73

**5. EVALUATION OF THE ALUMINUM-STEEL COMPOSITE ..... 77**

5.1 Overview ..... 77

5.2 Microstructure ..... 77

5.3 Mechanical Response ..... 79

5.3.1 Post-ARB Heat Treatment (3rd ARB cycle) ..... 80

5.3.2 Interfacial Strength ..... 84

**6. NUMERICAL ANALYSIS ..... 86**

6.1 Overview ..... 86

6.2 Modeling ..... 86

6.2.1 Geometry ..... 87

6.2.2 Assumptions ..... 88

6.2.3 Initial and Boundary Conditions ..... 89

6.2.4 Analysis ..... 89

6.3 Results and Discussion ..... 92

**7. CONCLUSION ..... 97**

**8. FUTURE WORKS ..... 100**

**REFERENCES ..... 101**

**VITA ..... 111**

# LIST OF FIGURES

**Figure 2.1** List of various reinforcements and matrix materials used to manufacture MMCs [5]. ..... 5

**Figure 2.2** Various manufacturing processes for MMCs [5]. ..... 6

**Figure 2.3** Microstructure of commercially pure titanium orientations and shapes of grains [8]. ..... 7

**Figure 2.4** Categorization of the microstructures based on the grain size of the metal [9]. ..... 8

**Figure 2.5** Illustration of (a) rolling process showing deformation (plastic) zone and (b) direction of rolling (friction) action [16]. ..... 10

**Figure 2.7** Schematic of principles of the ARB process [28]. ..... 14

**Figure 2.8** Mechanism of bond formation through fracture and extrusion by rolling [41]..... 17

**Figure 2.9** Worldwide research trend of ARB from 1999-2018 based on Google Scholar [41]. ..... 18

**Figure 2.10** Contrast in peel strength of aluminum strips against; (a) surface roughness, (b) delay time [50]. ..... 19

**Figure 2.11** Peeled surfaces of Ti (a-c) and Cu (d-e) from optical microscope (OM), rolled at three different $R_t$ values (a,d) 44%, (b,e) 56%, and (c,f) 62% [52]. ..... 20

**Figure 2.12** Variation in shear strength as a function of process (entry) temperature of the AA6111 [57]. ..... 22

**Figure 2.13** Trend in shear strength according to the rolling pressure of the AA6111 [57]... 23

**Figure 2.14** (a) Difference in average peel strength in different friction conditions (dry, rough, and lubricated surface) as a function of reduction [59], (b) Hardness versus the number of ARB cycles without lubrication [60]. ..... 24

**Figure 2.15** Trend in peeling force due to different heat treatment times and temperatures of Cu/Al interface after ARB [67].....26

**Figure 2.16** Trend in the strength of 1100 Al alloy tested at room temperature [14]. .....29

**Figure 2.17** Variation in the response of different conditions of Al2024 from stress-strain curves [74]. .....30

**Figure 2.18** Comparison of different tensile properties according to the increasing number of ARB cycles [76].....31

**Figure 2.19** Response of mechanical properties of steel processed by ARB, tested at room temperature [54].....33

**Figure 2.20** Variation in mechanical properties (a-d) of IF steel by ARB process as a function of cycles [79].....34

**Figure 2.21** Reduction of average grain size of CP-Ti as a function of ARB cycles [81].....35

**Figure 2.22** Stress-strain response of pure titanium processed after the ARB method [82]...35

**Figure 2.23** Demonstration of bumpers made by steel clad aluminum composite [86]. .....36

**Figure 2.24** Comparison in the hardness of AA6061 and AA5005 according to ARB cycles [69].....38

**Figure 2.25** Comparison of shear strength of three different layers' architecture under various rolling reductions after post brazing [99].....40

**Figure 2.26** Scanning electron microscope (SEM) image of interfaces at (a) 900$^{o}$C and (b) 950$^{o}$C [100].....41

**Figure 2.27** (a) Illustration of the SPT setup, (b) common LDC curve [104,105]. .....42

**Figure 3.1** Illustration of cyclic ARB process without the inclusion of additional Al2024 interlayer after the 1$^{st}$ cycle, here Al2024 is only used during the first cycle.....45

**Figure 3.2** Schematics of cyclic ARB process with the inclusion of additional Al2024 interlayer after the 1$^{st}$ cycle.....46

**Figure 3.3** The principal working of Al2024-IF steel composite by the ARB process [112]. 47

**Figure 3.4** Rolling mill used in the experimental procedure. 47

**Figure 4.1** Formation of Ti-IF steel composite rolled at 400°C through three cycles (1-3). 52

**Figure 4.2** Grain refinement of (a) as received IF steel, (b) ARBed IF steel after 3 cycles, (c) as received titanium, and (d) ARBed titanium after 3 cycles. 53

**Figure 4.3** SEM micrographs from fracture surfaces of Ti-IF steel composite rolled at 400°C after (a) two cycles and (b) three cycles. 55

**Figure 4.4** SEM micrographs from fracture surfaces of; (a) titanium, (b) titanium after the first cycle (ε = 0.8), (c) titanium after the third cycle (ε = 2.4), (d) IF steel, (e) IF steel after the first cycle(ε = 0.8), and (f) IF steel after the third cycle (ε = 2.4). 57

**Figure 4.5** Formation of aluminum interlayered Ti-Al2024-IF steel composite rolled at 480°C through three cycles (1-3). 59

**Figure 4.6** SEM micrographs from fracture surfaces of multi-metal (Ti-Al2024-IF steel) composite after (a) one cycle and (b) three cycles. 60

**Figure 4.7** True stress-strain curves of base metals and Ti-IF steel ARB composite rolled at 480°C. 62

**Figure 4.8** Modification in the average microhardness as; (a) comparison in constituent metals (Pre-ARB and Post-ARB) with increasing cycles and (b) through the cross-section of two-cycle ARBed composite. 63

**Figure 4.9** Tensile response of base metals and processed Ti-Al2024-IF steel composite after every ARB cycle. 65

**Figure 4.10** Average Vickers microhardness with the variation of (a) individual layers versus the number of cycles and (b) through-thickness of a sample after 3 ARB passes. 67

**Figure 4.11** Represents the response of fabricated Ti-IF steel sheets after the ARB with; (a) stress-strain curves and (b) the increasing number of cycles. 68

**Figure 4.12** Variation in the response of manufactured ARBed sheets after post-annealing (PA) with; (a) stress-strain curves, (b) increasing PA temperatures, and (c) ultimate conditions. ..70

**Figure 4.13** Stress-strain response of aluminum interlayered titanium-steel composite roll bonded at 400°C.....72

**Figure 4.14** Variation in the SPT results of Ti-Al2024-IF steel composite roll bonded at 400°C after three ARB cycles as (a) load-displacement curves, (b) shear strength as a function of displacement, and (c) ultimate shear strength versus the number of cycles. .....74

**Figure 4.15** Variation in the SPT results of Ti-IF steel composite roll bonded at 400°C after three ARB cycles as (a) load-displacement curves, (b) shear strength as a function of displacement, and (c) ultimate shear strength versus the number of cycles. .....75

**Figure 5.1** Optical micrographs of (a) aluminum as received, (b) three-cycle composite, (c) aged at 150°C/24h, (d) IF steel layers as received, (e) three-cycle composite, (f) three-cycle composite aged at 150°C/24h. .....78

**Figure 5.2** Engineering Stress-strain response of Al2024-IF steel composite after three ARB cycles.....80

**Figure 5.3** Graphical representation of precipitation hardening heating cycle. .....81

**Figure 5.4** Mechanical behavior of (a) as received constituent metals with ARBed composite, (b) aging response, and (c) variation in tensile properties with the increasing aging time.....82

**Figure 5.5** Comparison of bonding strength between three-cycle ARB composite with; (a) short aging, and (b) long aging period. .....84

**Figure 6.1** The FE model employed for the ARB of multi-metal composite (1$^{st}$ cycle). .....87

**Figure 6.2** Initial mesh size utilized in the analysis. .....88

**Figure 6.3** Illustration of the effective (a) (v-m) stress (MPa), and (b) plastic strain during the first rolling step. .....90

**Figure 6.4** Demonstration of the transferred effective plastic strain of the prior cycle before (a) second, and (b) third cycle rolling process. ..... 91

**Figure 6.5** Variation in von Mises stress levels of the layered composite after (a) 1st, (b) 2nd, and (c) 3rd rolling cycle. ..... 93

**Figure 6.6** Comparison between stresses gathered through simulations and experiments as a function of the number of cycles. ..... 94

**Figure 6.7** Variation in strain along the layered composite slab thickness in Ti-IF steel ARBed composite after each cycle. ..... 95

**Figure 6.8** Comparison between applied strain in experiments versus the strain acquired through simulations as a function of the number of cycles. ..... 96

# LIST OF TABLES

**Table 2.1** Description of commonly used SPD methods [9]. ..... 9

**Table 2.2** Summary of important factors and geometry changes during the ARB cycle in pure aluminum [29]. ..... 15

**Table 2.3** Characteristics of different types of ARB processed materials [29]. ..... 15

**Table 2.4** Organization, description, and properties of aluminum alloys [71]. ..... 28

**Table 3.1** The elemental composition of aluminum alloy. ..... 43

**Table 3.2** The elemental composition of IF steel (0.5mm). ..... 44

**Table 3.3** The elemental composition of IF steel (1mm). ..... 44

**Table 3.4** The elemental composition of commercially pure grade 2 titanium. ..... 44

**Table 4.1** Mechanical properties of aluminum interlayered titanium-steel composite by the ARB at 480°C. ..... 65

**Table 4.2** Mechanical properties of titanium-steel composite by the ARB at 400°C. ..... 71

**Table 4.3** Mechanical properties of aluminum interlayered titanium-steel composite by the ARB at 400°C. ..... 72

**Table 5.1** Tabular data extracted from stress-strain curves of primary metals and post-ARB heat-treated composites. ..... 83

**Table 6.1** Different meshing elements and their corresponding stresses of the model for the first cycle. ..... 88

**Table 6.2** Observed tensile yield strength (true), effective stress, and corresponding error of rolled composite after each cycle. ..... 94

# 1. INTRODUCTION

## *1.1 Motivation*

Energy efficiency plays an important role in our surroundings and environmental issues. The manufacturing of energy-efficient products is most critical on which different types of industries are working. Strength to weight ratio is the key issue in the automotive and aerospace industries these days. The use of lightweight materials instead of heavy materials leads to a reduction in emission and fuel consumption. It is important to fabricate alloys or composites that have the same mechanical properties as heavy material but are lightweight instead. Substituting high-density metals with low-density metals or alloys proves an effective strategy to cut vehicle weight. For example, the weight of the car body can be reduced from 300kg to 200 when an aluminum alloy structure is used [1]. Replacing lightweight aluminum ($2.7g/cm^3$) or pure titanium ($4.5g/cm^3$) instead of heavy steel ($7.8\ g/cm^3$) is critical in obtaining lightweight components. However, in the case of bulk production, cost plays an important role in the selection of material for the desired product as both aluminum and titanium are expensive than steel.

Fabrication of metal matrix composites (MMCs) balance all these factors and provides a material with better specific strength, cost-efficient, and enhanced mechanical properties. Strength, as well as toughness and ductility in material, can be considered important properties from a design point of view. Strenuous efforts have been given by the researchers to strengthen the material using diverse processes. Severe plastic deformation (SPD) is characterized by a high deformity process with refinement in grain size.

Accumulative roll bonding (ARB), the SPD process, was employed in this research to produce a multi-layered metal composite with a UFG structure. Owing to work hardening and grain refinement, the strength of the resultant composite can be enhanced significantly through

the ARB process. The focus of this study is to optimize the best conditions in acquiring favorable mechanical performance from the above-mentioned pure titanium and aluminum alloys with steel. Having dissimilar constituents in the laminated composite is beneficial in providing the advantageous feature of each constituent. Although ARB has been done on different combinations of dissimilar metals, this is the first time on the combination of titanium and steel. This work can contribute to literature as well as industrial application.

## *1.2 Research Objectives*

The main objective of the present work is to fabricate multi-layered titanium-steel and aluminum-steel composites and investigate their microstructural evolution and mechanical performance. Following are the steps through which the objectives are achieved.

- Manufacture multi-layered composites by utilizing different possible conditions and parameters gathered from the literature.
- Study the influence of different parameters and conditions on the bonding and strength of the composites.
- Investigate the effect of post heat treatment on the behavior of the resultant composites.
- Validate the experimental results with a numerical model of the process.

## *1.3 Work Summary*

Accumulative roll bonding (ARB) is utilized for the fabrication of lightweight multi-metal composites in this thesis. Literature review on the relevant subject comprises in the second chapter. The third chapter starts with the methodology used to solve the problem for this work. The first part involves the manufacturing of multi-metal composite while the second part encompasses the characterization of the resulting composite through microstructural evaluation and mechanical tests. The following chapter includes the results obtained from the microstructural observation and different mechanical tests of the ARB processed titanium-IF

steel composite. Testing results of fabricated aluminum-IF steel composite by ARB and post-ARB heat-treated composite are mentioned in chapter five. The experimental results were compared with simulations and results of the numerical method using ANSYS workbench 18.1, presented in chapter six. The idea of the finite element method (FEM) was applied in which deformation strain applied during ARB was calculated.

# 2. LITERATURE REVIEW

## *2.1 Overview*

Lately, great attention has been given to ultrafine-grained (UFG) materials to acquire enhanced mechanical properties. Several methods can be utilized to produce UFG materials, with all of them have advantages and disadvantages. Severe plastic deformation (SPD) on materials is a very common approach to alter the coarse grain (CG) to the UFG. Bulk production of materials having sub-micron grain size through SPD is one of the major benefits. This feature plays an important role in industrial purposes where mass fabrication is needed. The accumulative roll bonding (ARB) process has excellent potential in that aspect. This chapter thoroughly deals with previous studies related to process explanation, parameters, and mechanical behavior of materials produced by the ARB process.

## *2.2 Metal Matrix Composite (MMC)*

In this evolving modern age industry, there is always a need for attractive materials that can be used in extensive industrial applications. Recently, metal matrix composites (MMCs) have received great attention due to their superior mechanical properties and comprehensive use in industrial applications. The presence of mechanical properties like higher strength and toughness, which are usually absent concurrently in a single metal or its alloys, gives priority to MMCs over constituent metals [2]. MMCs consist of two parts: ductile metal or alloy matrix and reinforcement using other metal, organic or non-metallic compounds. Reinforcement in the shape of either sheets or particles can be used between metallic layers. The concept of producing MMCs is to improve the properties of a ductile matrix material by introducing a strong reinforcement in it. Properties like high strength to weight ratio, corrosion resistance, enhanced mechanical properties, and wear resistance can be obtained from MMCs. Generally, composites are known for their low weight and robust performance than other common

materials which allow them to be used in the aerospace and automobile industries. The advantage of having the ability to resist radiation, high temperatures, and electrical conductivities, allows MMCs to be used in nuclear industries as well as oil refineries [3,4]. It is very important to have a mutually compatible matrix and reinforcement materials, otherwise achieving strong interfacial bonding will be difficult, which will eventually produce composites with lower expected properties. Various reinforcement and matrix materials for the fabrication of MMCs are displayed in Figure 2.1. In this study, the usage of reinforcement as sheets will only be discussed.

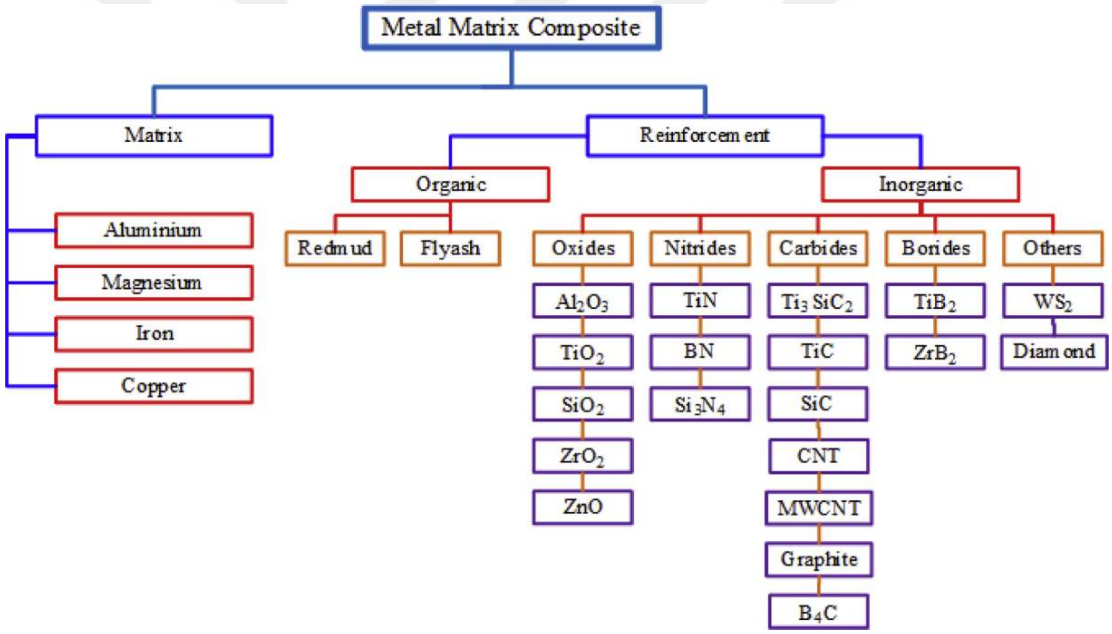



**Figure 2.1** List of various reinforcements and matrix materials used to manufacture MMCs [5].

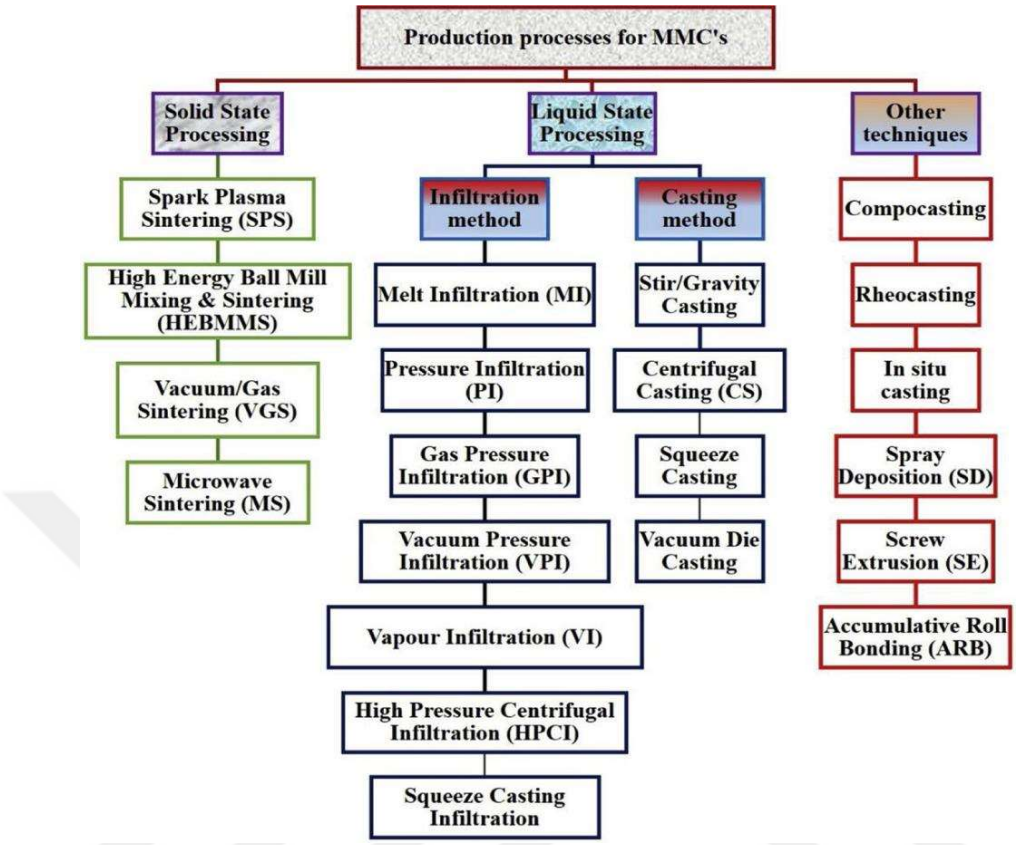



**Figure 2.2** Various manufacturing processes for MMCs [5].

A massive number of techniques were used by researchers worldwide to produce MMCs. Solid-state and liquid state processing are the main categories mentioned in Figure 2.2. Accumulative roll bonding (ARB) is one of the methods used for making composites, and only this will be discussed in this whole study.

## *2.3 Severe Plastic Deformation (SPD)*

Fundamentally, all metals are made up of atoms, and the arrangement of these atoms provides different crystal structures. These crystal structures can be categorized as single crystal and polycrystalline metal. In polycrystalline metals, these single crystals (grains) are interlocked in different orientations, as can be in Figure 2.3. The microstructural property, particularly grain size, affects the characteristics of many polycrystalline metals as it has a direct effect on different properties of metals [6]. A decrease in grain size substantially

increases the mechanical properties of the metals and, at high temperatures, yields superplastic ability. This effect on the properties can be understood from the Hall-Petch relation:

$$\sigma_y = \sigma_0 + kd^{-1/2} \quad (2.1)$$

where $\sigma_0$ is the friction stress, d is the grain size, and K is the constant [7].

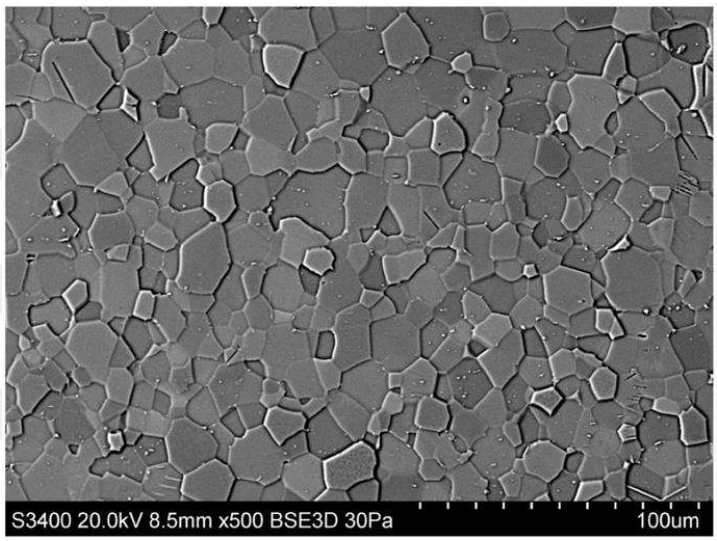



**Figure 2.3** Microstructure of commercially pure titanium orientations and shapes of grains [8].

The microstructure is categorized based on grain size, and Figure 2.4 illustrates the different structures of metals from coarse-grained (CG) to nano-grained. Based on the grain size, the structure of metals can be classified into four stages, i.e., coarse-grained, fine-grained, ultrafine-grained (UFG), and nano-grained or nanostructured (NS). The grain size varies from 10μm up to 100nm based upon the structure.

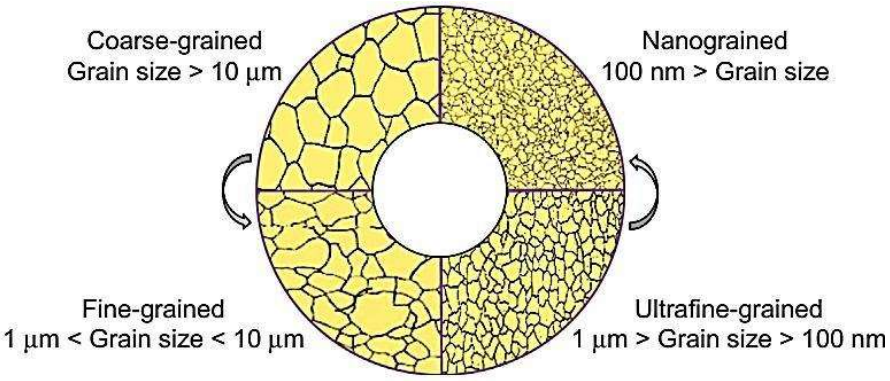



**Figure 2.4** Categorization of the microstructures based on the grain size of the metal [9].

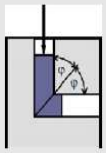
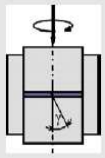
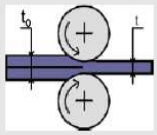
Typically, base metals have a coarse-grained structure which causes hindrance in providing high strength properties. Severe plastic deformation, the metal forming process, can be utilized to obtain UFG microstructure in the base metals and their alloys. Processing with SPD induces enormous plastic strain into the material, which consequently transforms into high-strength UFG material with high-angle grain boundaries. Refinement occurs through simultaneous shearing and transformation of phases with recrystallization methods (referred to as dynamic recrystallization). The fundamental mechanism of SPD techniques is to increase dislocation density through continuous induction of strain, which results in the formation of microstructures with high-angle and low-angle grain boundaries upon ambient temperature.

There are several SPD processes used worldwide includes equal channel angular pressing (ECAP), high-pressure torsion (HPT), friction stir processing (FSP), accumulative roll bonding (ARB), extrusion, and others [10-14]. These methods can be utilized to achieve UFG microstructure, and as a result, improve mechanical properties like strength levels, wear resistance, and hardness. Among SPD methods mentioned above, commonly used processes are represented with schematics and achievable equivalent strain in table 2.1 [9].

SPD methods have some limitations as only ultra-fine levels can be produced by industries for continuous operation, while nanoscale levels can only process in laboratories and

remain obsolete for industrial operation. Furthermore, many techniques utilize expensive equipment and procedures, large load capabilities, complicated nature of processes, limited sample size, and finally provides low production efficiency. To overcome these limitations, an ARB method was introduced in 1998 to achieve ultrafine-grained nanomaterials, which is a simple, economical, and bulk production method. ARB has promising industrial applications for the continuous manufacturing of large, laminated materials [15]. Only the ARB method, as an application of severe deformation, is researched in this study.

**Table 2.1** Description of commonly used SPD methods [9].

| Process name | Schematic representation | Equivalent plastic strain |
|---|---|---|
| Equal channel angular extrusion (ECAE) (Segal, 1977) |  | $\varepsilon = n\frac{2}{\sqrt{3}}\cot(\varphi)$ |
| High-pressure torsion (HPT) (Valiev et al., 1989) |  | $\varepsilon = \frac{\gamma(r)}{\sqrt{3}}, \gamma(r) = n\frac{2\pi r}{t}$ |
| Accumulative roll-bonding (ARB) (Saito, Tsuji, Utsunomiya, Sakai, 1998) |  | $\varepsilon = n\frac{2}{\sqrt{3}}\ln\left(\frac{t_0}{t}\right)$ |

## *2.4 Conventional Rolling*

In metalworking, rolling is a simple metal forming process in which metal stock is deformed plastically by coursing it through one or more pairs of rolls. The purpose of this process is to not only reduce the thickness of the workpiece with uniformity but also to acquire desired mechanical properties from processed material [16]. During the whole rolling process, sheet metal receives high shear stresses along with high compressive stresses which helps in the uniform deformation. These stresses arise in the product due to the squeezing of rolls together with the application of friction force between rolls and sheets. Cold rolling and hot

rolling are two main types used in laboratories and industries to manufacture a new product or deform existing material into the desired one. It is easily understandable from the names of these two methods that, one is carried out at room temperature and the other at high temperature, depends upon materials compatibility and its desired usage. Thickness (initial $h_0$, final $h_f$) and velocity (initial $V_0$, $V_f$) of the rolling sheet are the most critical parameter of rolling methods as indicated in Figure 2.5, where $\alpha$, R, $\omega$ are the angle of contact, radius, and rotational speed of rolls, respectively. Finally, w and L are the width and contact length (plastic zone) of the sheet.

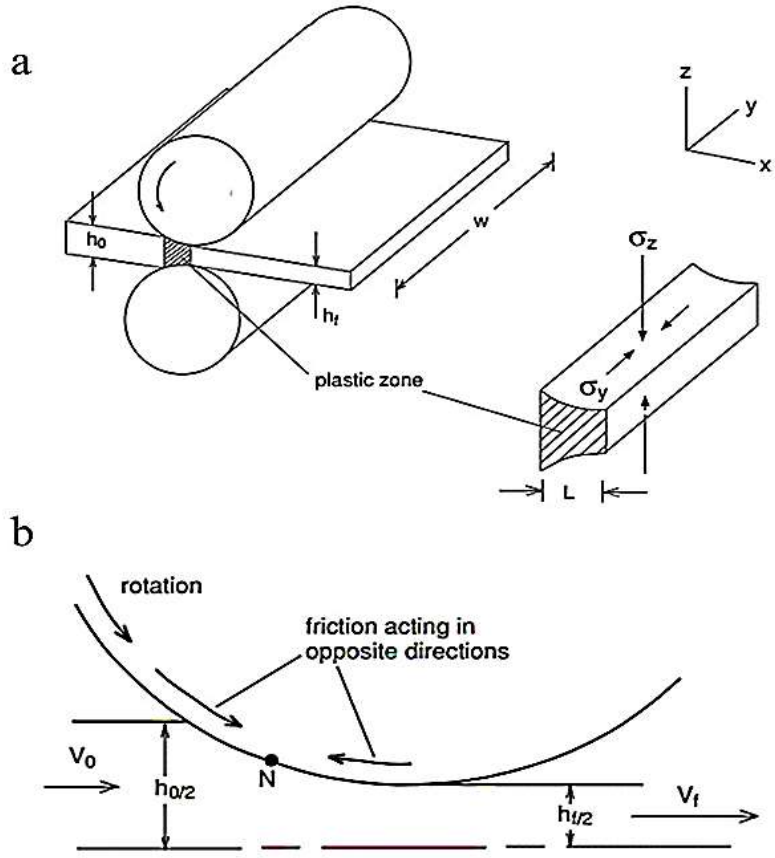



**Figure 2.5** Illustration of (a) rolling process showing deformation (plastic) zone and (b) direction of rolling (friction) action [16].

Generally, the rolling process is assumed to be two 2-D in flat shape materials, because deformation is very negligible in width as compared to the length and thickness of the material. Deformation values, i.e., reduction in cross-section and strain can be measured from equations (2.2) and (2.3) respectively.

$$\Delta h = h_0 - h_f \tag{2.2}$$

$$\varepsilon_h = {\Delta h}/{h_0} \tag{2.3}$$

The velocity of the rolling metal can be calculated from equation (2.4).

$$v_0 . h_0 . w_0 = v_f . h_f . w_f \tag{2.4}$$

As mentioned earlier, in the flat rolling process, the expansion in width is negligible.

$$w_0 = w_f \tag{2.5}$$

Mathematically, the deformation (plastic) zone in Fig. 2.5 can be measured by equation (2.6).

$$L = [R(h_0 - h_f)]^{-1/2} \tag{2.6}$$

The summary of the whole mechanism of the rolling method is following; When a specimen is fed into the rolls, due to friction between the specimen's surface and rolls, it is pulled between the rolls through to the departure side. In terms of the speed of the specimen, it travels slowly till the first point of contact. Reaching a deformation zone, the specimen's speed becomes equal to the roll's rotational speed which is called neutral point. Specimen travels at a speed higher than the speed of the roll after a neutral point. At this point, the frictional force starts to oppose the material flow as its direction becomes reversed. Opening between the roll should be appropriate enough to grip the specimen and then draw it out through the rolls, otherwise, it will likely be stuck between them. This phenomenon of push and pull is explained in Figure 2.6.

Condition of pull will only occur, if

$$F_2 \geq F_1 \tag{2.7}$$

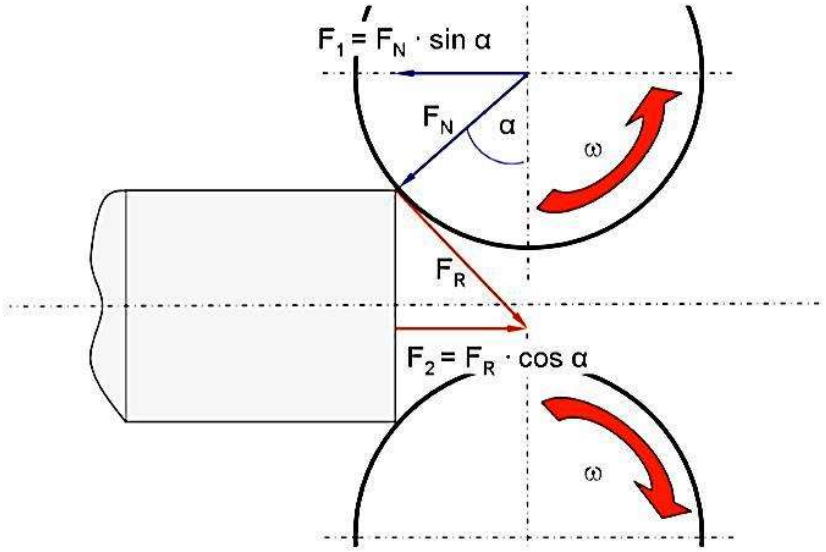



**Figure 2.6** Illustration of rolling forces through the whole process [17].

The rolling process may produce different types of flaws in rolled sheets due to the complex interaction between the sheet metal and rolls. Waviness, edge cracking, non-uniform thickness, and bending of the rolling plate are some defects that can occur due to rolling methods.

## *2.5 Accumulative Roll Bonding (ARB)*

Accumulative roll bonding (ARB) is one of the severe plastic deformation (SPD) processes used to fabricate sheet metal matrix composites with enhanced mechanical properties and tailored microstructure. It is simple, repetitive unidirectional rolling to impart large strain on different materials, consequently, provide deformed grain size. The presence of ultra-fine grained (UFG) microstructure in a material corresponds to improved mechanical behavior [15]. Due to low-cost production and simplicity during the process, ARB is preferable to be used as

a continuous operation industrially over the other SPD methods. Also, the ARB process can bond both similar and dissimilar materials, which is also beneficial in obtaining multiple layers and UFG in microstructure by the accumulation of large strain [18]. Through the processing of ARB, bonding of many materials is achieved which is not possible by traditional bonding processes. ARB process is an excellent candidate to fabricate composite to be used in lightweight structural applications in several industries including aerospace, automotive, and marine [19].

### 2.5.1 Basics and Bonding Mechanism

ARB is a solid-state joining method that includes repetitive steps of surface preparation, stacking, rolling, and cutting [14]. Surface preparations involve degreasing and wire brushing of contacting surface by acetone/alcohol and a steel brush. When the rolling pressure is applied, due to friction and reduction in thickness, heat is generated which helps clean surfaces to be bond along with high pressure. To achieve sufficient solid-state bonding, the deformation of stacked layers must be enough. The whole ARB process is demonstrated schematically in Figure 2.7. Rolling can be done at room temperature and sometimes at a high temperature depending upon the nature of the materials. To improve the bonding quality and formability between sheets, pre and post-rolling heat treatment is usually performed on the stacked sandwich [20-27].

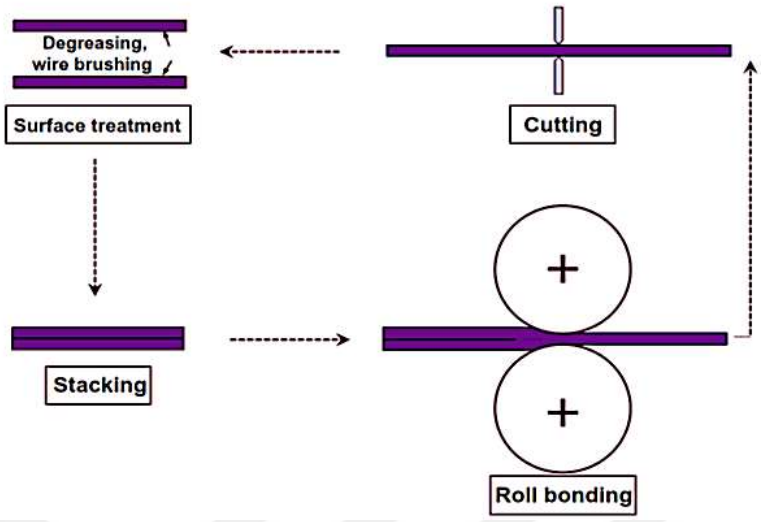



**Figure 2.7** Schematic of principles of the ARB process [28].

According to each number of cycles and layers, reduction in thickness and equivalent strain can be measured in the ARB process, every cycle provides a 50% reduction in thickness as summarized in Table 2.2. Every 50% reduction ratio is equivalent to 0.8 von Mises strain that increases 0.8n times as each number of cycles increases. New thickness obtained after each cycle can be determined by the relation

$$t = t_0/2^n \tag{2.8}$$

The following relation will be used to calculate the total true strain for each processed cycle.

$$\varepsilon = (2/\sqrt{3})n.\ln(1-r) = 0.8n \tag{2.9}$$

where (n) and (r) are the number of cycles and the reduction in thickness of each cycle, respectively.

The reason for attaining high strength in the processed material after ARB is dominantly due to the elongated UFG. Table 2.3 outlines some of UFG materials' grain size and strength.

**Table 2.2** Summary of important factors and geometry changes during the ARB cycle in pure aluminum [29].

| No. of cycles | 1 | 2 | 3 | 4 | 5 | 6 | 7 | 8 | 9 | 10 | $n$ |
|---|---|---|---|---|---|---|---|---|---|---|---|
| No. of layers | 2 | 4 | 8 | 16 | 32 | 64 | 128 | 256 | 512 | 1024 | $2^n$ |
| No of bonded boundaries | 1 | 3 | 7 | 15 | 31 | 63 | 127 | 255 | 511 | 1023 | $2^n-1$ |
| Layer interval (μm) | 500 | 250 | 125 | 62.5 | 31.2 | 15.6 | 7.8 | 3.9 | 1.9 | 0.96 | $1000/2^n$ |
| Total reduction (%) | 50 | 75 | 87.5 | 93.8 | 96.9 | 98.4 | 99.2 | 99.6 | 99.8 | 99.9 | $(1-1/2^n)\times 100$ |
| Equivalent strain | 0.8 | 1.6 | 2.4 | 3.2 | 4.0 | 4.8 | 5.6 | 6.4 | 7.2 | 8.0 | $\left(\frac{2}{\sqrt{3}}\ln 2\right) n = 0.8\,n$ |

Conducting ARB at low temperatures tends to produce a structure with fine grain size which subsequently gives two- or three-times higher strength than conventional grain size, but at the expanse of lower ductility in the material because of the plastic instability [30]. Tsuji et al. [31, 32] observed low temperature superplasticity during the ARB method in UFG aluminum alloy. Also, fabrication of UFG through ARB is faster than conventional rolling which makes ARB more useful than conventional rolling in the refinement of grain structure [33].

**Table 2.3** Characteristics of different types of ARB processed materials [29].

| Materials [mass %] | ARB Process | Microstructure | Grain size [μm] | Tensile strength [MPa] |
|---|---|---|---|---|
| 4N-Al | 7 cycles at RT | pancake UFG | 0.67 | 125 |
| 100-Al (99 % Al) | 8 cycles at RT | pancake UFG | 0.21 | 310 |
| 5052-Al (Al-2.4Mg) | 4 cycles at RT | ultrafine lamellae | 0.26 | 388 |
| 5083-Al (al-4.5Mg+0.57Mn) | 7 cycles at 100°C | ultrafine lamellae | 0.08 | 530 |
| 6061-Al (Al-1.1Mg-0.63Si) | 8 cycles at RT | ultrafine lamellae | 0.10 | 357 |
| 7075-Al (Al-5.6Zn-2.6Mg-1.7Cu) | 5 cycles at 250°C | pancake UFG | 0.30 | 376 |
| OFHC-Cu | 6 cycles at RT | ultrafine lamellae | 0.26 | 520 |
| Cu-0.27Co-0.09P | 8 cycles at 200°C | ultrafine lamellae | 0.15 | 470 |
| Ni | 5 cycles at RT | ultrafine lamellae | 0.14 | 885 |
| IF steel | 7 cycles at 500°C | pancake UFG | 0.21 | 870 |
| 0.041P-IF | 5 cycles at 400°C | pancake UFG | 0.18 | 820 |
| SS400 steel (Fe-0.13C-0.37Mn) | 5 cycles at RT | ultrafine lamellae | 0.11 | 1030 |
| Fe-36Ni | 7 cycles at 500°C | ultrafine lamellae | 0.087 | 780 |

The bonding mechanism is explained by four major theories which are the following:

- Film theory
- Energy barrier
- Recrystallization
- Diffusion bonding

Film theory suggests that two clean metal surfaces have a main role in creating a bond. When they come into close contact during rolling, fracture of hard (surface) layer and flow of ductile layer causes mechanical bonding between them. Specifically, this theory is a chief mechanism in low-temperature ARB [34,35]. Energy barrier theory opposes film theory and proposes that when metal surfaces come into contact, no bond is created. Erdmann-Jesnitzer [36] suspects that diffusion is related to the energy barrier, while Parks [37] resolved that recrystallization is the energy barrier. However, Semenov's [38] finding deducted that bonding for copper (Cu), aluminum (Al), and silver (Ag) occurred at liquid nitrogen temperature which is against diffusion and recrystallization. He proposed that crystal misorientation at the contact surfaces originates energy barrier. It is concluded that bonding occurs from film theory in which oxides and contaminants are removed from surfaces, creates a rough and hard surface. During rolling operation, brittle layers from the surfaces are broken up and ductile layers are extruded, allowing to form a bond with cracked surfaces due to the rolling pressure from either side of layers. This mechanism is supported by optical and scanning electron microscopies (SEM) [39,40]. Figure 2.8 displays a schematic illustration of the entire film theory.

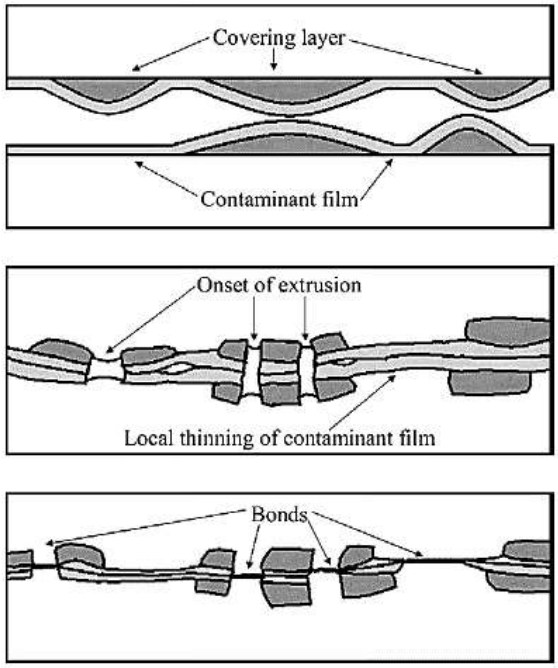



**Figure 2.8** Mechanism of bond formation through fracture and extrusion by rolling [41].

### 2.5.2 Process Parameters

Several factors have effects in providing optimum properties of the fabricated composite, including types and orientation of stacking metals, thickness and surface preparation of base components, and bonding and rolling conditions [42,43].

*2.5.2.1 Types of materials*

Types of metal matrix composites (MMCs) is solely depending upon the different types of materials used to produce them, the most important parameter in ARB. Single metal [44], double metal [45], and multi-metal with reinforcing agents [46] are some that fall into the category of MMCs. The number of articles published between 1998 and 2018, according to Google Scholar, is represented in Figure 2.9. It is evident and easily assumable that ARB of similar materials was researched dominantly in the early years. Experimenting on dissimilar materials/reinforcement started from 2007 prominently, this trend became more relevant till

2014. The extent of research has been increased in recent years, where dissimilar materials received more devotion from researchers worldwide.

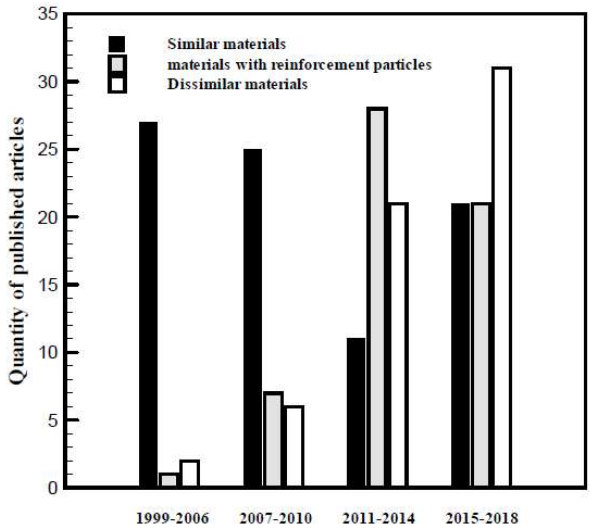



**Figure 2.9** Worldwide research trend of ARB from 1999-2018 based on Google Scholar [41].

Approximately, 50% of the studies on the ARB have been carried out on Al alloys in similar materials, while other materials that have been used are steel, copper, titanium, and magnesium alloys. Aluminum is an easily fabricated alloy and widely used, more than 70%, in dissimilar metal bonding methods. Compatibility between dissimilar materials is very important in obtaining a good, bonded composite.

*2.5.2.2 Surface Preparation*

Surface characteristics such as roughness and cleanliness, significantly influence mechanical strength [47]. Oxides can be formed on the surface of different metals during hot forming processes or thermal treatment. Moreover, lubricants used during these processes such as grease, oil, moisture, and chemical compounds can contaminate the surface, therefore, act as bonding barriers. These contaminants must be eliminated, especially before rolling at ambient temperatures, otherwise, it would lessen the strength [48,49]. Both chemical and/or

mechanical treatments can be carried out to remove contaminants from the surface of a material.

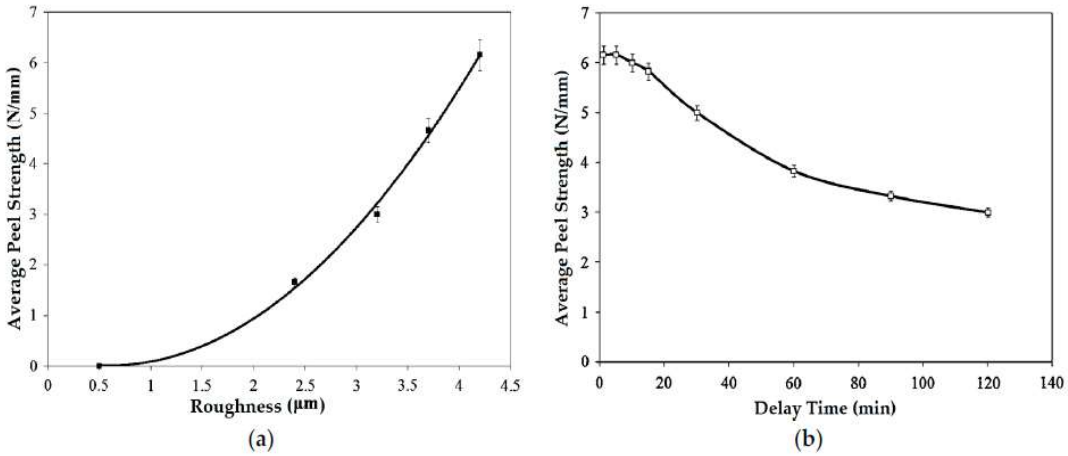



**Figure 2.10** Contrast in peel strength of aluminum strips against; (a) surface roughness, (b) delay time [50].

Among different surface preparation methods, degreasing in acetone followed by wire brushing is by far a widely used process that gives better bond strength. It has also been observed that reducing delay time in surface preparation before rolling will enhance adhesion between two materials. Figure 2.10 demonstrates the effect of surface preparation and delay time on the peeling strength of processed material. It can be observed that increasing the roughness of surfaces and allowing less delaying time before rolling has provided higher peel strength. During rolling, brittle surface layers and unavoidable oxide films break which allow virgin (ductile) layers to be extruded and ensue better bonding between sheets. Also, the rolling process should be carried out inside the first 10 min as Figure 2.10 (b) suggested [50].

*2.5.2.3 Reduction in Each Cycle*

Thickness reduction is the major condition to governed plastic strain, consequently, provide bonding quality. Thickness reduction, termed threshold thickness ($R_t$), is necessary to achieve good bonding. The amount of $R_t$ depends upon working temperature which decreases

when the working temperature reaches up to recrystallization temperature. Sufficient bonding can be acquired without recrystallization if the working temperature is less than half of the melting temperature of the material [51].

Hosseini et al. [52] performed a microscopic examination on Ti/Cu peeling surfaces to observe evidence of mechanically affected bond strength at different reductions. They suggested by increasing $R_t$, the total surface cracks area increases which raise the extent of virgin metal extrusion, subsequently leads to expanded fusion areas and improved bond strength, as displayed in Figure 2.11.

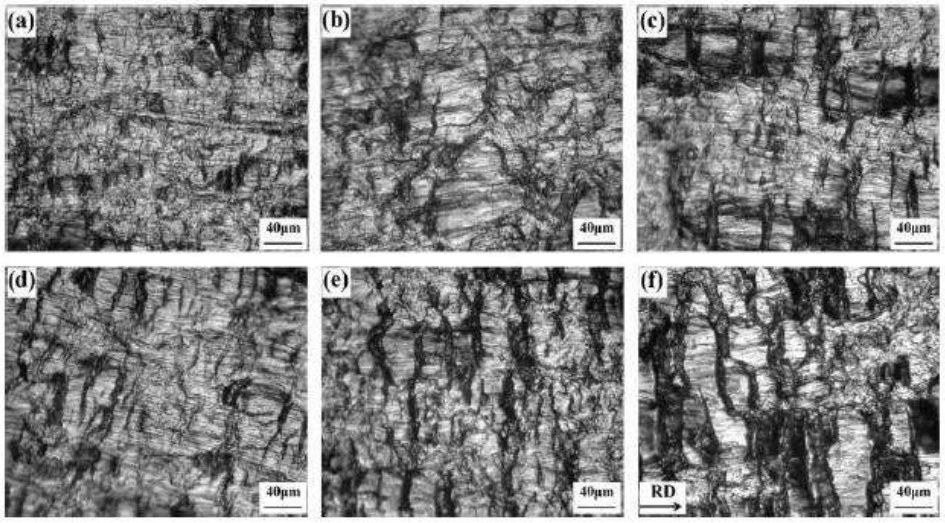



**Figure 2.11** Peeled surfaces of Ti (a-c) and Cu (d-e) from optical microscope (OM), rolled at three different $R_t$ values (a,d) 44%, (b,e) 56%, and (c,f) 62% [52].

In terms of chemically affected bond strength, a width of the diffusion layer of Al/Ti composites after ARB was measured at different $R_t$ values and concluded that it has a direct relation with thickness reduction, thus bond strength increases with high $R_t$ values [53].

*2.5.2.4 Temperature*

Working temperature is critical in affecting thermal stability, microstructure, bonding between sheets, and consequential mechanical properties [54]. Initially, ARB was performed

at high temperatures, which is now being carried out at low and/or room temperatures along with elevated temperatures. Generally, the rolling temperature has a direct correlation with bonding, i.e., increasing temperature expands diffusion layer thickness of interface between two sheets subsequently enhance bond strength. Although the main purpose of using temperature is to increase strength by improving bonding between layers, sometimes, it can also lessen the strength by initiating factors like recrystallization and recovery. Recovery of accumulated plastic deformation is inevitable even at low temperatures, so rolling must be done below the recrystallization temperature of the metals used. Recrystallization temperature is below half of the melting point; thus, the rolling temperature should be varied for each material based on it. If other factors, mentioned before this, can provide quality bonding without increasing temperature, then the final strength of the material will be greater than with temperature.

The temperatures of more than 200°C give quality bonding for most of the aluminum alloys. Slamova et al. [55,56] studied the importance of preheating followed by rolling on thermal stability. Preheating combined with heat generated during the rolling process are the reasons for the initiation of partial recrystallization and recovery on the accumulative roll bonded Al-Fe-Mn-Si. Sometimes, increasing temperature could lead to the generation of oxide layer depending upon the type of metal, which reduces the quality of bonding between sheets. The effect of process temperature versus shear strength can be observed in Figure 2.12 [57]. Zhan et. al [58] also reported that the strength of the final ARBed AZ31 alloy was reduced by increasing rolling temperature.

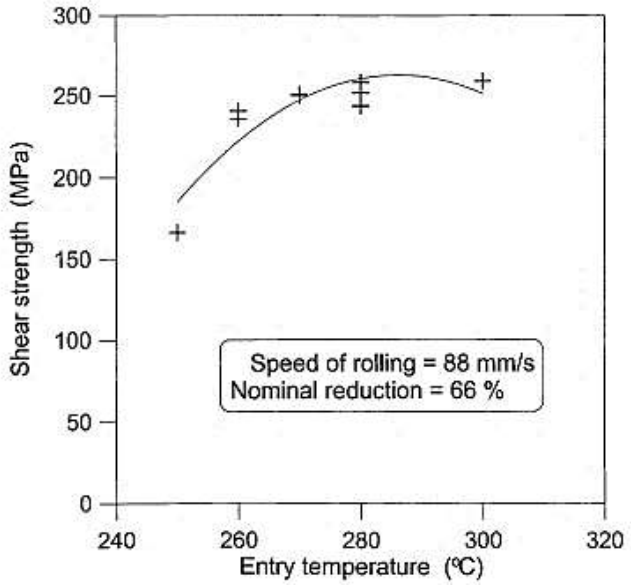



**Figure 2.12** Variation in shear strength as a function of process (entry) temperature of the AA6111 [57].

*2.5.2.5 Roll Diameter and Rolling Speed*

To obtain hardness, fine structure, and quality bonding in the composite, roll diameter and rolling speed are decisive factors. Decreasing the speed of the rolling process will provide diffusion of adjacent layers and enough time to contact pressure that results in stronger bonding. Large roll diameter increases deformation areas, thus more distribution of the equivalent strain on the specimen and vice versa. While rolling pressure will increase the shear strength of the processed material, as can be seen in Figure 2.13, which is similar to the rolling reduction parameter. The experiment performed in the AA6111 revealed that large roll diameter and slow rolling speed helped in obtaining maximum bond strength [57]. So, it can be concluded that the optimum parameter is to have a slow speed in securing better strength.

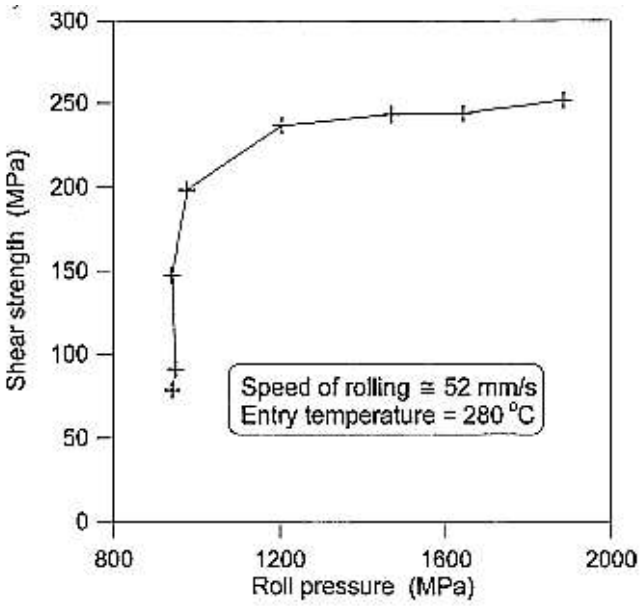



**Figure 2.13** Trend in shear strength according to the rolling pressure of the AA6111 [57].

*2.5.2.6 Friction at the Roll Interface*

It is very common to perform ARB without lubricants between rolls and sheet metal, as most of the studies have suggested. In this regard, the friction factor comes into the contention for producing strongly bonded sheets. Figure 2.14 indicates the effect of different friction coefficients on the peel strength and hardness of processed material. Jamaati and Toroghinejad [59] conducted ARB at different friction conditions such as with lubricant, rough, and dry surfaces, and observed that peel strength was increased when friction coefficient was high between rolls and sheets due to high contact pressure, as indicated in Figure 2.14 (a).

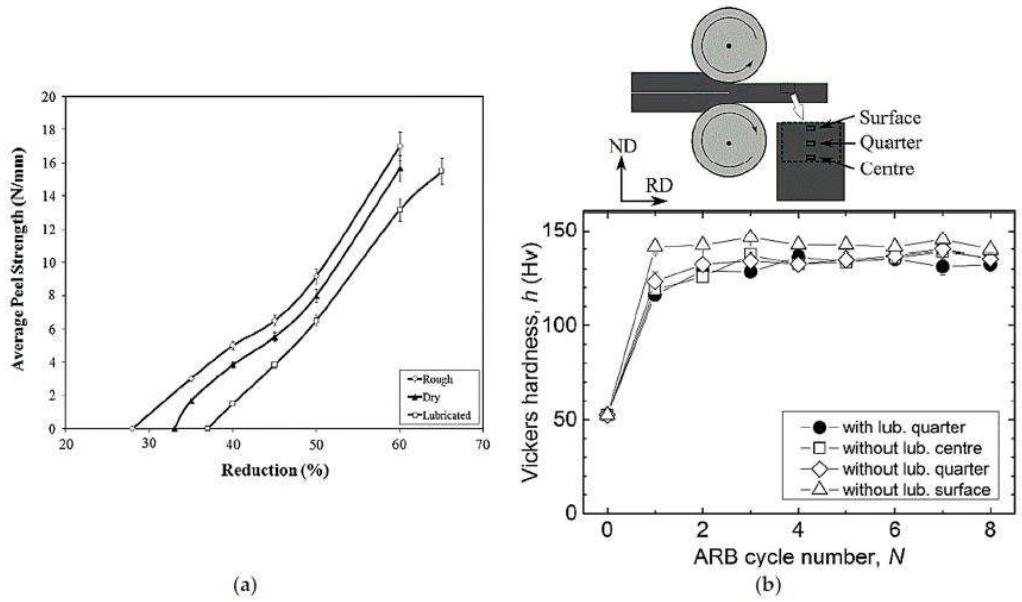



**Figure 2.14** (a) Difference in average peel strength in different friction conditions (dry, rough, and lubricated surface) as a function of reduction [59], (b) Hardness versus the number of ARB cycles without lubrication [60].

Miyajima et al. [60] studied the effect of friction at different places of ARB processed Cu, i.e., surface, quarter, and center. As displayed in Figure 2.14 (b), the highest strain occurs adjacent to the surface with high friction coefficient between rolls and specimen due to additional shear strain (referred to as redundant shear strain) and the lowest at the center [61]. This strain remains in the ARBed structure as every surface layer moves to the center in the ensuing cycle. Lastly, no lubricant condition accelerates grain refinement due to the redundant shear strain.

*2.5.2.7 Number of Cycles and Layers*

Deformation and bonding between sheets are concurrently affected by an increasing number of layers or cycles [62]. Jang et al. [63] observed the tensile strength of 2- and 3-layer Cu composite after ARB, which is determined by material strength along with applied equivalent strain. Initially, strength is normally higher for more stacked layers compared to a

smaller number of layers up to a critical point after that response becomes almost identical. In terms of the number of cycles, the strengthening mechanism in the starting cycles is due to work hardening, while grain refinement and grain boundary strengthening contribute to the major strengthening of rolled specimen subsequently. Krallics and Lenard [64] studied the ARB of different metals and the effects of the number of cycles on processed materials. They suggested after some cycles, bond strength improved owing to the reduction of delamination area and increasing number of bond layers in the structure.

*2.5.2.8 Post-ARB Heat Treatment*

Materials obtained after ARB are usually poor in formability as they have limited ductility. Heat treatment is a viable choice to deal with this problem where medium/large strain is accumulated in the samples. It recrystallizes (i.e., nucleation and growth) and provides extended recovery, results in microstructural coarsening of grains [65,66]. Investigation of annealing treatment on fabricated Cu/Al/Cu clad composite was done by Sheng et al. [67] after one cycle rolling, and results are reported in Figure 2.15. Evidently, bond strength and bonding quality were significantly improved by appropriate heat treatment, while low temperature and short annealing time also varied the bond strength. However, the strength of processed material drastically decreased due to the deterioration of layers through the growth of brittle intermetallic compounds (IMCs) at high temperatures and longer annealing times. Finally, the formability of processed sheets is improved by interlayer diffusion and recrystallization due to annealing.

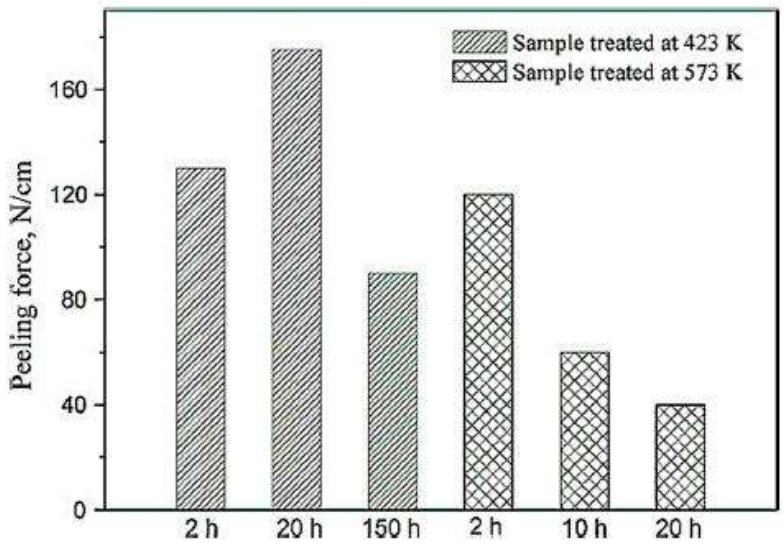



**Figure 2.15** Trend in peeling force due to different heat treatment times and temperatures of Cu/Al interface after ARB [67].

## *2.6 Advantages of the ARB Process*

Achieving reliable materials with nano or ultrafine grain structure involves either advanced methods or expensive die in all SPD techniques which increase the cost of production. Moreover, most of the SPD methods involves complication in the method as well as limitation in the workpiece as they include large apparatus. Whereas the ARB method is simple with no limitation in the size of the workpiece as any capacity of rolling mill is available and performs a similar process according to requirements. For example, ECAP has the advantage of producing bulk workpieces with limited (large) dimensions, while ARB provides variable dimensions due to the capacity of the rolling mill [68]. In this regard, ARB is preferable in industrial processes in comparison with the other SPD techniques due to its simple and more economical approach.

## *2.7 ARB Processed Materials*

### 2.7.1 Aluminum Alloys

The demand for aluminum and its alloys in the extensive applications of automotive, aerospace, and marine industries as a structural component has been increased significantly in the last few decades. This led to the evolution of the development of manufacturing techniques that can improve the mechanical properties of aluminum [69]. Nowadays, reducing fuel consumption and controlling $CO_2$ emission is very challenging in material selection for different industries. Therefore, aluminum is the appropriate choice to be used as a structural part and component as it has suitable properties like lightweight, formability, machinability, and lastly high strength.

Cast alloys and wrought alloys are two different series on which aluminum alloys are generally classified. Both alloys are typically expressed by four digits (#xx.x and #xxx) where starting # is the principal element in the aluminum and other numbers indicate the quantity of alloying elements. 2XXX and 6XXX are two of the main categories of the wrought aluminum alloys containing Cu and Mg, respectively as the principal alloying element [70]. Representation and description of the wrought aluminum alloys are mentioned in Table 2.4 [71].

**Table 2.4** Organization, description, and properties of aluminum alloys [71].

| Alloy Series | Principal Alloying Element | Definition and Properties |
|---|---|---|
| 1xxx | 99% minimum Aluminum | Controlled pure aluminum alloys, this series are generally used in the electrical and chemical industries. |
| 2xxx | Copper | The 2xxx series aluminum alloys, which is the major alloying element of copper, is generally used in the aviation industry due to its high yield strength as high as 455 MPa. |
| 3xxx | Manganese | Utilized as general-purpose alloys for building industry and other numerous products. |
| 4xxx | Silicon | Silicon is the principal alloying element and 4xxx series are utilized as welding rods and brazing sheet. Silicon addition range from 0.6 to 6.2%. |
| 5xxx | Magnesium | 5xxx series are the aluminum/magnesium alloys which are magnesium addition range are 0.2 to 6.2%. This series has high weldability, so they are used for different applications. |
| 6xxx | Magnesium and Silicon | Aluminum/magnesium and silicon alloys have 1% magnesium and silicon additions. These additions produce magnesium-silicide, which is ensures the ability to become solution heat treated for enhanced strength. |
| 7xxx | Zinc | Zinc addition range is 0.8 to 12%. 7xxx series are contain highest strength aluminum alloys. These alloys are utilized in aircraft, aerospace, and sporting equipment applications. |
| 8xxx | Other Elements | This series contains iron, lithium, or tin. |

As mentioned earlier, most of the severe plastic deformation studies especially ARB was successfully conducted on different aluminum alloys. In fact, more than 50% of ARB experiments were done on aluminum alloys in the fabrication of similar and dissimilar composites that result in the considerable enhancement of mechanical properties in the last two decades. For example, Figure 2.16 displays the strength of UFG aluminum alloy fabricated at

elevated temperatures utilizing the ARB method, which was increased up to 3.7 times than the raw materials with the expanse of decreasing elongation [14].

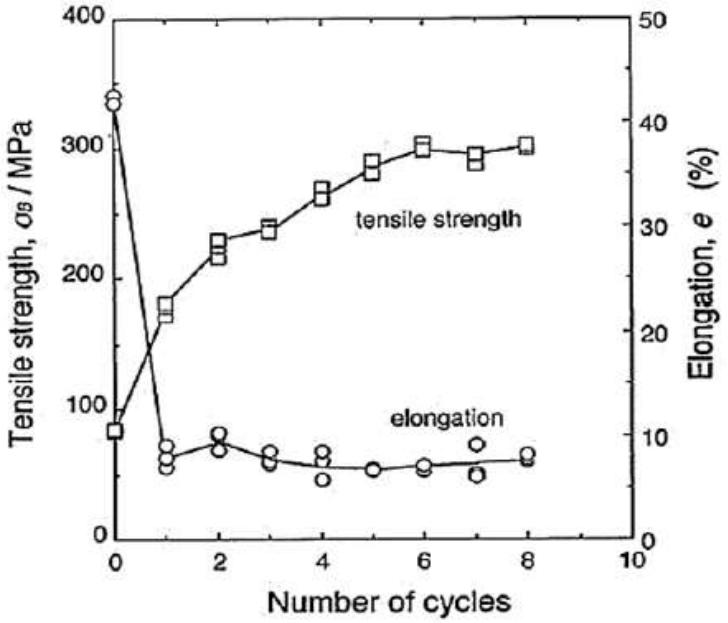



**Figure 2.16** Trend in the strength of 1100 Al alloy tested at room temperature [14].

The Al2024 is an alloy of aluminum that contains copper (2-10%) as a principal alloying element with the inclusion of other minor alloying elements such as manganese, zirconium, magnesium, silicon. The purpose of the copper element is to improve the strength of aluminum alloys as well as promote precipitation hardening in the alloy. Al2024 is used commercially as a structural part that provides appropriate mechanical properties, available in the form of sheets [72]. The Al2024 alloy has unique properties for instance good machinability and workability, fatigue resistance, sensitivity to temperatures, and finally, suitable strength which allow it to be used as structural parts in various products like clock parts, aircraft structure, missile parts, truck wheels, orthopaedic and veterinary products [73]. Application of the SPD process on Al2024 provides a significant number of dislocation and fine grain sizes, consequently present enhanced strength with the expanse of the lower ductility.

Different types of ARB strategies were applied to improve the elongation of Al2024 along with relatively high strength. Naseri et al [74] utilized a process in which two annealed strips of Al2024 were used and rolled at room temperature under 50% reduction thickness to fabricate a two-layered Al2024 sheet in the first cycle. But before the second cycle, an annealed Al2024 strip, similar in thickness as two layers sheet, was introduced between the first cycle processed composite and rolled bonded with a 50% reduction ratio to consist of five layers Al2024 sheet. They repeated a similar step up to four cycles and acquired results are reported in Figure 2.17 along with UFG Al2024 and annealed 2024. Elongation was improved from approximately 4% to 10% with a relatively good strength of 365MPa.

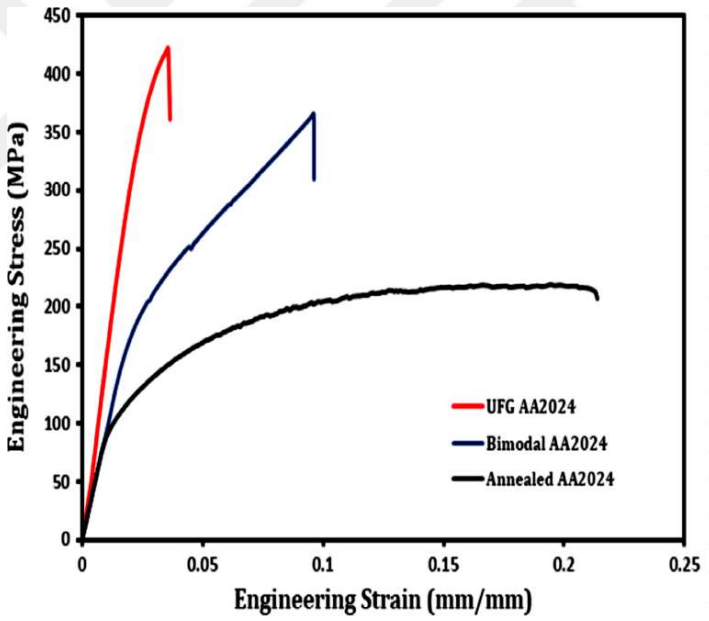



**Figure 2.17** Variation in the response of different conditions of Al2024 from stress-strain curves [74].

Another approach was tried to refine the ductility of aluminum alloy Al2024 by solid solution treatment in which rolling was performed at cryogenic temperature followed by aging. The results achieved after the mentioned approach were 11% elongation, 635MPa tensile strength [73]. Zheng et al. [75] applied the cross-rolling process after ARB and reported that

the strength of the material was raised gradually by increasing the number of ARB cycles followed by the cross-rolling process. A maximum UTS was achieved up to 600MPA, while only 1.7% elongation at fracture was attained. Strain hardening capacity was mentioned as the major reason for the loss of acquired ductility after severe cold working. To improve the ductility, aging treatment was performed at 100°C for 20h, and reported results showed the increase of both ductility and UTS which reached about 7% and 635MPa, respectively. During the aging process, nano-precipitates were formed that improved the ability of strain hardening eventually enhanced mechanical properties.

Alvand et al. [76] investigated the effect of the ARB process on the microstructure evolution and mechanical properties of aluminum alloy (Al2024) sheets, the results achieved are demonstrated in Figure 2.18. Hardness, yield, and ultimate tensile strength were consistently raised throughout the ARB process and reached approximately 140HV, 345MPa, and 450MPa, respectively, after 7 cycles.

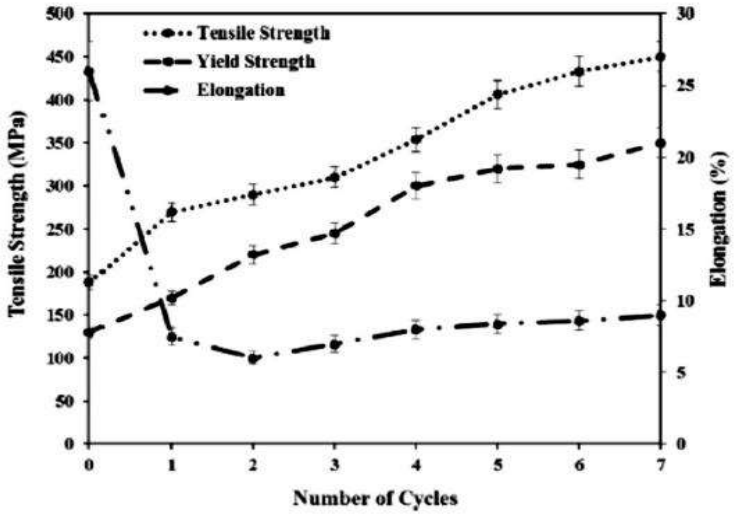



**Figure 2.18** Comparison of different tensile properties according to the increasing number of ARB cycles [76].

### 2.7.2 Steel

The interstitial free (IF) steel is a very different kind of steel that consists of few impurities and low content of alloying elements. Typically, the content of major alloying elements, i.e., carbon and nitrogen, are less than 30 ppm and 40ppm, respectively. Substantial volumes of IF steels have been manufactured during recent years and classified into three varieties that are Nb stabilized, Ti stabilized, and steel containing both Nb and Ti. The function of inducing Nb and Ti is to eliminate the formation of solutes in the final product after processing. IF steels are famous for having high formability (40-45%) and are being used extensively to produce outer body components of automobiles. These steels are accessible in low strength (yield strength < 170MPa) along with high strength (yield strength > 210MPa) grades. IF steel can be produced by both hot and cold rolling with subsequently annealed to attain desirable properties [77,78].

The grain refinement through the ARB process improves the strength of materials without elements addition and this condition of strengthening provides recycling of the parts. Bulk steel strips were fabricated with UFG utilizing ARB methods by Tsuji et al. [54] and improvements in tensile properties during the process are demonstrated in Figure 2.19. It can be stated that the behavior of properties (strength and elongation) is similar to the aluminum alloy mentioned previously.

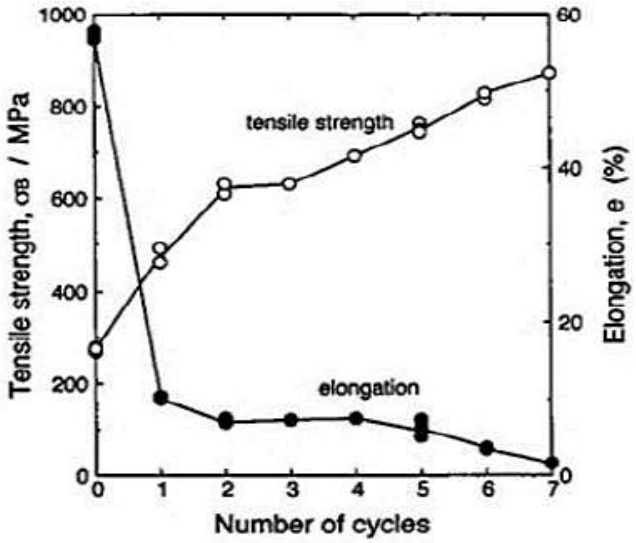



**Figure 2.19** Response of mechanical properties of steel processed by ARB, tested at room temperature [54].

Tamimi et al. [79] employed the ARB process on IF steel sheets to manufacture multi-layered UFG material at 500°C for ten cycles. They verified that increasing the ARB cycles continuously raised the hardness and strength of processed IF steel. These properties were increased more than two and three times, respectively, than starting annealed condition of IF steel as displayed in Figure 2.20. In Figure 2.20 (d), the reduction rate of elongation is significant after the first ARB cycle which becomes minimal for ensuing cycles.

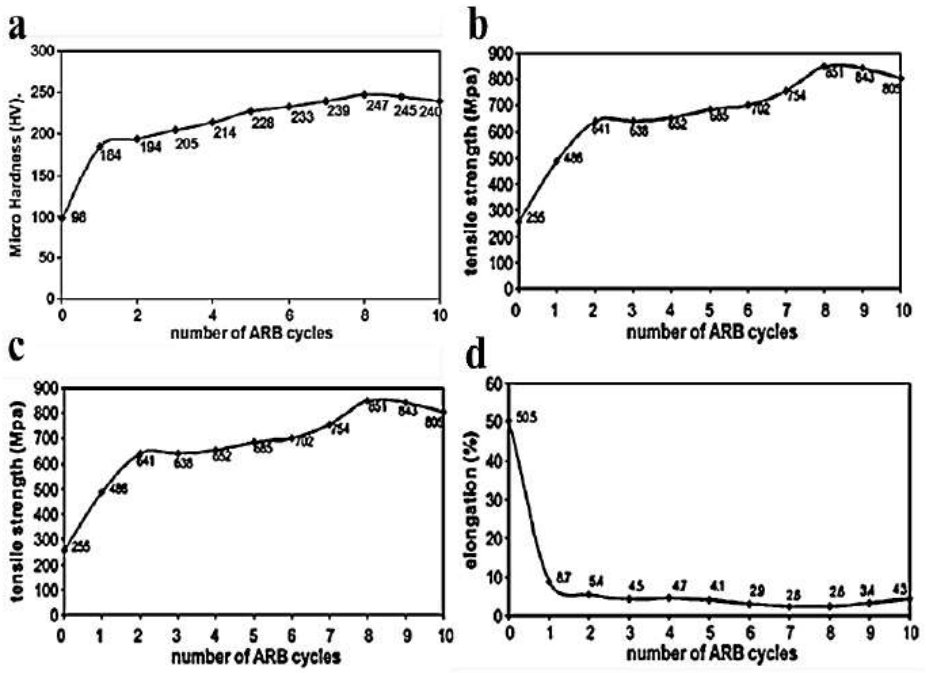



**Figure 2.20** Variation in mechanical properties (a-d) of IF steel by ARB process as a function of cycles [79].

### 2.7.3 Titanium

Titanium and its alloys are known for having excellent corrosion resistance and high specific strength, first applied in orthopaedics and aviation industries. Commercially pure titanium (CP-Ti) and Ti-6Al-4V are two dominant alloys that have been used in the implants for several years. CP-Ti was used in the dental application owing to its oxide layer formation on the surface, consequently high corrosion resistance, and high ductility, while joint replacement components were made of Ti-6Al-4V due to its higher mechanical properties [80].

Milner et al [81] applied severe deformation through the warm ARB process on CP-Ti to achieved UFG structure. They reported that an average grain size of 100nm (Figure 2.21) was attained after 7 ARB cycles along with amplified mechanical strength reached 900MPa. Processed titanium after final ARB cycles was still able to elongate up to 10%, show good workability.

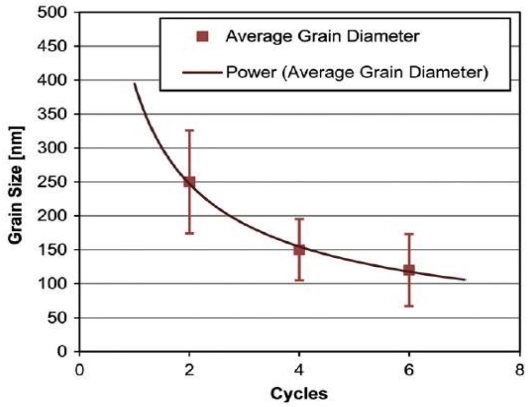



**Figure 2.21** Reduction of average grain size of CP-Ti as a function of ARB cycles [81].

The effect of strain hardening and grain refinement on the mechanical behavior and microstructural evolution was studied after applying the ARB method at room temperature on pure titanium. Results reported in Figure 2.22 explain that the strength of processed material was increased substantially after the first cycle, which continued to rise for later cycles with a moderate rate. The overall strength of ARBed material was increased 2.5 times compared to the initial material along with a similar amount of loss in ductility. Strength was increased due to strain hardening in the early cycles of ARB due to dislocation density and in later cycles, the rise was occurred due to grain refinement in the structure [82].

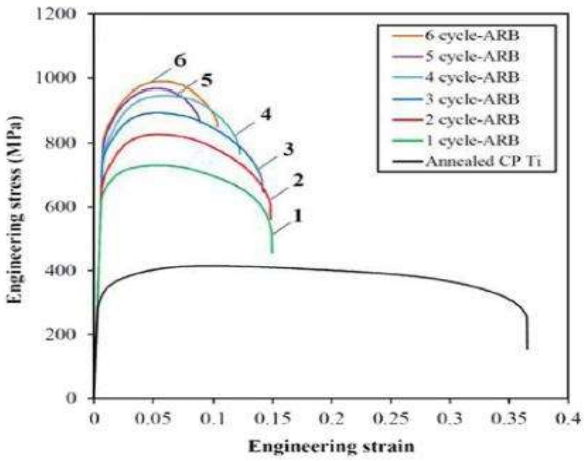



**Figure 2.22** Stress-strain response of pure titanium processed after the ARB method [82].

### 2.7.4 Dissimilar Metals

Layered metal composites (LMCs) are applicable in various applications, but the main drawback of these composites is the high fabrication price which reduced their use in industrial applications. These multi-layered composites have recently been produced by deformation processes for instance “repeating rolling” [83]. Due to low cost in-process and mass production capability as well as superior mechanical properties, the ARB method has removed hindrance in the fabrication of LMCs. These dissimilar LMCs are being widely used in defense, aircraft, and marine industries [84,85]. As displayed in Figure 2.23, a mixture of aluminum and steel is employed to offer strength and corrosion to the bumper of the car according to the requirement [86]. Multiple experiments have been operated to prevent damages to the elements inside the laminated sheet and maximize the advantages. In the previous two decades, magnesium and aluminum are started to be used dominantly in the automotive industry as they are lightweight metals. Beneficially, dissimilar metals combination presents new features, unlike base metals.

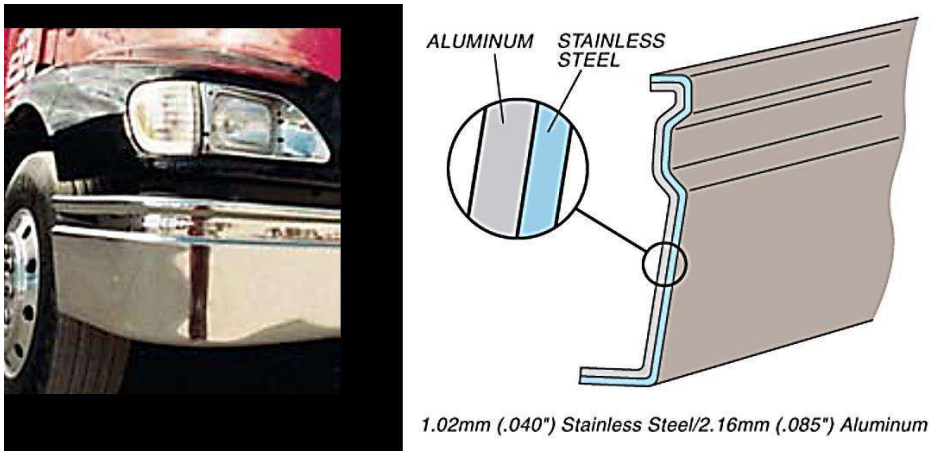



**Figure 2.23** Demonstration of bumpers made by steel clad aluminum composite [86].

The most common method of producing multi-layered materials from dissimilar sheet metals is repetitive rolling. ARB method is quite different than other SPD processes to produce dissimilar materials, as layered composite is achieved after ARB which is usually not attainable in other SPD techniques. There has been active interest in the research areas of manufacturing and processing of advanced materials due to the aforementioned advantage offered by the ARB process.

Similar metals processing remained a focus of the research rather than dissimilar materials since the processing of the former is easy [87]. Insufficient bonding between different metals during processing consequentially affects the strength of processed material. Additionally, plastic instability occurs earlier in a hard layer than the ductile one which initiates necking and fragmentation in the former as the strain increases [84,88]. The reasons are differences in mechanical properties and solubility between elements of two dissimilar metals.

Generally, the ARB provides two kinds of microscopic morphological structures in multilayer metal composites. At first, necking followed by fragmentation of the hard layer is uniformly distributed to produce a reinforcing phase in the ductile matrix after several ARB cycles [90,91]. This breakdown of structure offers load distribution among constituent layers. Secondly, the architecture of the layers is maintained for several cycles even after the occurrence of severe thickness reduction between layers [91,92].

Countless research has been done on similar and dissimilar metals [81,82,86, 89-93]. As this study involves only dissimilar materials, a few examples will be highlighted in this category. Hausöl et al. [94] conducted an ARB study on various grades of aluminum alloy and observed superior properties from the processed materials. Experiments were conducted on combinations of Al6014/Al5754 and Al1050/Al5754, in which Al1050 and Al6014 were acted

as external clad and Al5754 as core material. Results show excellent strength and good ductility as well as high surface quality from both sandwiches in optimum condition.

The laminated composite was fabricated using Al5005 and Al6061 by the ARB process up to 4 cycles. Preheating was employed for 10 min at 200°C to assist the bonding between dissimilar alloys. Reported results showed a similar behavior as the ARB method suggested, hardness and strength were increased two times more than original values. As the ARB cycles increase, the ductility was reduced substantially after the first cycle. Ductility was remained constant after further processing. Additionally, the hardness of the layer AA6061 was relatively higher than AA5005 in the dissimilar composite as seen in Figure 2.24 [69].

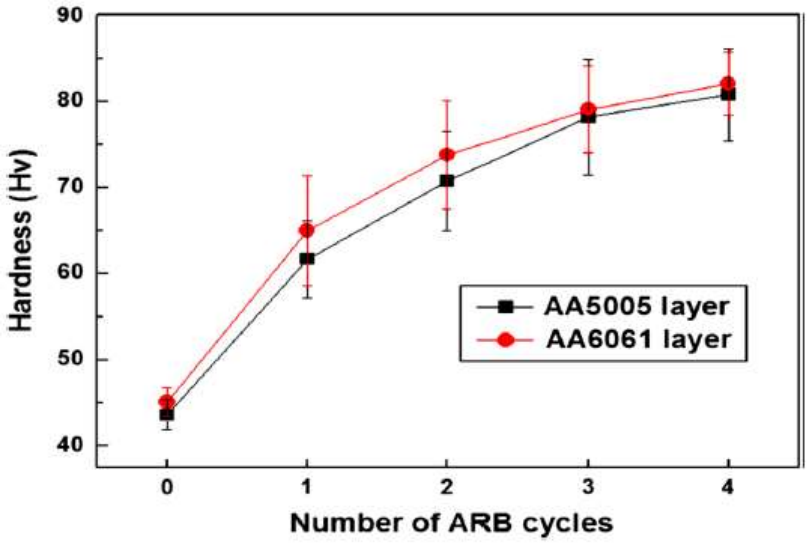



**Figure 2.24** Comparison in the hardness of AA6061 and AA5005 according to ARB cycles [69].

The density of aluminum (2.7g/cm$^3$) and titanium (4400g/cm$^3$) is less than IF steel (7.8g/cm$^3$) that gives the lightweight advantage to aluminum and titanium parts. Alternatively, Young's modulus of IF steel (205MPa) is higher than both aluminum (70MPa) and titanium (110MPa). To compensate and obtain the same structure in the final product, the thickness or content of ductile metal should be more than hard metal. Moreover, the overall cost of

aluminum and titanium is higher than steel that limits their use in many vehicular applications. Thus, the use of the ARB method offers compatibility in many applications as well as reduces cost.

Semiatin et al. [95] observed the formability and bonding ability in aluminum (Al) and stainless steel (SS) in two types of three-layers stacking architecture, i.e., Al-SS-Al and SS-Al-SS, depend on localized necking and diffusion. The arrangement of layers governs localization leading to ultimate fracture. Similarly, the ARB method was performed on aluminum and IF steel sheets, in which initial sheets were rolled at constant thickness with varying preheating temperatures (200$^{o}$C, 250$^{o}$C, 300$^{o}$C, and 400$^{o}$C). Evaluation of results revealed that increasing preheating temperatures raised the activation energy of the atom for bonding, consequently, promotes bonding strength of the composite [96].

### 2.7.5 Roll Bonding of Dissimilar Alloys Using Interlayers

In the case of titanium and steel, researchers found difficulties in bonding directly due to their high melting temperature nature and inferior ability to form a solid solution at room temperature. At elevated temperatures, the formation of brittle intermetallic compounds between them causes embrittlement in joints [97,98]. The problem is solved by introducing one or multiple mutual soluble interlayers between titanium and steel that promote bonding and ultimately provide a strengthened material. Liu et al. [99] introduced brazing-rolling, a new two-stage method, to fabricate titanium clad steel composite utilizing Cu and Ag interlayers to aid reliable bonding between base metals. In this technique, both sandwiches (Ti-Ag-steel and Ti-Cu-steel) were slowly heated (5$^{o}$C/min and 10$^{o}$C/min) up to 750$^{o}$C and 850$^{o}$C to insert a brazing effect. Sandwiches were subsequently rolled at different reduction ratios to provide even stronger bonding. Results displayed in Figure 2.25 show the shear strength of multiple processed composites. Maximum shear strength of about 270MPa was obtained from Ag interlayer composite which gave better results comparatively.

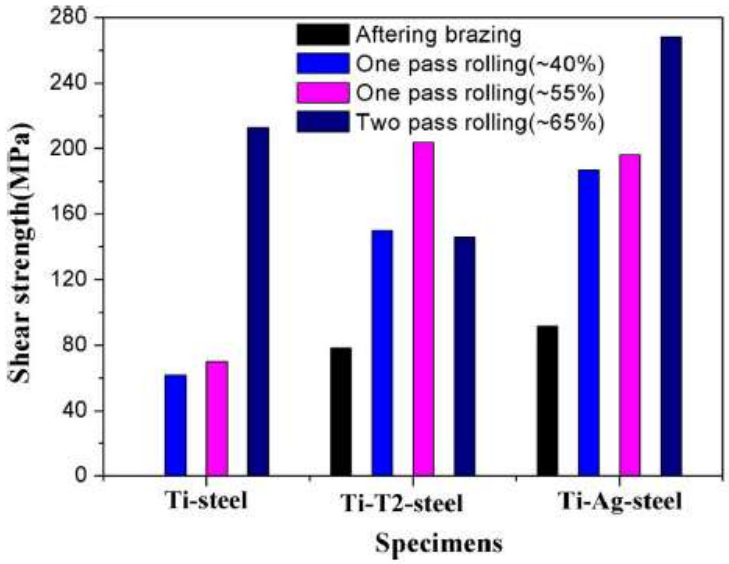



**Figure 2.25** Comparison of shear strength of three different layers' architecture under various rolling reductions after post brazing [99].

Diffusion bonding was applied on the first-time IF steel and titanium (Ti-6Al-4V) alloy to achieve sufficient bonding and consequently effective strength. The coupled specimen was heated up to 900$^{o}$C and 950$^{o}$C under a pressure of 5 MPa and cooled to room temperature in the air to complete the bonding process. Figure 2.26 exhibits the formation of brittle intermetallic compounds at the bonding zone that decreases the shear strength of processed sheets [100].

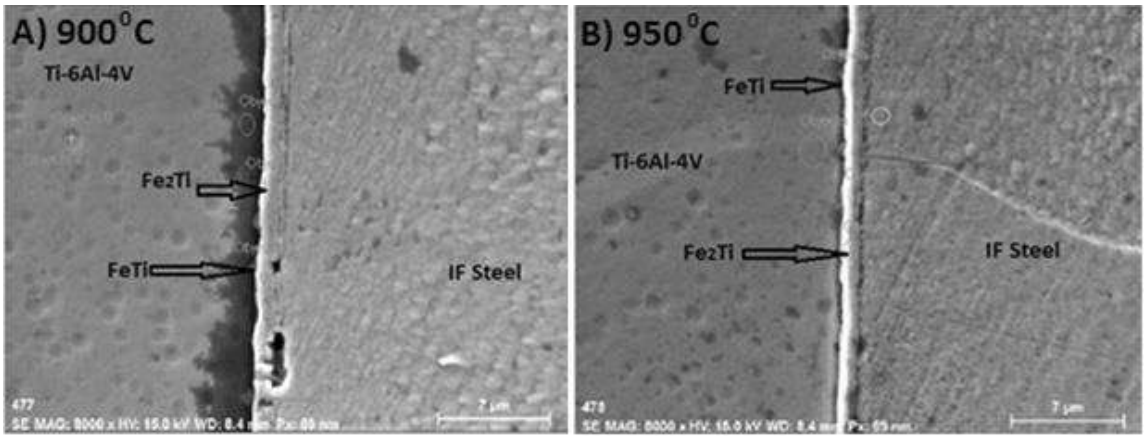



**Figure 2.26** Scanning electron microscope (SEM) image of interfaces at (a) 900ºC and (b) 950ºC [100].

## *2.8 Application of Shear Punch Test in Evaluating Mechanical Behavior*

Evaluation of sheet metal processed by ARB is very important prior to the use in various applications. Shear punch test (SPT) is used to evaluate and estimate the manufactured sheet's formability [101]. The advantage of SPT is that it can provide an evaluation of the small test samples [102]. Shear yield strength (SYS), ultimate shear strength (USS) and shear elongation can be successfully calculated using the SPT method [103].

The test sample is mounted between two dies in this test and a flat cylindrical punch is forced through it. A circular disk is obtained from the deformed area as a result, similar to the punch's diameter. The applied load is recorded as a function of displacement that provides a load-displacement curve (LDC), resulting in shear stress vs displacement. Schematics of the whole setup with an obtained curve are demonstrated in Figure 2.27. Shear stress can be measured from equation 2.10 by recording all parameters under constant displacement rate [104,105]. Shear punch testing is useful in characterizing the heat-affected zone of welded materials [106, 107], biomaterials [104], and composites [108,109].

$$\tau = \frac{\mathrm{p}}{\pi d_{(\mathrm{avg})}\,\mathrm{t}} \tag{2.10}$$

where P, $d_{(avg)}$, and t are applied load, the average diameter of die and punch, and sample thickness, respectively.

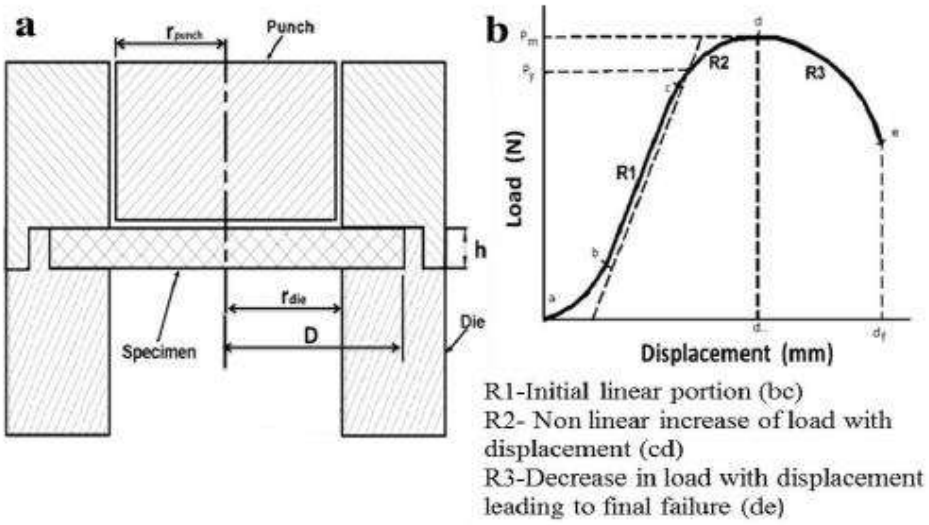



**Figure 2.27** (a) Illustration of the SPT setup, (b) common LDC curve [104,105].

The small punch test is similar to the shear punch test but differs with respect to the shape of the punch and fracture of the specimen. Punch shapes in the form of flat and hemispherical are used in shear punch and small punch test, respectively. Moreover, the shear punch test results in a shear cut, while the small punch test produces a bulge in the disk. The small punch test is mostly used to observe the degradation and wear mechanism of material through fatigue life where cyclic loading is applied [110]. The shear punch test is used in this study because it provides the shear strength of the material that can be correlated with tensile strength [111].

# 3. EXPERIMENTAL METHODS

## *3.1 Materials*

Various materials were utilized in the present study that includes interstitial free (IF) steel, Al2024 aluminum alloy, and commercially pure grade 2 titanium (Ti). This work is divided into two different categories, i.e., multiple-layer clad materials, dissimilar materials. For the first category, a titanium-IF steel laminated metal composite was investigated while a combination of Al2024-IF steel metal composite was studied in the second category. Titanium and IF steel were used in as-received condition whereas Aluminum 2024 was utilized after performing full annealing on it, known as O temper condition. All sheets were cut in different dimensions depending upon the capacity of the rolling mill and the behavior of diverse materials. The initial thickness of titanium was 0.55mm, while Al2024 and IF steel were employed in two sizes (1mm and 0.25mm) and (1mm and 0.5mm), respectively, depending on different categories of this work. Fully annealed Al2024 (0.25mm) acted as an interlayer between 0.55mm titanium and 1mm IF steel to produce titanium-IF steel composite, while Al2024 (1mm) and IF steel (0.55mm) sheets were utilized in aluminum-IF steel composite. The IF steel was used in different thicknesses in two categories to make a compatible composite with corresponding metals. The chemical compositions of Al2024, IF steel, and titanium are reported in Table 3.1, Table 3.2, 3.3, and 3.4, respectively.

**Table 3.1** The elemental composition of aluminum alloy.

| **Metal** | **Chemical Composition (%)** | | | | | | | | |
|---|---|---|---|---|---|---|---|---|---|
| | Si | Cu | Mn | Mg | Zn | Cr | Ti | Fe | Al |
| **Al2024** | 0.08 | 4.48 | 0.54 | 1.49 | 0.04 | 0.01 | 0.036 | 0.12 | Bal |

**Table 3.2** The elemental composition of IF steel (0.5mm).

| Metal | Chemical Composition (%) | | | | | | | | | |
|---|---|---|---|---|---|---|---|---|---|---|
| | C | P | Cr | Mn | Mo | Ni | Cu | Ti | Al | Fe |
| **IF steel** | 0.0015 | 0.008 | 0.025 | 0.128 | 0.003 | 0.014 | 0.03 | 0.069 | 0.025 | Bal |

**Table 3.3** The elemental composition of IF steel (1mm).

| Metal | Chemical Composition (%) | | | | | | | | | |
|---|---|---|---|---|---|---|---|---|---|---|
| | C | P | Cr | Mn | Mo | Ni | Cu | Ti | Al | Fe |
| **IF steel** | 0.0013 | 0.0114 | 0.029 | 0.1167 | 0.003 | 0.016 | 0.03 | 0.0745 | 0.032 | Bal |

**Table 3.4** The elemental composition of commercially pure grade 2 titanium.

| Metal | Chemical Composition (%) | | | | | |
|---|---|---|---|---|---|---|
| | C | H | N | O | Fe | Ti |
| **Titanium** | 0.1 | 0.015 | 0.03 | 0.25 | 0.3 | Bal |

## *3.2 Processing of Accumulative Roll Bonding*

The ARB process is a successive rolling process that consists of four repetitive steps such as surface preparation of layers, layers assembling, rolling, and cutting [112]. These steps continue till the desired properties and microstructure is obtained. Figure 3.1 demonstrates the whole process to carry out a successful rolling bonding of Ti-IF steel composite. The process started with surface preparation in which sheets were firstly de-greased by acetone until their surface was completely clean, followed by wire brushing using circular steel brush rotating at a speed of about 3600 rpm to make the surface rough that aids in the bonding of layers [2].

Sheets were stacked in the desired order and fixed from the edges with steel wire to prevent slipping when the stacked sandwich is passed through the rolls. After surface preparation, the stacked sheets should pass through the roll within 180 seconds to provide sufficient bonding and prevent the formation of oxides between layers. However, several studies suggested that preheating of sheets should be beneficial in providing successful bonding depending upon the metals used [99,113]. Therefore, the stacked sample of Ti-Al2024-IF steel was preheated in two ways at 480°C/10min and 400°C/10min before each rolling cycle. The third step was rolling in which preheated samples were passed instantly through the rolls, applying a 50% reduction in thickness in two passes which is equal to 0.8 von Mises strain [113]. Finally, the rolled sheet was cut in half and the whole process was repeated for two more cycles. Previously, ARB of commercially pure titanium and IF steel was performed between the temperature range of 400-550°C [79, 81]. The processing temperatures, i.e., 400°C and 480°C, were chosen based upon literature studies.

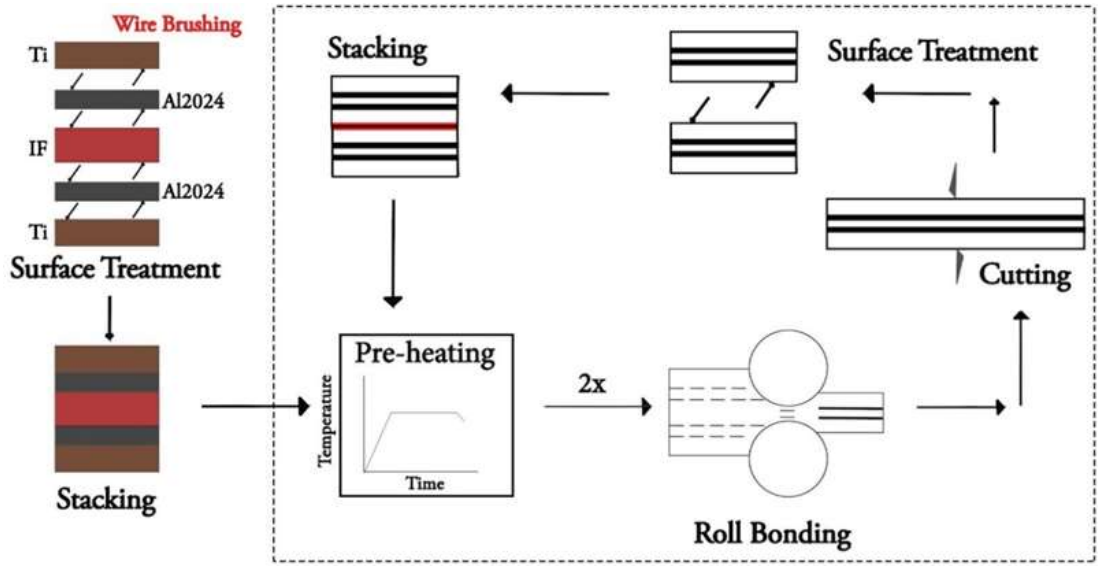



**Figure 3.1** Illustration of cyclic ARB process without the inclusion of additional Al2024 interlayer after the 1st cycle, here Al2024 is only used during the first cycle.

To find out the effect of interlayer and comparison in properties, an additional Al2024 interlayer was inserted after every rolling cycle as illustrated in Figure 3.2, and similarly, roll bonded at 480°C/10min and 400°C/10min for three cycles. This is to observe the effect of bonding on the microstructural and mechanical behavior of processed composite.

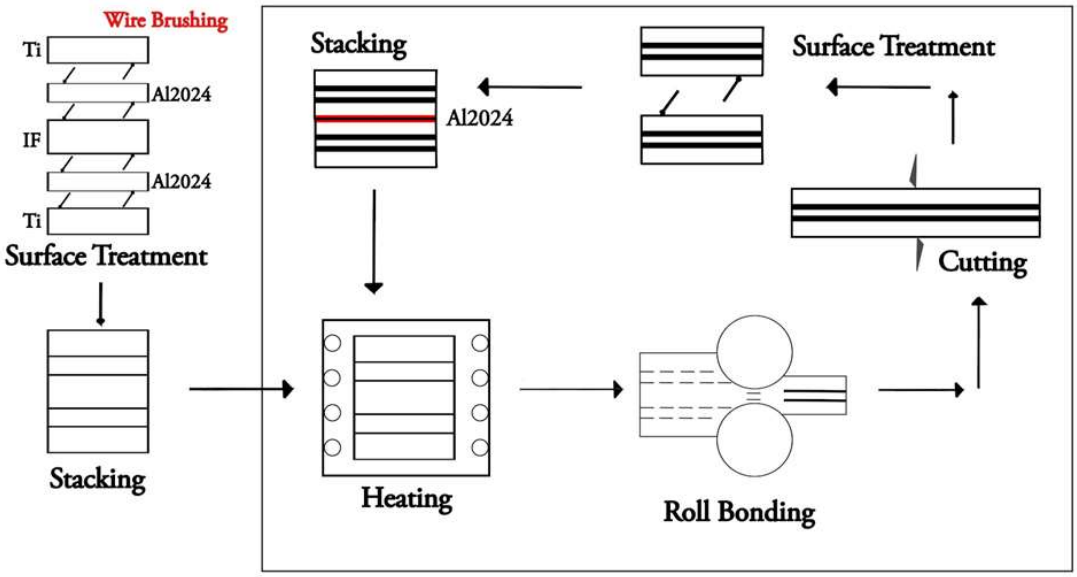



**Figure 3.2** Schematics of cyclic ARB process with the inclusion of additional Al2024 interlayer after the 1st cycle.

The ARB processing related to Al2024-IF steel (Figure 3.3) was only different with respect to preheating time and temperature which was 410°C/5min. Similarly, to the previous case, a 50% reduction in thickness was attained in one pass and the whole process was repeated for 3 cycles which induced a total von Mises strain of 2.4 on the sheets. The initial thickness of aluminum and IF steel sheets were 1mm and 0.5mm, respectively. Rolling cycles were performed on a rolling mill displayed in Figure 3.4 with rolls diameter and rolling speed of 150mm and 10 rpm, respectively.

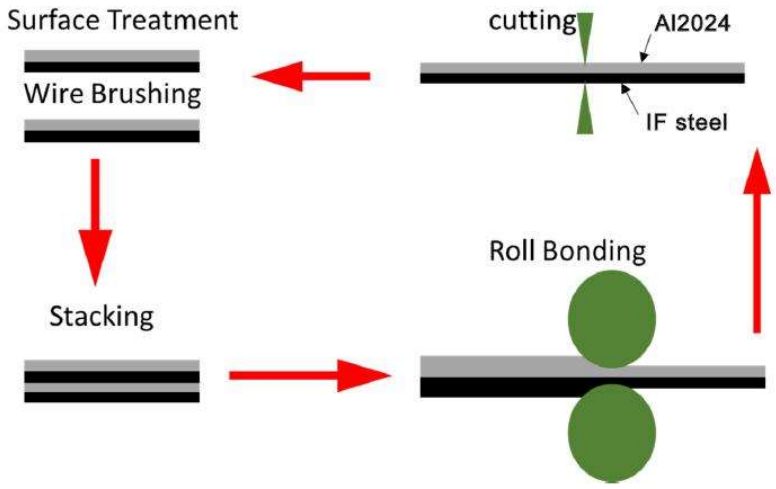



**Figure 3.3** The principal working of Al2024-IF steel composite by the ARB process [112].



**Figure 3.4** Rolling mill used in the experimental procedure.

## *3.3 Post-ARB Heat Treatment*

Post heat treatment is usually done to provide recovery in ductility and impart precipitation hardening in specific rolled layers [65]. A short post-annealing (PA) was performed on three cycles ARB processed composite of Ti-IF steel at 300°C, 400°C, and 500°C for 10min followed by water quenching at room temperature.

In the case of Al2024-IF steel composite, a lengthy PA was conducted on three cycles ARBed composite where samples were heat-treated for 30min at 420°C subsequently quenched in a water bath. These samples were followed by artificial aging (AA) at 150°C for 30min, 1hr, 2hr, 4hr, 12hr, and 24hr to observe the effect of duration on the formation and distribution of precipitates in the aluminum layers as well as improving the performance of the final composite [114,115].

## *3.4 Microstructural Characterizations*

It is very important to observe the material's structure to understand its behavior. The structure consists of atomic arrangements and microscopic abnormalities on the grain level. The following steps were utilized to evaluate the structure of materials.

Metallography samples were cut in 10x10mm$^2$ dimensions in rolling (RD) and transverse direction (TD). Samples were cut from the center of the processed sheets to avoid the edge crack. These samples were mounted with epoxy resin that helped in holding during processing and testing. Mounted composites were grounded and mechanically polished before etching.

Microstructural properties in a broader way were observed through optical microscopy. Therefore, polished samples were chemically etched by immersion in different reagents. Marshal's and Kroll's reagents were utilized to differentiate between IF steel layers and

titanium layers, respectively [79,116]. The optical light microscope was used to obtain microstructure from cross-sections as well as surfaces of individual layers.

Deep structural morphology of processed layers was conducted on a scanning electron microscope. The fracture surface mechanism was aimed to be observed using a JEOL scanning electron microscope (SEM) functioning at 15kv accelerating voltage. Only titanium-steel composites were experimented on SEM to find their fracture mode and layers' delamination.

## *3.5 Mechanical Behavior Evaluation*

All samples (as received and post-ARB) were cut from cross-section followed by grinding and polishing to measure microhardness effectively. Individual layers' hardness after every cycle was measured from the surface of the specimens using Vickers microhardness tester under the loading condition of 0.5kgf for 10s. Hardness was conducted from five different points and the mean hardness was calculated. The same procedure was applied in through-thickness hardness measurements in which the thickness of the specimen was divided into ten equally spaced points. For example, Ti/IF steel composite had 1350μm thickness, so load was applied after every 135μm distance of the whole thickness, and the average of the measurements provided the hardness of the composite.

Mechanical characteristics of the material are very important for evaluating the material's ability to be used in applications. Tensile testing can be used to calculate strength properties from stress-strain curves. Tensile specimens were cut in dog bone shape with 15mm gauge length by electro-discharge machine (EDM) following standard ASTM E646-98, along the rolling direction. All samples (Pre-ARB, Post-ARB, and post-annealed-ARB) were tested at ambient temperature under a constant strain rate of 0.001 $s^{-1}$.

Shear punch testing (SPT) was conducted to observe the effect of the ARB method on the shear properties of composites, eventually provide evidence of bonding strength. The SPT

setup includes a die, specimen holder, and cylindrical punch (flathead) as indicated in Fig. 3.7. The diameter of the punch and die's opening was 3mm and 3.10mm, respectively whereas the length of the punch was 10mm. Disc-shaped miniature specimens, with a diameter of 6.5mm were extracted from ARBed composite using EDM. These compression tests were performed at ambient temperature at a crosshead speed of 0.35mm/min, resulting in load-displacement curves (LDC). All tests were conducted three times on the Intron testing machine likewise to tensile tests and average values were reported.

# 4. EVALUATION OF THE TITANIUM-STEEL COMPOSITE

## *4.1 Overview*

In the present chapter, characteristics of resultant titanium-steel composites via the ARB method were analyzed using microscopic examination, microhardness, uniaxial tensile, and shear punch test. All the examinations were not conducted on every case but for appropriate cases. Tensile testing was made basic criteria for all cases upon which other tests were carried out.

## *4.2 Microstructure*

In materials engineering, evaluation of microstructure is the first thing conducted in order to understand the behavior of newly processed material as it influences the response of the material. So, it is wise to perform a thorough analysis of the microstructure to understand the behavior of the material processed.

### 4.2.1 ARBed Ti-IF Steel Composite

Variation in layer thickness and grain refinement with the increasing number of ARB cycles was examined for all the samples processed at 400°C rolling temperature. All the samples were observed from a longitudinal cross-section and surface of the individual layers under a light optical microscope, displayed in Figure 4.1 and Figure 4.2. Individual layers became thinner and transformed into non-uniform layers from straight edges as the number of ARB cycles increases. This shows the beginning of the necking process and subsequent sturdy bonding between layers. The presence of voids or unbonded regions was almost impossible to observe as the ARB cycles increased. Due to the existence of dissimilar constituent layers, the deformation of layers was non-homogenous from the surface to the center of the rolled sheets as the rolling progressed. Outer layers showed additional shear strain typically referred to as

redundant shear strain as the ARB cycles raised [61]. Reasons are friction between sample and rolls along with variation in deformation mode across dissimilar layers.

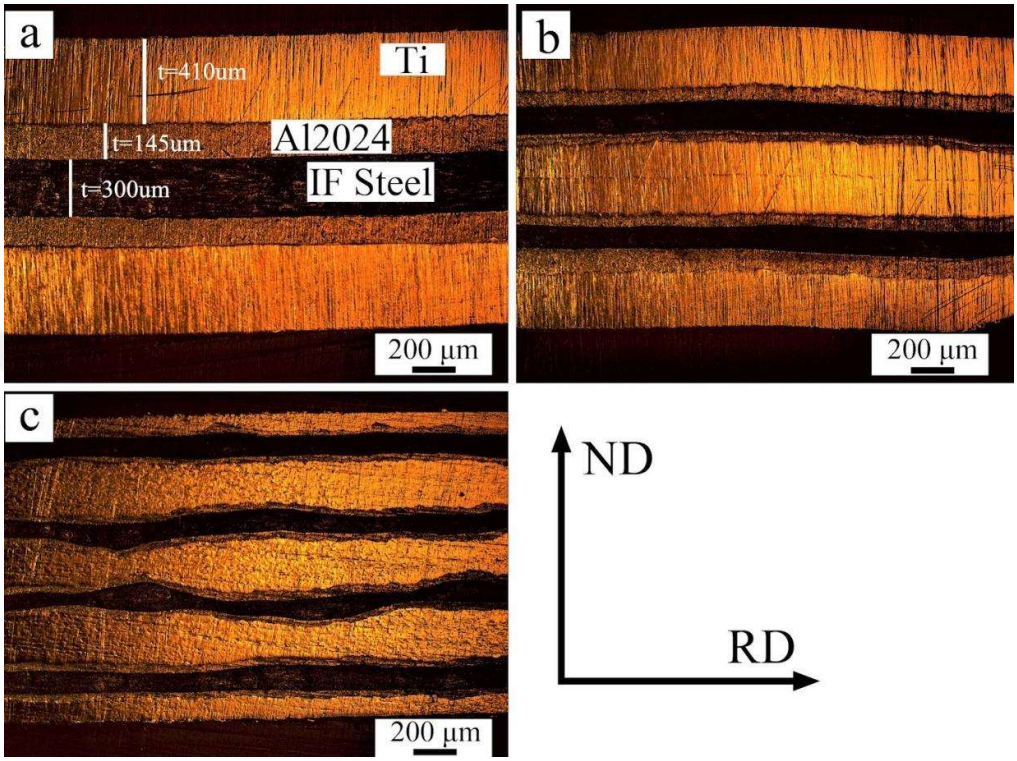



**Figure 4.1** Formation of Ti-IF steel composite rolled at 400°C through three cycles (1-3).

A better bonding was achieved, and a more uniform layered structure was attained after the final cycle. This explains that more strain can be withstood by the material until crack initiation occurs in this case.

Figure 4.2(a-d) represents the grain refinement of primary constituents of the composite as the number of ARB cycles increases. The average grain size of IF steel and titanium were measured as 28µm and 18µm, respectively, before the ARB process. Both metals exhibited lamellar structures, with IF steel having a high aspect ratio of grains after three ARB cycles. Two types of boundaries can be understood from the grain structures which are lamellar boundaries (LB) and interconnecting boundaries (ICB). The linkage of two LBs with ICB formed the whole structure along the rolling direction (RD) which is prominent in titanium

after 3 cycles than IF steel. Lamellar boundaries were dominant in IF steel due to higher deformation rate as well as low content of impurities.

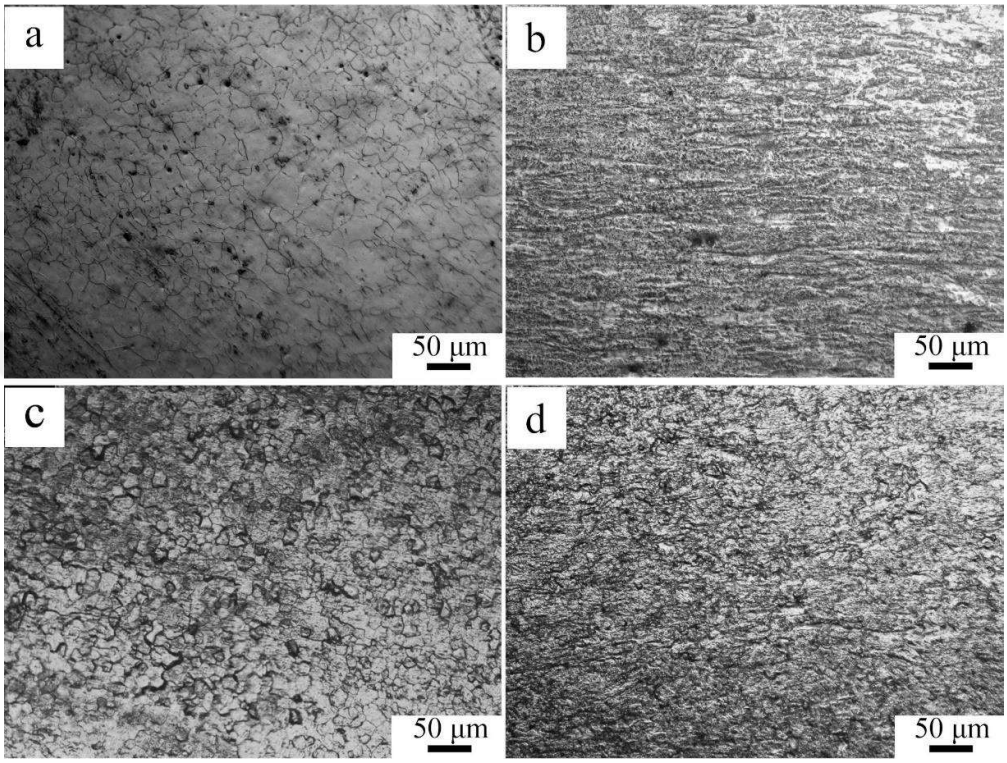



**Figure 4.2** Grain refinement of (a) as received IF steel, (b) ARBed IF steel after 3 cycles, (c) as received titanium, and (d) ARBed titanium after 3 cycles.

After the completion of the ARB process, an average grain size of 5µm was obtained in both materials but larger refinement was occurred in IF steel as compared to titanium. Reasons could be the lower dislocation density and low content of impurities in the IF steel component. Also, the strain hardening rate is comparably higher in the case of IF steel which explains higher grain refinement behavior. Finally, the formation of several shear bands after three cycles confirms the interlocking of layers [117].

*4.2.1.1 Fracture Morphology*

The fracture morphology of Ti-IF steel composite rolled at 400°C was carried out under a scanning electron microscope from the surface of the tensile sample tested at a strain rate of $0.001s^{-1}$. The bonding quality and failure mechanism of the processed composite can be understood from the SEM micrographs. Figure 4.3 indicates the effect of deformation on the failure surfaces of the composite after several ARB cycles. As the purpose of fracture morphology is to understand the bonding strength of the interface region so, there are three interface regions which are Al2024/IF, Al2024/Ti, and Ti/Ti, and the amount of delamination of these explains the strength of interfacial bonding between these layers. Deep delamination was apparent at the Al2024/IF region whereas the other two interface regions showed adequate bonding after two ARB cycles as can be seen in Figure 4.3(a). The delamination in the third cycle became shallow and indistinct compared to the former two cycles' fracture interfaces. Normally, further strain induction by the addition of the ARB cycles increases interfacial bonding of the prior cycle due to interdiffusion of the elements [76,118].

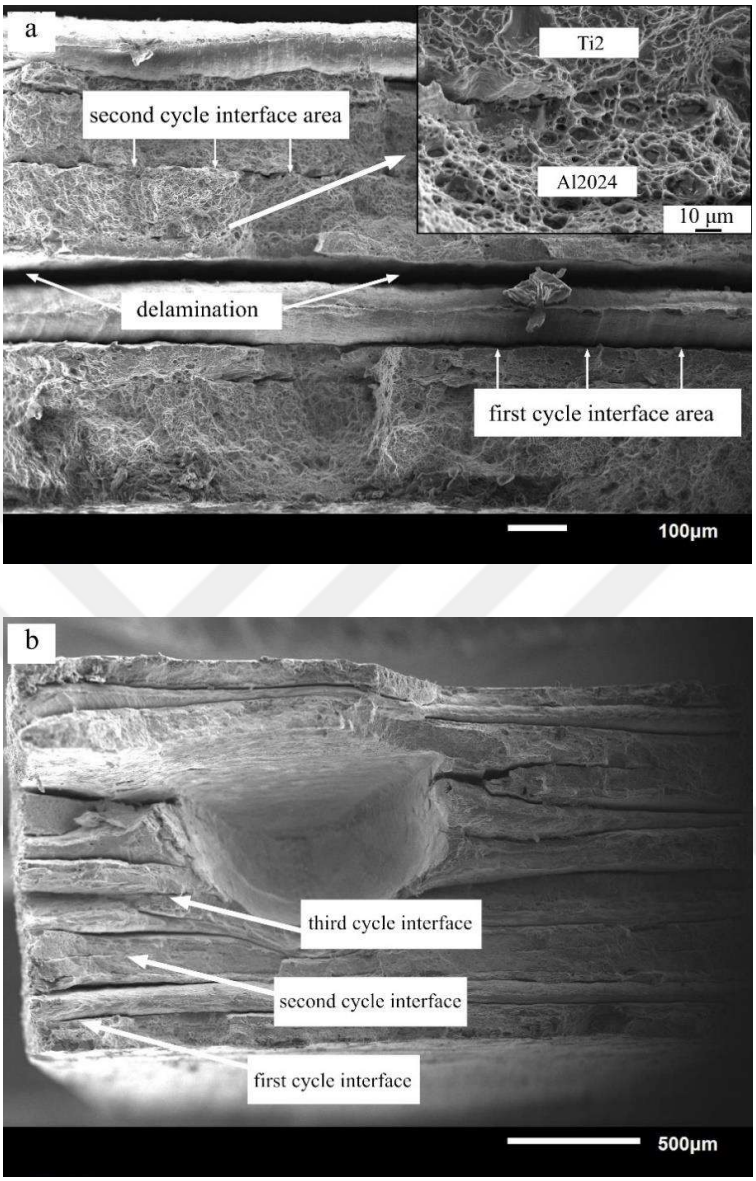



**Figure 4.3** SEM micrographs from fracture surfaces of Ti-IF steel composite rolled at 400°C after (a) two cycles and (b) three cycles.

High rolling pressure mechanically inter-diffuses atomic elements of both metals. As displayed in Figure 4.3(b), the interface regions established after the first two cycles turned into indistinguishable interfaces after the 3$^{rd}$ cycle which is also mentioned in previous studies of the ARB process [76,112]. Still, the Al2024/IF interface area was slightly delaminated even after the strain accumulation of three cycles due to its weakest linkage among the other bonded

areas. It is safe to say that the cracking of layers started from the Al2024/IF bonded region in each cycle upon fracture.

The failure mechanism of individual constituents of Ti-IF composite can be understood from the investigation of fracture surfaces at high magnification levels in Figure 4.4. It exhibits the modes of fracture in pre-ARB and post-ARB titanium and IF steel constituents. A common ductile fracture was observed from primary titanium and IF steel metals in Figures 4.4(a) and (d), respectively, as deep dimples were exhibited from the fracture surfaces with equiaxed and hemispheroidal shape [116,119,120]. Typically, the appearance of a grey fibrous form of dimples on the surface gives the idea of ductile fracture, and the reduction or disappearance of these shear zone indicates a slight brittle fracture. Due to the application of moderate strain after the first cycle, a similar ductile fracture was detected from the fracture surface. Compared to titanium fracture, shear zones on the IF steel surface began to disappear after the 1$^{st}$ ARB cycle as demonstrated in Figures 4.4(b) and (e). The deformation rate in IF steel metal (56%) was approximately double compared to titanium metal (29%) after one cycle.

Generally, the nucleation of the micro-voids occurs close to the interface region, and the growth of these voids by coalescence to each other leads to rupture. This fracture arises due to the presence of brittle IMCs at the interface area [120]. Figures 4.4(c) and (f) indicate the beginning of brittle rupture in the composite as deep dimples changed into shallow and elongated ones classified as shear dimples after the third ARB cycle. Work hardening enhanced grain refinement which causes the reduction in the dimple size.

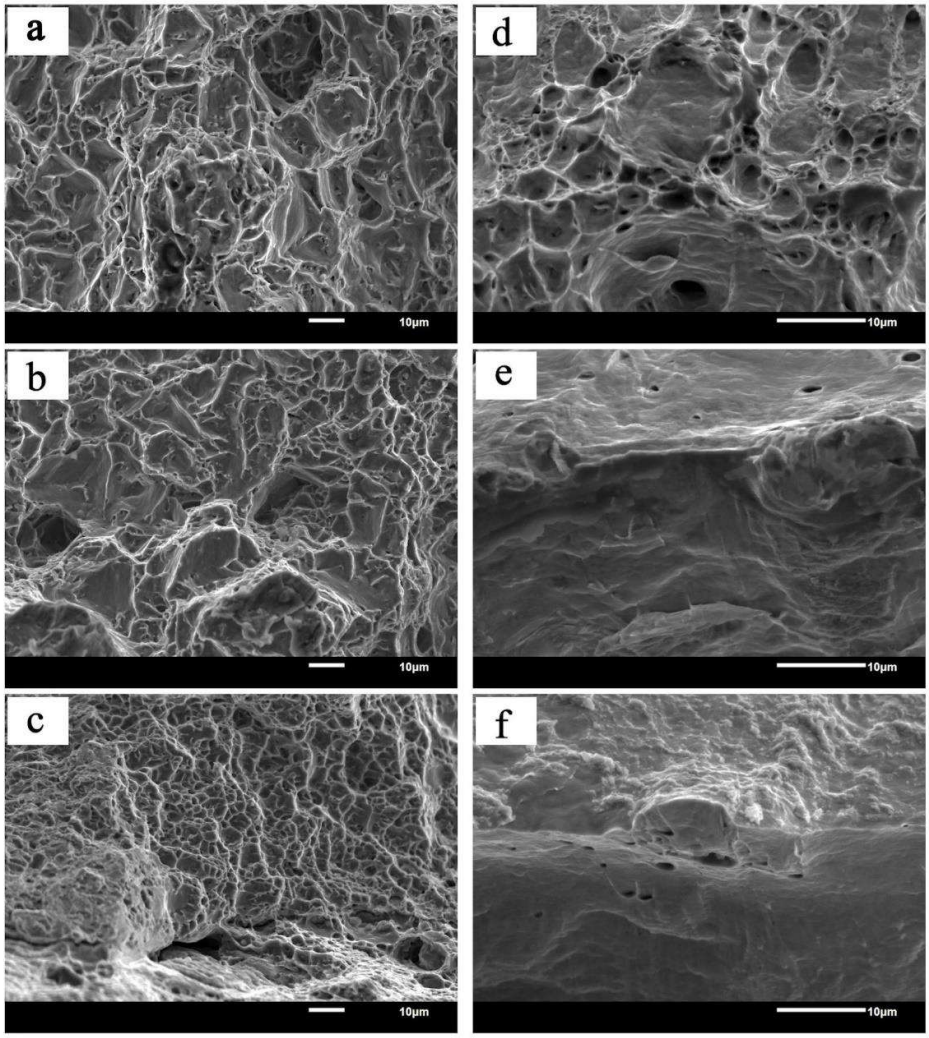



**Figure 4.4** SEM micrographs from fracture surfaces of; (a) titanium, (b) titanium after the first cycle (ε = 0.8), (c) titanium after the third cycle (ε = 2.4), (d) IF steel, (e) IF steel after the first cycle(ε = 0.8), and (f) IF steel after the third cycle (ε = 2.4).

### 4.2.1 ARBed Ti-Al2024-IF Steel Composite

Microstructural observation in Figure 4.5 was obtained from a longitudinal cross-section of the composites rolled at 480°C temperature along the rolling direction. An additional Al2024 interlayer was added after each cycle to improve the bonding between layers at a relatively higher temperature. A continuous decrease in layer thickness from cycle 1 to cycle 3 shows the formation of sufficient bonding between layers and consequentially high strength in

the composite. The presence of a void at the interfaces between layers indicates the brittle behavior and crack initiation sites in the structure. Generally, these unbonded voids occur in the first cycle and disappear with subsequent rolling but in this case, they occurred in every cycle due to the incompatible nature of different metals at high rolling temperatures. After the first cycles, straight edges of layers are apparent which transforms into a non-uniform thickness in ensuing cycles, the implication of the necking process [121,122].

Additional Al2024 interlayer can be seen at the middle of $2^{nd}$ and $3^{rd}$ cycle ARB processed composites which increased the overall bonding strength of the composite. Thickness reduction of individual layers with the increasing number of ARB cycles can be noticed in the micrographs. Thickness reduction was maximum in IF steel after the first cycle which is 56%. Aluminum and titanium layers showed thickness reduction of 36% and 29%, respectively. A sufficient bonding was achieved but the layered structure was comparatively non-uniform after the last cycle as can be seen in Figure 4.5. This explains that it is unwise to apply another rolling cycle due to the brittle behavior of the composite. More strain may lead to catastrophic failure of the material.

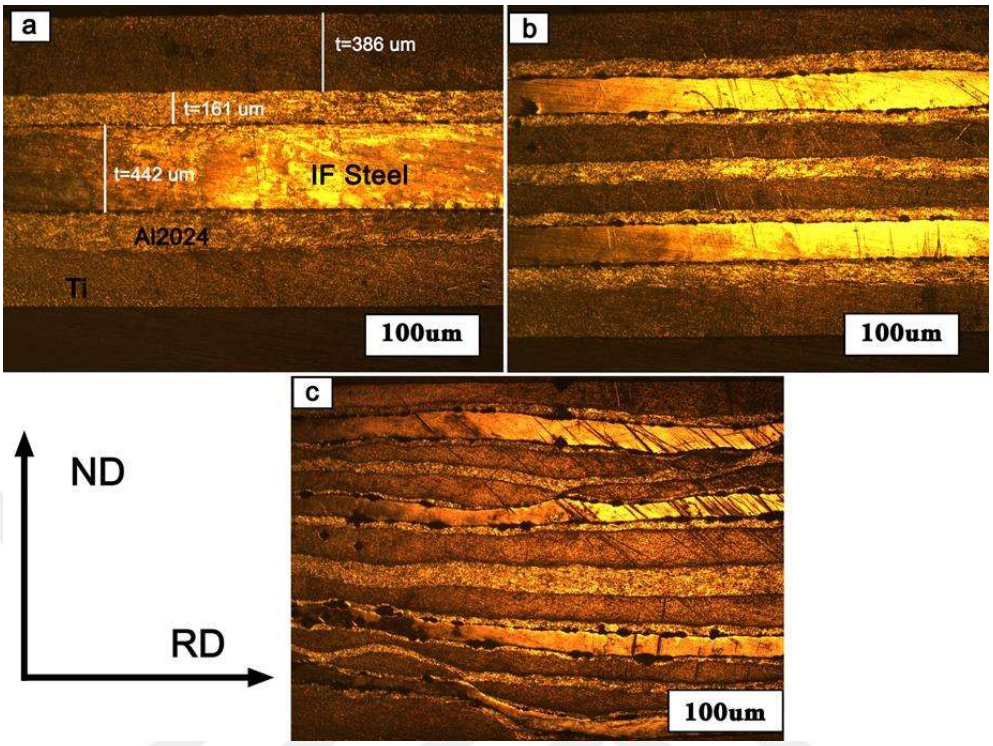



**Figure 4.5** Formation of aluminum interlayered Ti-Al2024-IF steel composite rolled at 480°C through three cycles (1-3).

As explained previously that the ARB process is very simple and appropriate in manufacturing multi-metal composite, difficulties can still appear during processing. Variation in roughness during the wire brushing and improper brushing on different layers can affect the reliability of the composites. Due to this, residual oxides and contaminants can remain on the surface of the layers which encourages the formation of brittle intermetallic compounds between reactive metal combinations such as titanium and steel. Also, simple heating conditions and high rolling temperatures influence the making of brittle intermetallic compounds as compared to controlled vacuum conditions and lower rolling temperatures.

*4.2.1.1 Fracture Morphology*

Fracture morphology, as mentioned before, was carried out under SEM to analyze the fracture behavior and interface strength of the aluminum interlayered Ti-IF steel composite rolled at 480°C. Delamination was too much in the case of the Al2024/IF steel interface region,

whereas Ti/Al2024 interface was remained in contact after the first cycle, as displayed in Figure 4.6(a). Also, the failure mode of the IF steel sheet in comparison to the other two sheets was brittle as deep dimples were observed in both Al2024 and titanium sheets which was not the case in IF steel. Figure 4.6(b) demonstrates the failure of the processed composite after three cycles and a better bonding can be observed in all the interfaces, which is normal as the number of cycles and rolling pressure increases. There is still some shallow delamination close to IF steel layers from where the crack initiated and propagated which led to the rupture of layers. Elongated and shallow dimples on the fracture surfaces of titanium and aluminum sheets indicate the conversion of ductile to brittle fracture. An overall better bonding of layers after three ARB cycles can be seen in Figure 4.6(b) as compared to Figure 4.3(b) where the additional Al2024 interlayer did not introduce after the first cycle, but the fracture of the final composite was more brittle in this case.

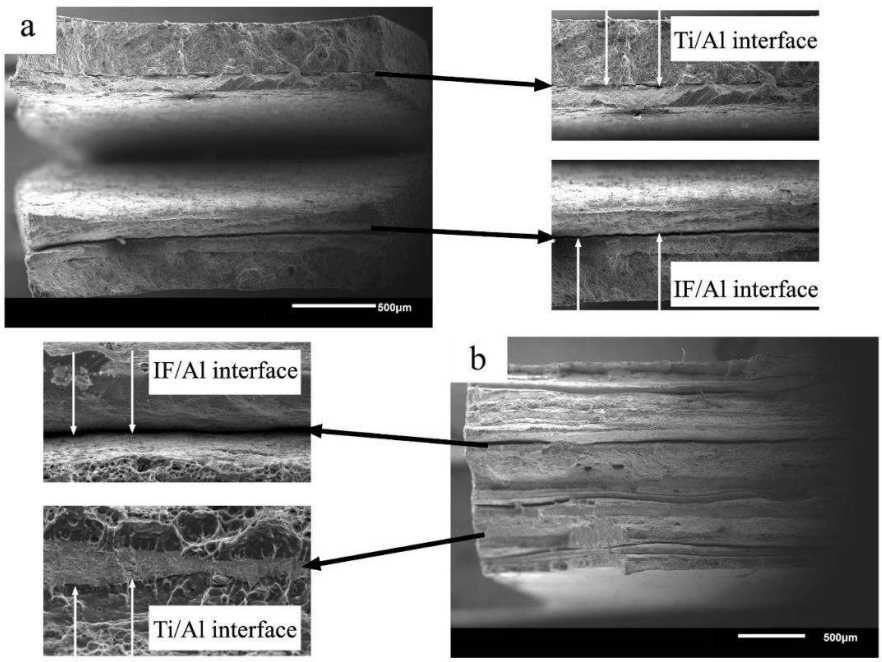



**Figure 4.6** SEM micrographs from fracture surfaces of multi-metal (Ti-Al2024-IF steel) composite after (a) one cycle and (b) three cycles.

## *4.3 Mechanical Response*

Modifications in microstructure, discussed in the previous segment, correspond well with the mechanical behavior of the sheet metal composites under severe plastic deformation. Hall-Patch equation represents the crucial relationship between the structure and properties. It describes that the increase in hardness and strength of the material is attributable to the refinement of grains. This was well proved by the outcomes of microhardness and tensile tests after the ARB method.

### 4.3.1 Ti-IF Steel Composite Rolled at 480°C

In the first case of titanium and IF steel, a three-cycle Ti-IF steel composite was fabricated at a rolling temperature of 480°C without the inclusion of an aluminum interlayer after the first cycle. The resultant composite was uniaxially tested under tension to observe the response, results are indicated in Figure 4.7. True stress-strain curves of base metals and three-cycle ARB composite show that the decrease of substantial ductility without increasing much strength after the ARB process. Also, fracture of the final composite indicates the bad bonding quality between different interfaces as layers ruptured in step mode with the increase of strain value. This approach is not appropriate in obtaining a sound composite that can be used in structural applications. Due to this, other tests were not carried out on this case.

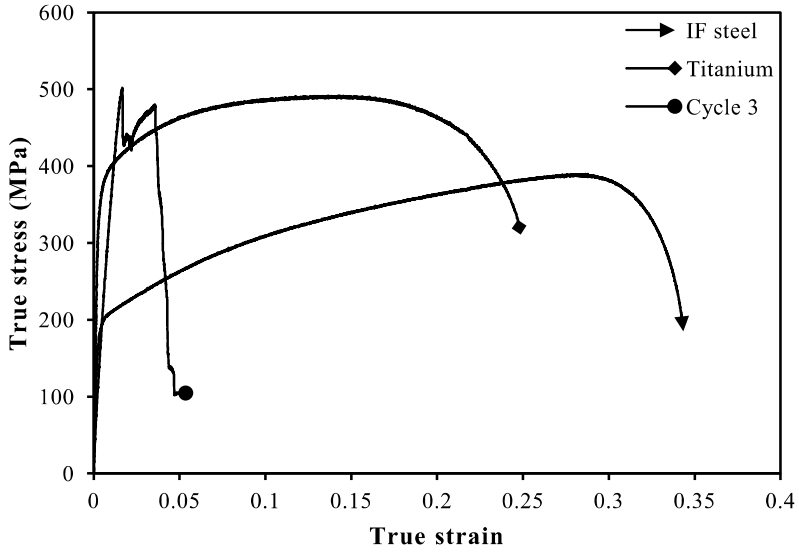



**Figure 4.7** True stress-strain curves of base metals and Ti-IF steel ARB composite rolled at 480°C.

### 4.3.2 Ti-Al2024-IF Steel Composite Rolled at 480°C

The second case includes the manufacturing of titanium and IF steel composite with the introduction of an aluminum interlayer after every cycle, rolled at 480°C temperature. To observe the variation in the composite after rolling, each cycle composite was tested, and the results are mentioned in this section. The average Vickers microhardness of Ti-Al2024-IF steel ARBed composite as a function of the numbers of cycles and thickness is displayed in Figure 4.8. Microhardness values of constituent metals (before and after the ARB) are represented in Figure 4.8(a), along the rolling direction after each cycle. A significant rise is recorded in hardness for all the constituents after the first cycle which is understandable. The upcoming cycles also enhanced the hardness but to a lesser extent [110]. In the initial cycle, the rise is approximately two-fold as compared to the initial values for IF steel and Al2024 sheets, but titanium indicates a steady increase [82, 112, 123]. Strain hardening rate and increase in dislocation density caused this behavior in the former components than the latter [82]. A similar

steady increase in the hardness can be observed in each sheet due to the change in the hardening mechanism from strain hardening to grain refinement in the remaining cycles [79]. Generally, the saturation would be achieved at a high strain as the number of cycles increases.

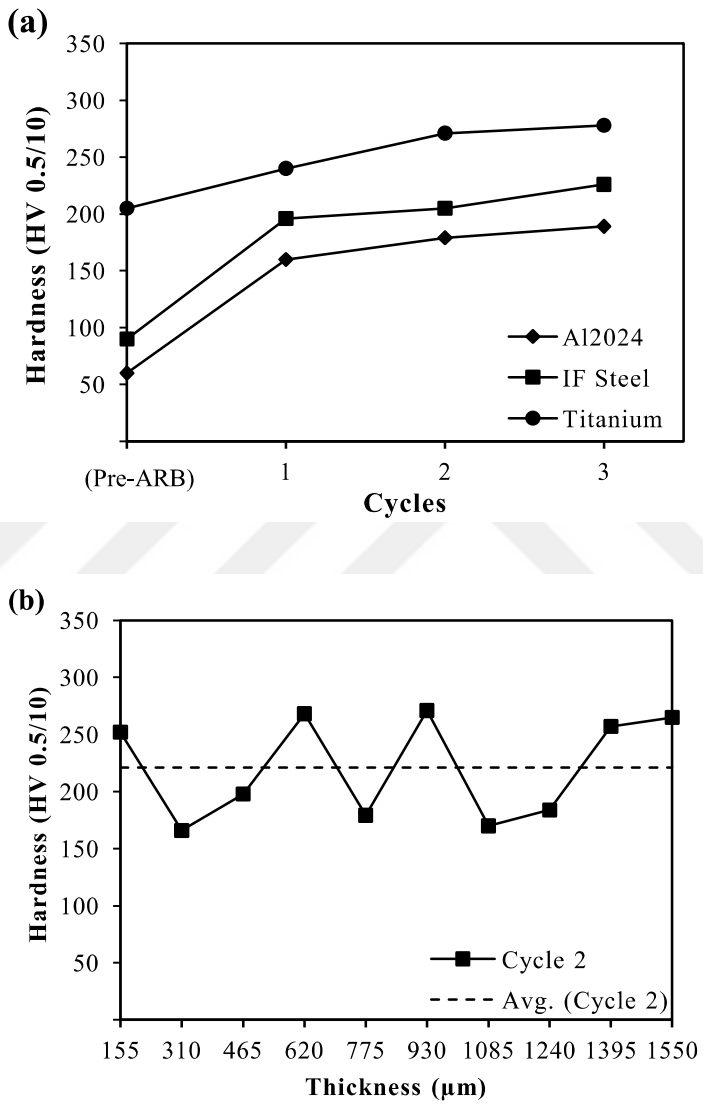



**Figure 4.8** Modification in the average microhardness as; (a) comparison in constituent metals (Pre-ARB and Post-ARB) with increasing cycles and (b) through the cross-section of two-cycle ARBed composite.

As displayed in Figure 4.8(b), variation in hardness values can be observed over the thickness of the composite processed after two cycles. The hardness levels vary expectedly

depending on the behavior of each layer and the location of the measurements [87, 124]. Going through the thickness of the composite, different metal layers and their interfaces had variable hardness levels after every cycle at different locations, but the average hardness indicated similar results in both types of measurements. This kind of variation in hardness levels in the composite proves beneficial in obtaining a ductile and strengthened structure that facilitates load transfer between different layers [98, 121]. The average values of primary metals and overall composites with the increasing number of cycles are noted in Table 4.1.

Tensile properties of the present composite were investigated after each cycle and consequent response and properties are presented in Figure 4.9 and Table 4.1. The pattern is completely obvious in the ARB process that improvement in true yield and tensile strength of the composite occurs, in contrast to the decrease in ductility. This can be attributed to the high dislocation density due to the strain hardening in early cycles, grain refinement with the development of micro sub-grains during the next cycles, and the overall presence of residual stresses in the composite [98, 125]. As illustrated in Figure 4.9, the true ultimate tensile stress (UTS) of approximately 670MPa was achieved after the final cycle which is 1.83 and 1.36 times higher than the base IF steel and titanium metals, respectively. Similar to the hardness value of this composite, the rise in the strength levels was significant after the first cycle that became steady for ensuing cycles. Generally, the elongation of the processed sheet reduces substantially through the current SPD method [125]. A ductility of around 2.2% was attained after three ARB cycles that make this composite incompatible for structural purposes.

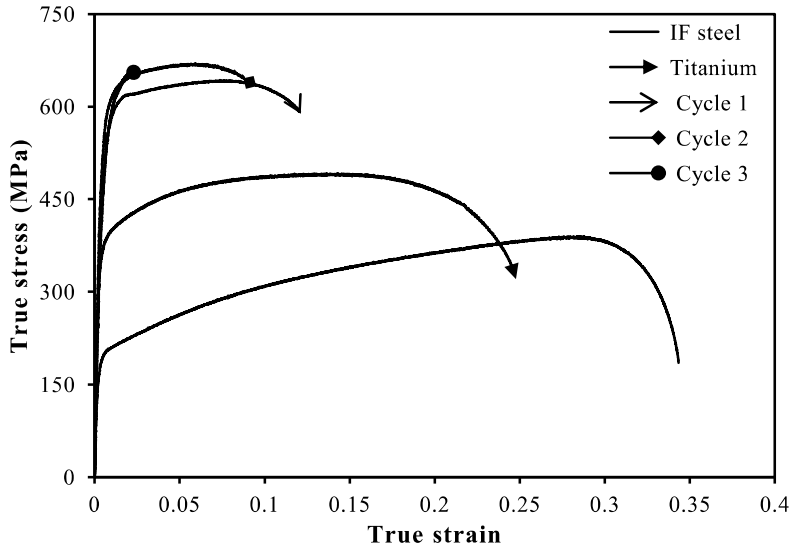



**Figure 4.9** Tensile response of base metals and processed Ti-Al2024-IF steel composite after every ARB cycle.

**Table 4.1** Mechanical properties of aluminum interlayered titanium-steel composite by the ARB at 480°C.

| Samples | Mechanical Properties | | | |
|---|---|---|---|---|
| | $YS_{(T)}$ (MPa) | $UTS_{(T)}$ (MPa) | $El_{(T)}$ (%) | Hardness (HV) |
| IF Steel | 202 | 365 | 34 | 90 |
| Titanium | 372 | 490 | 25 | 205 |
| Cycle 1 Ti-Al2024-IF | 536 | 641 | 12 | 199 |
| Cycle 2 Ti-Al2024-IF | 555 | 668 | 9 | 220 |
| Cycle 3 Ti-Al2024-IF | 522 | 660 | 2.2 | 239 |

### 4.3.3 Ti-IF Steel Composite Rolled at 400°C

This case involves similar processing in fabricating a titanium-steel composite without the addition of an aluminum interlayer after first cycle, but a slight difference in the rolling temperature which was 400°C. An additional layer was not used between the layers after the first ARB cycle to obtain a proper ARBed structure in the composite. The resultant composite was tested after each cycle and presented in this section (Table 4.2) to observe the variation of mechanical properties. Figure 4.10 illustrates the average microhardness along the RD of an individual component of the composite as well as across the thickness of the third cycle ARBed sheet. Understandably, a continuous rise in the hardness values was attained throughout the rolling cycles which is normal in the ARB processed composite. Like the previous section, an increase in the hardness value is substantial after the first cycle which becomes moderate afterward as presented in Figure 4.10(a). IF steel showed the highest increase in hardness compared to the others after the ARB process due to the high level of strain hardening.

Measurements across the composites were carried to observe the hardness variation at different locations, reported in Figure 4.10(b). Typically, higher values of hardness can be observed close to the surface, center, and interface region [124]. Friction between rolls and workpiece imparts the additional shear strain (redundant shear strain) close to the surface that transfers to the middle in the subsequent cycles. Wire brushing of layers before rolling triggers work hardening ultimately increase the hardness values close to the interfaces. Apart from these reasons, the presence of multiple metals also influences bigger fluctuation in the values across the thickness of the composite. Nonetheless, the average of the measurements for all the cycles indicates a steady increase in the hardness value.

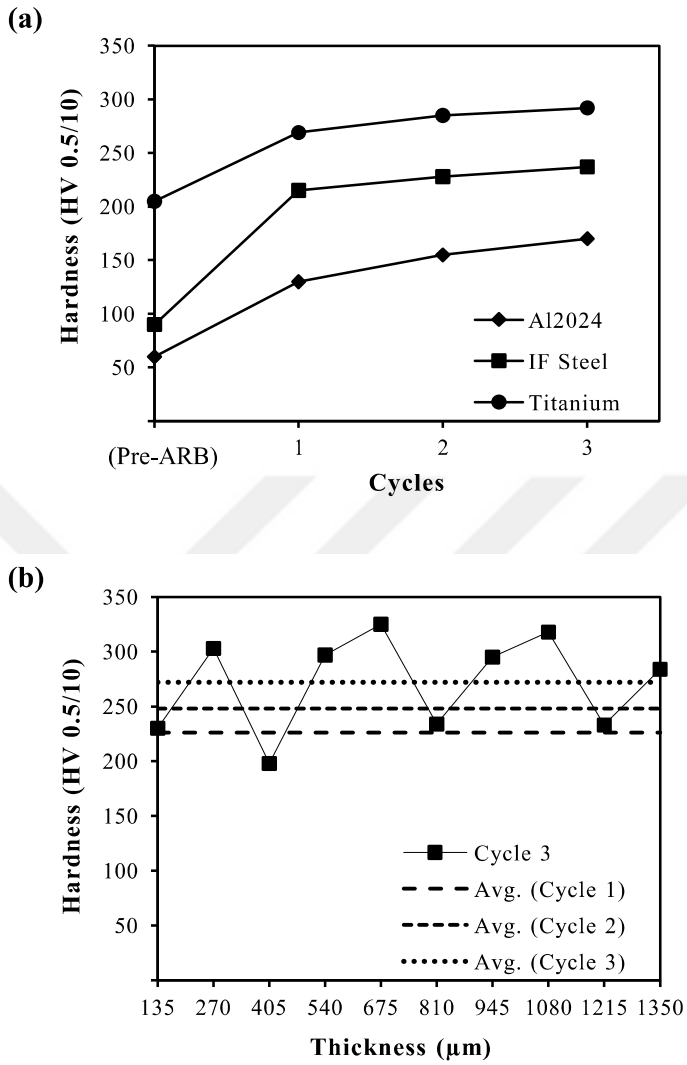



**Figure 4.10** Average Vickers microhardness with the variation of (a) individual layers versus the number of cycles and (b) through-thickness of a sample after 3 ARB passes.

Figure 4.11(a-b) illustrates the strength of the Ti-IF steel composite sheets using true stress-strain curves and their multiple attributes after each ARB cycle, roll bonded at 400°C. Resembling the previous section composite, a rise in the stress levels is significant which exceeds both primary metals. In contrast to strength, limited failure ductility was achieved for all the composites, as demonstrated in Figure 4.11(b). The above-mentioned pattern was occurred due to the creation of dislocation, presence of residual stresses, and grain refinement

which is obvious in most of the materials after ARB. An abrupt increase in strength with a mere loss of ductility between the first two cycles indicates a decent mechanical performance.

Generally, strengthening in material occurs due to dislocation strengthening or strain hardening in the early cycles of ARB whereas, at later stages, grain refinement or grain boundary strengthening causes an increase in tensile strength [87,120]. The peak stress of about 700MPa was acquired after the final cycle which is 1.92 and 1.43 times of as-received IF steel (365MPa) and pure titanium (470MPa), respectively. A lower ductility of 4% is noticeable after the third ARB cycle which is highest in any case mentioned in this study, but still inadequate for structural application. Correspond to enhanced strength, this is the main limitation in the SPD methods [125]. Full data are listed in Table 4.2.

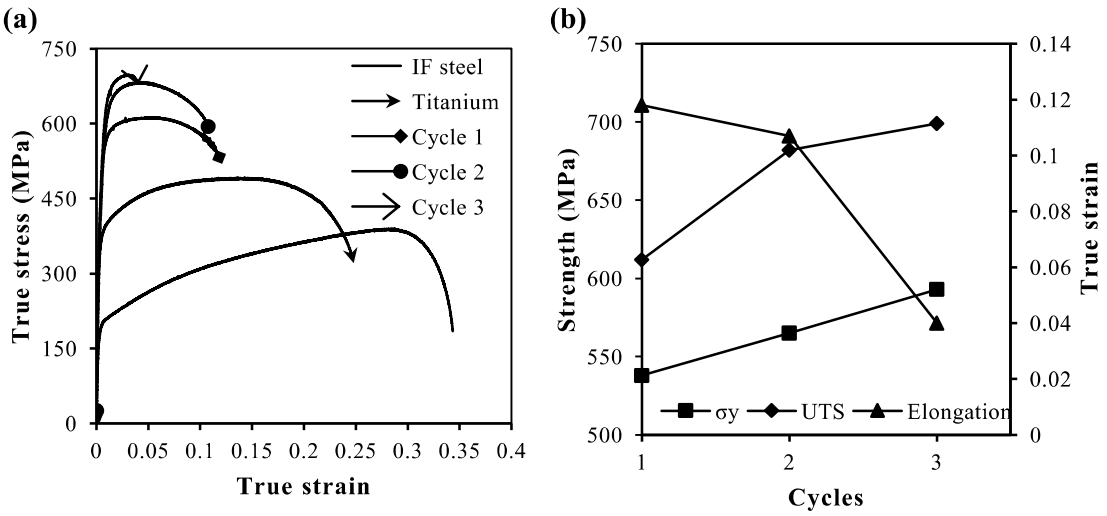



**Figure 4.11** Represents the response of fabricated Ti-IF steel sheets after the ARB with; (a) stress-strain curves and (b) the increasing number of cycles.

*4.3.3.1 Post-ARB Annealing (PA)*

To enrich the overall performance of the third cycle composite, post-ARB annealing (PA) was conducted at several temperatures and findings of these are presented in Figure 4.12(a-b). The post-annealing cycle consists of heating the third cycle ARBed sheet for 10min at 300°C, 400°C, and 500°C [65]. Among these temperatures, a comparable response of stress-strain to third cycle composite was demonstrated when heated at 300°C. A rise was exhibited for subsequent temperatures, i.e., 400°C and 500°C where the true strain was reached near to 0.07. An increase in the post-annealing temperatures led to the change in stress-strain owing to the elimination of residual stress, removal to voids and dislocation, and recrystallization or recovery of primary metals [126,127].

The decrease in yield point and continuous rise in tensile strength in the curves after 300°C indicates the development of precipitation hardening phenomena in the composite. As only aluminum's recrystallization temperature was crossed, the aforementioned phenomena could only have occurred in the Al2024 layer [128, 129]. Ultimately, true tensile strength up to 650MPa accompanied by ductility of around 7% was achieved after post-annealing of three-cycle ARBed composite. The best possible composites were achieved after optimum conditions are presented in Figure 4.12(c).

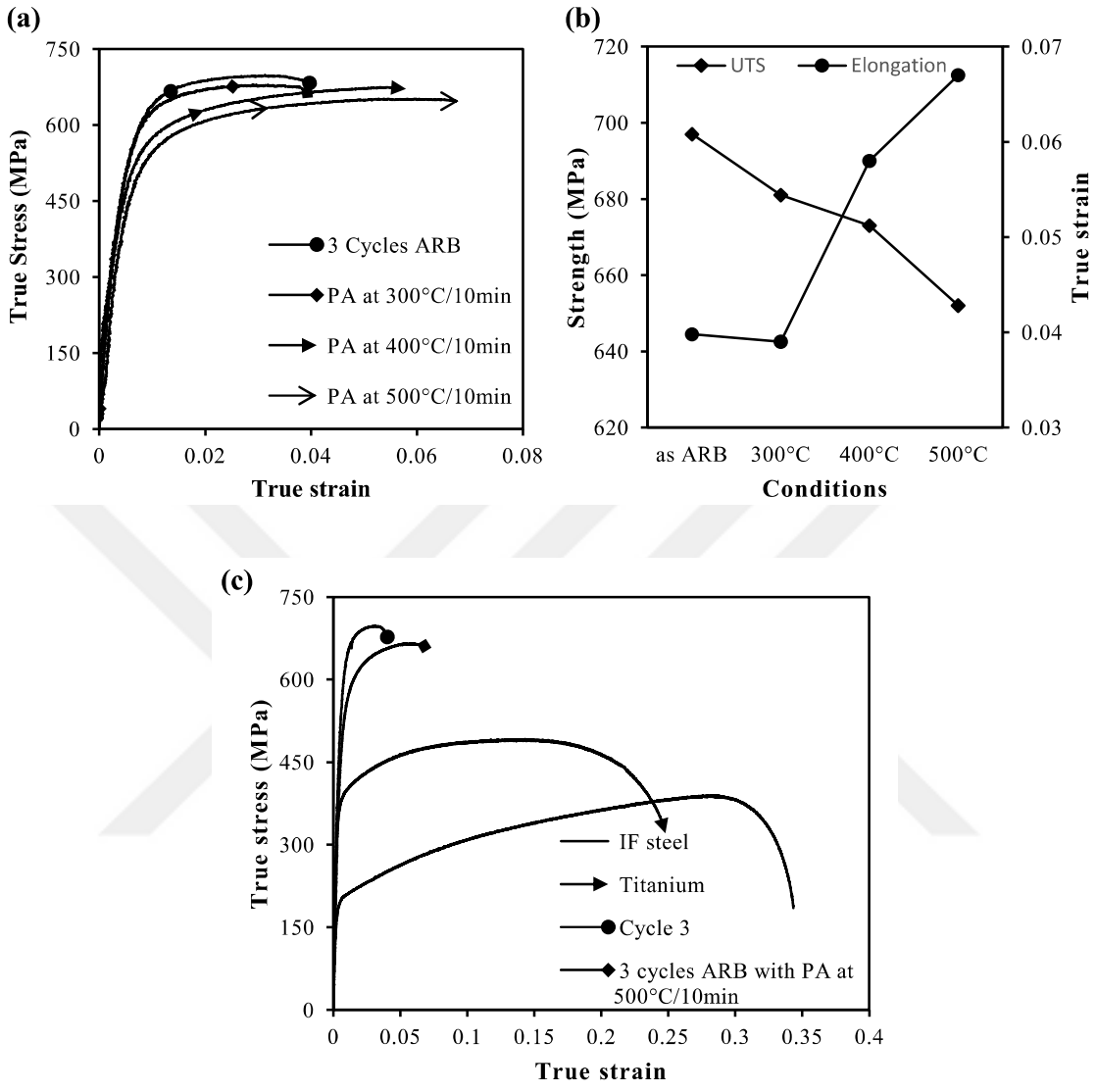



**Figure 4.12** Variation in the response of manufactured ARBed sheets after post-annealing (PA) with; (a) stress-strain curves, (b) increasing PA temperatures, and (c) ultimate conditions.

**Table 4.2** Mechanical properties of titanium-steel composite by the ARB at 400°C.

| Samples | Mechanical Properties | | | |
|---|---|---|---|---|
| | $YS_{(T)}$ (MPa) | $UTS_{(T)}$ (MPa) | $El_{(T)}$ (%) | Hardness (HV) |
| IF Steel | 202 | 365 | 34 | 90 |
| Titanium | 372 | 490 | 25 | 205 |
| Cycle 1 Ti-IF steel | 538 | 612 | 12.5 | 226 |
| Cycle 2 Ti-IF steel | 565 | 682 | 11.4 | 248 |
| Cycle 3 Ti-IF steel | 593 | 699 | 4.2 | 272 |

### 4.3.4 Ti-Al2024-IF Steel Composite Rolled at 400°C

In the final case, a titanium-IF steel composite was fabricated with the introduction of an aluminum interlayer after every cycle, rolled at 400°C temperature. A uniaxial tensile test was performed to observe the response of the composite compared to the previous case, resultant stress-strain behavior is illustrated in Figure 4.13. Even though strength exceeds both base metals by far but still lesser than the former case. There was an abrupt increase in strength for the first cycle curve along with decent elongation. Later cycles did not demonstrate a noticeable increase in strength levels due to induction of new aluminum (Al2024) layer after first and second cycles which produced improper ARB structure. True stress barely crossed 610MPa after three cycles which is 90MPa lower than the best three-cycle ARBed composite in this study. A brittle failure elongation of about 2.5% was gained after the final cycle composite. A better performance was obtained from the second cycle composite where UTS and ductility were 628MPa and 9%, respectively. Complete properties extracted from the stress-strain curve are noted in Table 4.3.

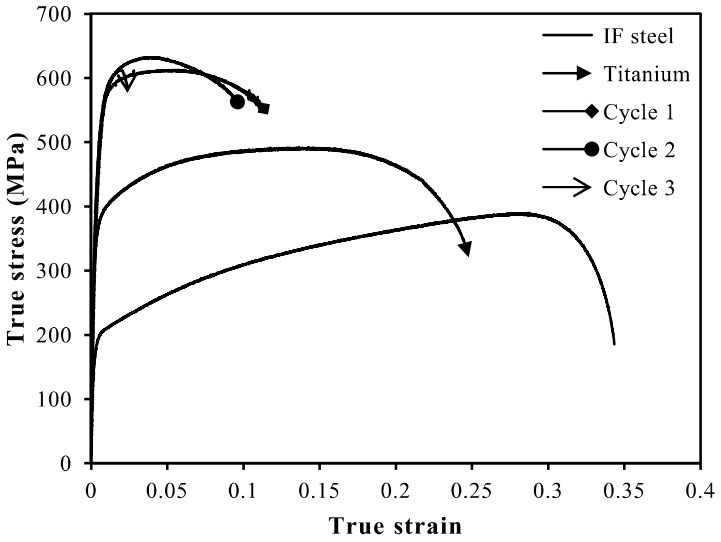



**Figure 4.13** Stress-strain response of aluminum interlayered titanium-steel composite roll bonded at 400°C.

**Table 4.3** Mechanical properties of aluminum interlayered titanium-steel composite by the ARB at 400°C.

| Samples | Mechanical Properties | | |
|---|---|---|---|
| | $YS_{(T)}$ (MPa) | $UTS_{(T)}$ (MPa) | $El_{(T)}$ (%) |
| IF Steel | 202 | 365 | 34 |
| Titanium | 372 | 490 | 25 |
| Cycle 1 Ti-Al2024-IF steel | 485 | 611 | 11.3 |
| Cycle 2 Ti-Al2024-IF steel | 537 | 628 | 9.3 |
| Cycle 3 Ti-Al2024-IF steel | 490 | 612 | 2.4 |

## *4.4 Interfacial Strength*

To prove the bonding quality after the ARB process, shear punch testing can be done that provides shear properties of the processed composite. The composite produced at 400°C rolling temperature offered the best results so, SPT was only performed on the two composites (with and without Al2024 interlayer) to observed and compared the bonding strength between them. Load-displacement curves (LDCs) were acquired from SPT, showed the maximum load obtained by the composite before the punch fractured the composite, presented in Figure 4.14 and Figure 4.15.

A continuous increase in the load can be noticed from the curve after every cycle caused by the accumulation of dislocations in the material due to work hardening. This trend confirms the enhancement of interlayer bonding strength for the trailing cycle at higher strain. After the first cycle, the force was increased substantially in the second and slightly in the third cycle (reached up to 5600N) which is in the agreement with the tensile test results of section 4.3.4. Moreover, the non-uniform behavior of curves in Figure 4.14 indicates the improper ARBed structure of the composite as an additional aluminum interlayer was added after each rolling cycle. The LDCs curves were transformed into shear strength after applying equation 2.10 and consequent results are mentioned in Figure 4.14(b,c). It was mentioned in the fracture morphology that the following cycle improves the bonding quality of the previous cycle's interface which ultimately increases the strength of the composite.

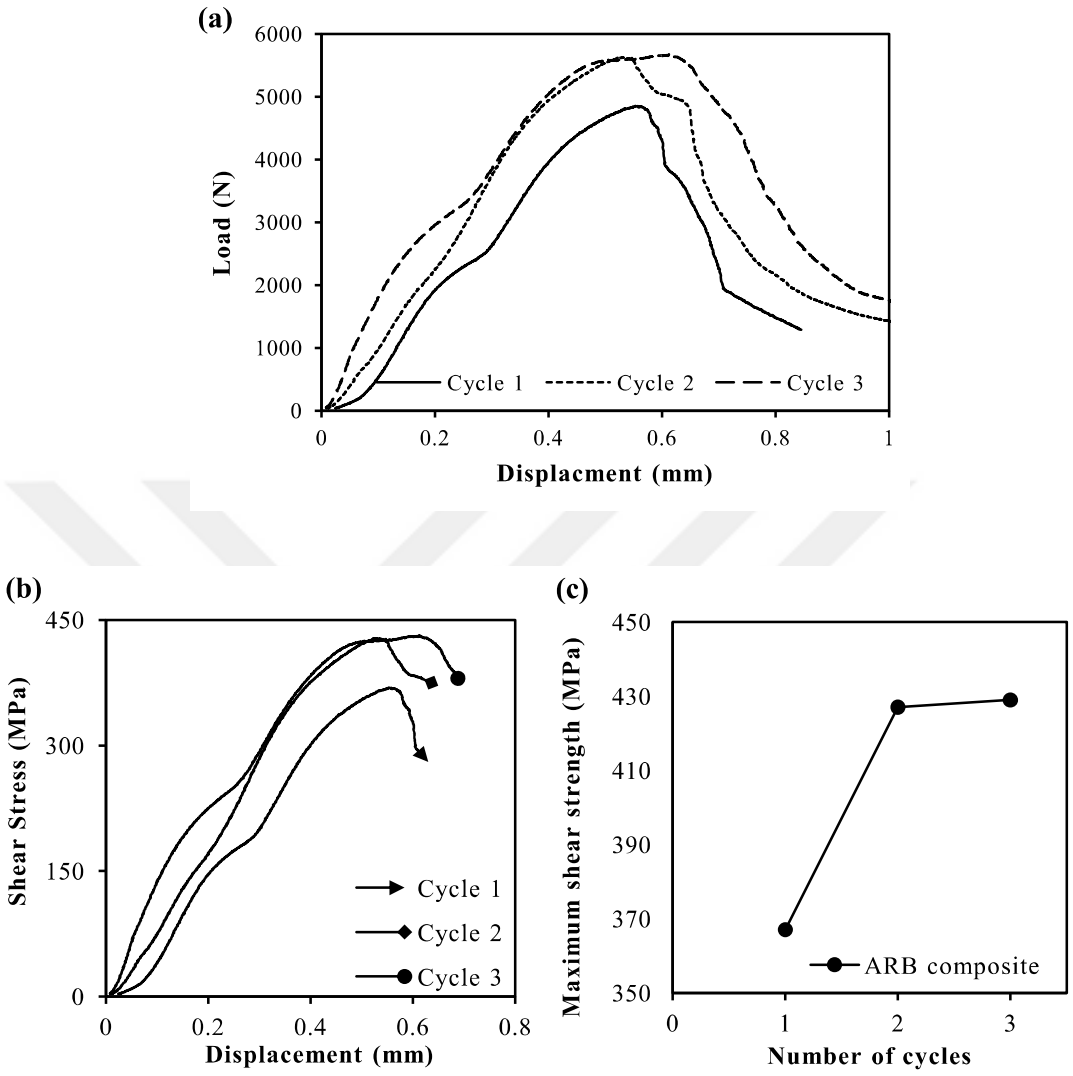



**Figure 4.14** Variation in the SPT results of Ti-Al2024-IF steel composite roll bonded at 400°C after three ARB cycles as (a) load-displacement curves, (b) shear strength as a function of displacement, and (c) ultimate shear strength versus the number of cycles.

Figure 4.15(a) demonstrates the LDCs of titanium-steel composite roll bonded at 400°C after three cycles without the inclusion of Al2024 interlayer after the first ARB cycle. The curves are similar to previous SPT results, with a slight difference in the maximum load withstood by the final composite. Consistent growth in the curves is evident after three ARB cycles which is obvious. Continuous application of strain by powerful rolling pressure allows mutual embedding of layers consequently elevates interlayer bonding and shear strength [99].

A maximum load of 5700N was resisted by the final composite before fracture. Comparatively more uniform and less deflection can be detected from these curves than prior ones, owing to the uniformity of the ARBed structure in the composite. Similarly, the LDCs curves were transformed into shear strength after applying equation 2.10 and consequent results are mentioned in Figure 4.15(b,c). SPT results prove that enhancing rolling pressure enriches the shear strength of the composite.

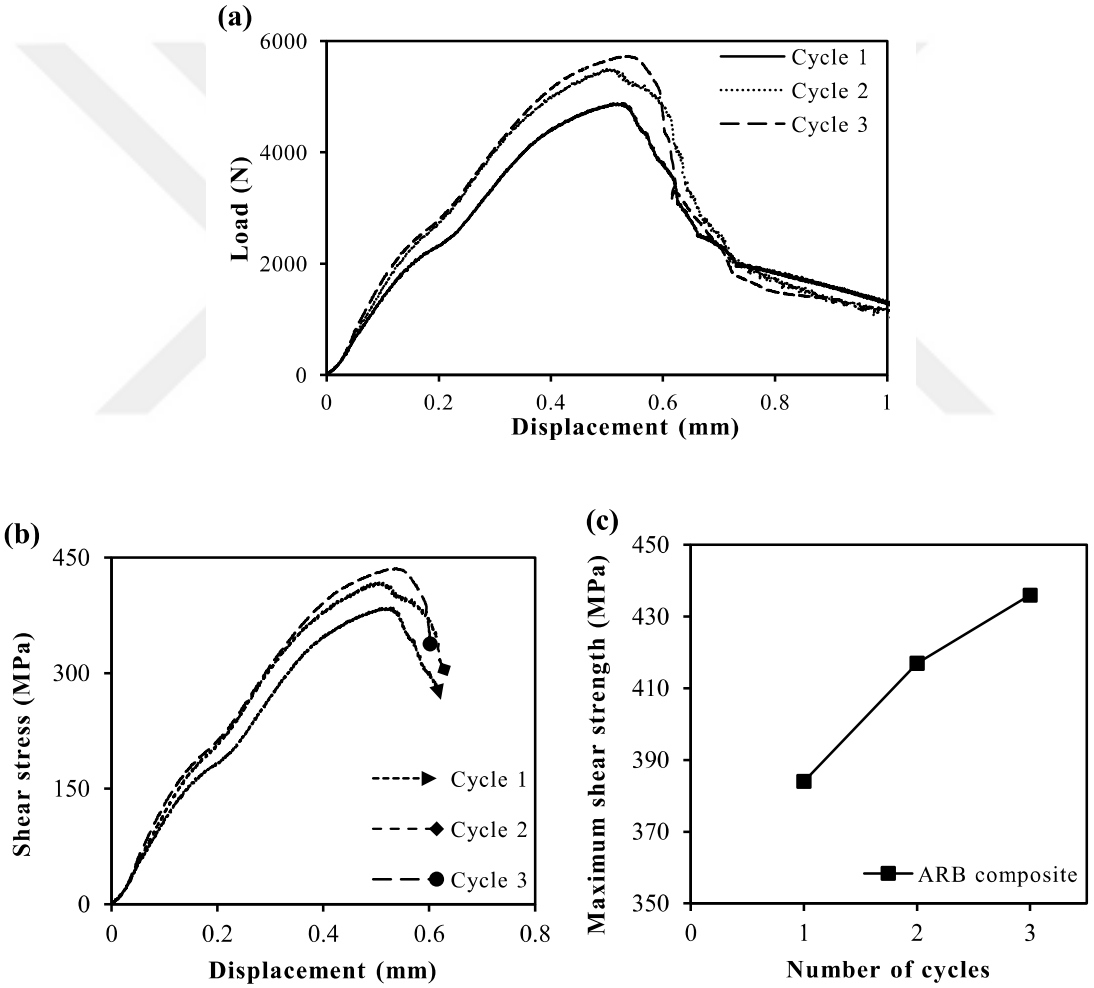



**Figure 4.15** Variation in the SPT results of Ti-IF steel composite roll bonded at 400°C after three ARB cycles as (a) load-displacement curves, (b) shear strength as a function of displacement, and (c) ultimate shear strength versus the number of cycles.

The shear punch test was only performed on titanium-IF steel composites (with and without aluminum interlayer after 1st cycle) roll bonded at 400°C. These results can be correlated with uniaxial tensile results for similar composites through only observation [111]. A similar trend can be observed from obtained curves. The increase in ultimate tensile strength (UTS) and ultimate shear strength (USS) is almost identical. Ti-IF steel composite at 400°C showed continuous rise after each cycle whereas Ti-Al2024-IF steel composite at 400°C initially expressed an increase in strength but became stagnant for the third cycle.

Overall, the titanium-IF steel composite (without Al2024 interlayer after the first cycle) rolled at 400°C gave the best performance due to strong bonding between layers along with work hardening on it. The purpose of additional Al2024 interlayer after each cycle in titanium-IF steel composite (especially at 480°C) was to increase interfacial bonding and subsequently strength of the composite. Even though bonding was increased, and decent strength was achieved, the final composite became brittle due to the working and non-uniform ARB layered structure.

# 5. EVALUATION OF THE ALUMINUM-STEEL COMPOSITE

## *5.1 Overview*

In the present chapter, a metal matrix composite was fabricated using lightweight metal aluminum with IF steel by the ARB process, and the mechanical characteristics of the resultant composite were examined using uniaxial tensile testing. Firstly, a three-cycle ARB composite was produced which was then post-annealed to observe the occurrence of precipitate hardening in the material.

## *5.2 Microstructure*

Both (aluminum and IF steel) layers were etched to observe the behavior of grains after heat treatment of ARBed composite. Figure 5.1(a, d) and Figure 5.1(b, e) indicate the coarse grain structure of as-received metals and their obvious fine grain structure after three ARB cycles due to the continuous accumulation of strain after each cycle. The average grain sizes of Al2024 and IF steel were 30μm and 28μm, respectively. Grain refinement is more in the case of aluminum compared to IF steel that explains the indistinctive nature of aluminum microstructure after three cycles, Figure 5.1(b). A micrograph of the composite aged at 150°C/24h can be viewed in Figure 5.1(c, f), which demonstrates the partial coarsening of the average grain size in both aluminum and IF steel layers. The dislocation density decreases partially due to the limited recovery at lower annealing temperatures.

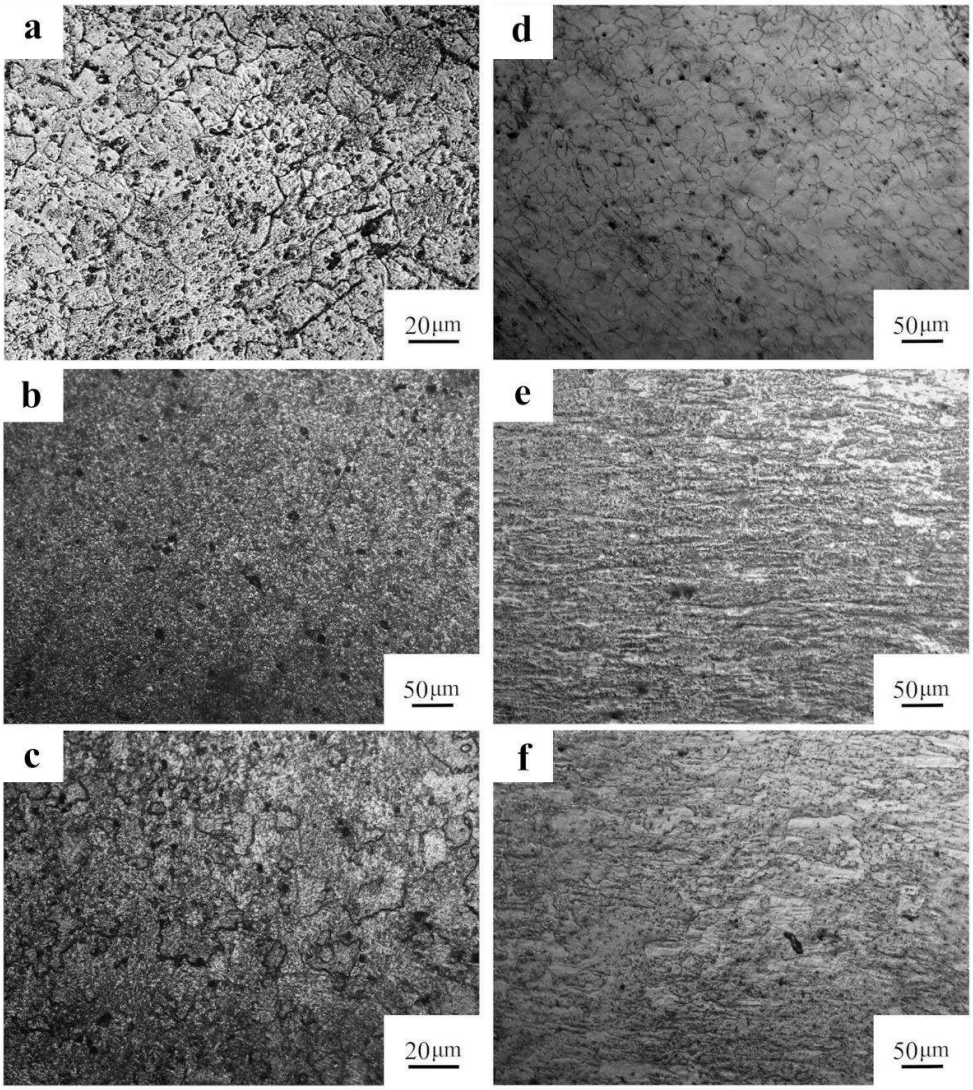



**Figure 5.1** Optical micrographs of (a) aluminum as received, (b) three-cycle composite, (c) aged at 150°C/24h, (d) IF steel layers as received, (e) three-cycle composite, (f) three-cycle composite aged at 150°C/24h.

## *5.3 Mechanical Response*

The mechanical properties of aluminum-steel composite were studied by tensile test under $0.001s^{-1}$ strain rate at ambient temperature. The outcome behavior of the sheets with the increasing number of cycles is illustrated in Figure 5.2. Enhancement in the strength levels is apparent after each cycle with the expanse of limited ductility compared to the initial metals of the composite. The highest strength of about 450MPa was achieved along with 5% elongation after three ARB cycles. The ultimate strength of the composite is 2.6 and 1.5 times the initial conditions of aluminum and IF steel, respectively. Work hardening of constituent layers by the addition of strain causes a decrease in the mobility of dislocations in the early rolling cycles, while grain subdivisions and refinement in later cycles enhanced strength and reduce ductility substantially [79, 130]. A slight increase in the ductility after initial cycles can be seen which is in the agreement with previous studies [61, 76].

In the UFG materials, it is proposed that the improvement in elongation can be credited to the bimodal distribution microstructure of grains (micro and nano) at higher ARB cycles. Furthermore, the emergence of a restoration mechanism which is continuous recrystallization and recovery leads to the improvement in ductility [15, 131]. To further recover the ductility of the composite with a slight reduction in the strength, a three-cycle ARBed sheet was subjected to heat treatment. The focus is to obtain a composite consisting of both decent strength and ductility that can be utilized in engineering applications.

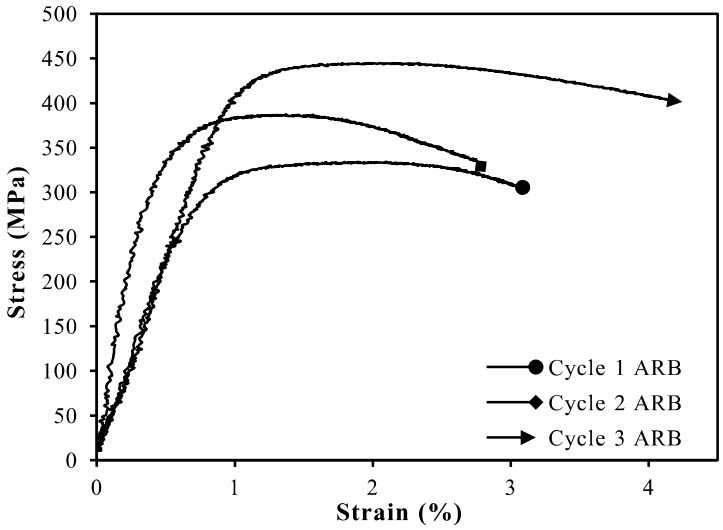



**Figure 5.2** Engineering Stress-strain response of Al2024-IF steel composite after three ARB cycles.

### 5.3.1 Post-ARB Heat Treatment (3rd ARB cycle)

To trigger the precipitate hardening phenomena, an extensive post-annealing cycle was performed on a three-cycle ARBed Al2024-IF composite. The idea was to monitor the effect of time on the formation and saturation of precipitates inside the material. A thorough explanation of the heating mechanism was mentioned in the experimental section, but the full post-annealing cycle is demonstrated in Figure 5.3. Samples were firstly heated at 420°C (just above annealing temperature) followed by water quenching which then artificially aged (AA) at 150°C for several intervals.

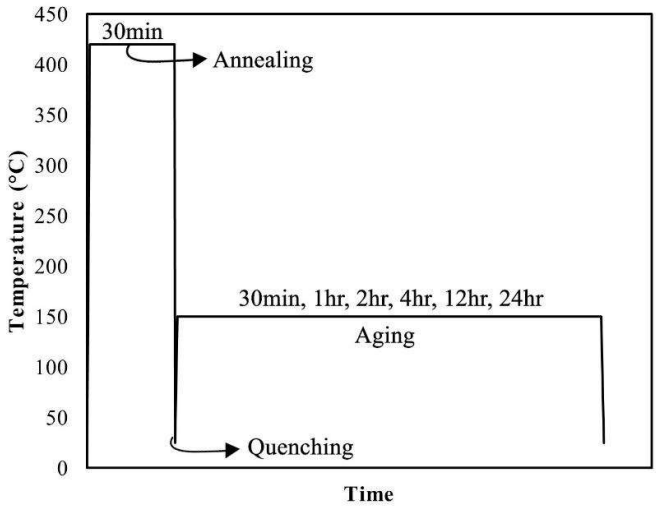



**Figure 5.3** Graphical representation of precipitation hardening heating cycle.

Attained post-annealed samples were tested uniaxially and compared with base metals and final cycle ARB composite. Figure 5.4 displays the variation in tensile behavior of the samples with increasing aging time. There is an abrupt reduction in stress value in contrast to elongation levels that increased substantially from final composite to aging samples. Strength was reached at 397MPa (previously 445MPa) while ductility was increased almost twice (9%) after aged for 30min. The same trend was followed by the sample aged for 1hr. Removal of residual stress, saturation in the dislocation, and further recovery in the base metals suggest a typical behavior of the composites [132]. Generally, when metals are heated below the recrystallization temperature, it only removes the strain formed in the sheets by the rolling process, consequently, allow increment in elongation and loss in strength. In this case, the heating temperature (420°C) was favorably high for the Al2024 layer, it is expected to observe precipitation hardening phenomena as the aging time increase.

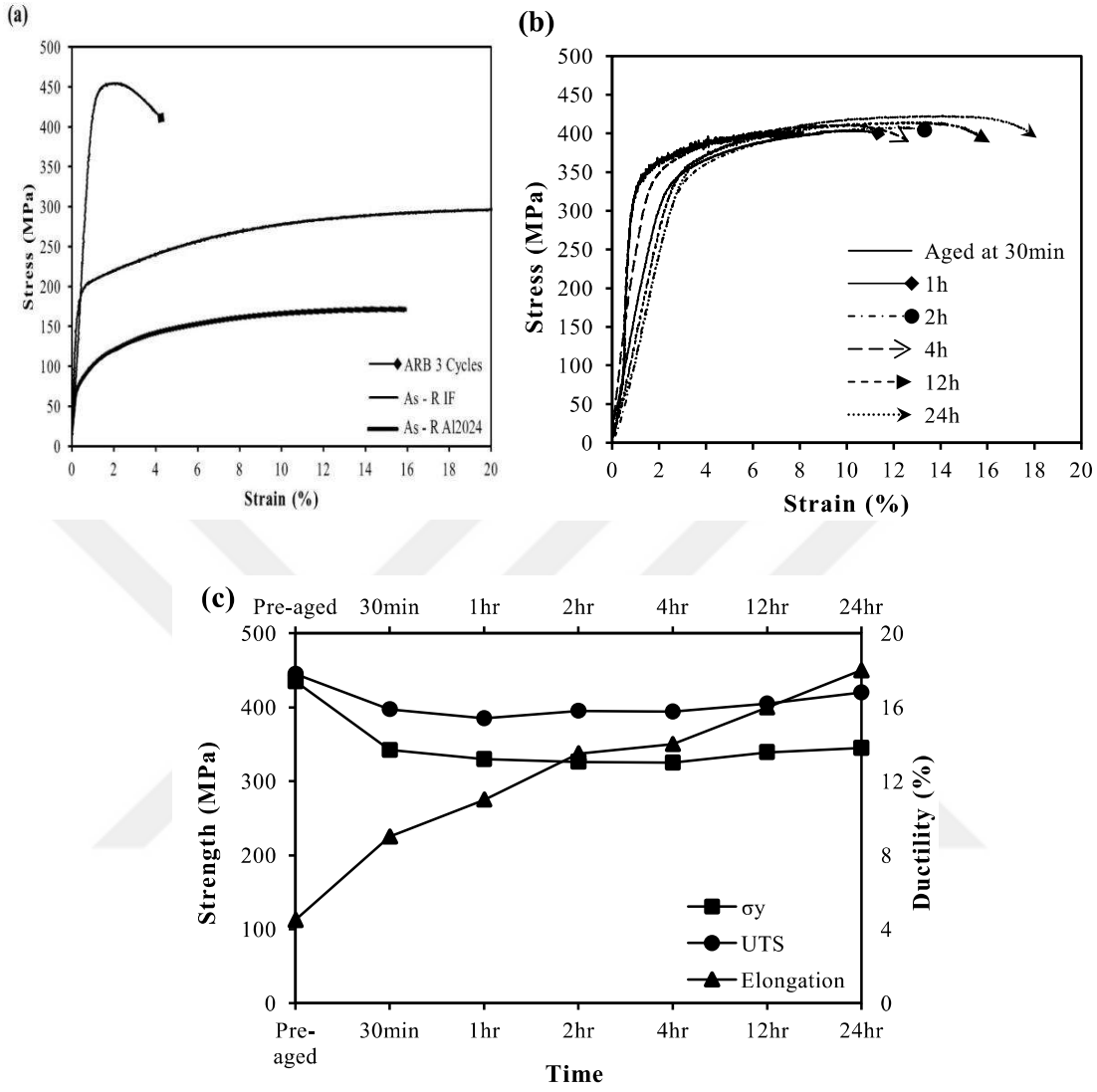



**Figure 5.4** Mechanical behavior of (a) as received constituent metals with ARBed composite, (b) aging response, and (c) variation in tensile properties with the increasing aging time.

For 2hr aging time, the stress value was increased marginally along with the increase in elongation value that remained almost constant for 4hr. This is the period when the growth of precipitates occurs together with coarsening of grain size, allow to obtain decent strength while improving ductility [133]. The aforementioned conditions are the threshold of strength as a further increase in aging time will only improve strength together with ductility. Strength was reached to 420MPa while 18% elongation was apparent in the composite, as displayed in Figure 5.4(b). Longer aging time assisted in attaining a reasonable size of precipitates along

with fine distribution throughout the aluminum layer [115, 133, 134]. Complete data of all aging conditions extracted from stress-strain curves are noted in Table 5.1. Figure 5.4(c) presents a statistical look at the strength levels of all the conditions of composite, where fluctuation in strength can be noticed as aging time increases.

**Table 5.1** Tabular data extracted from stress-strain curves of primary metals and post-ARB heat-treated composites.

| Samples | Conditions (Aging Time) | Mechanical Properties | | |
|---|---|---|---|---|
| | | YS (MPa) | UTS (MPa) | El (%) |
| **Al2024-O** | - | 80 | 175 | 16 |
| **IF Steel** | - | 194 | 299 | 41 |
| **3 ARB Cycles** | - | 435 | 445 | 4.5 |
| **AA 30min** | 30min | 342 | 397 | 9 |
| **AA 1hr** | 1hr | 330 | 385 | 11 |
| **AA 2hr** | 2hr | 326 | 395 | 13.5 |
| **AA 4hr** | 4hr | 325 | 394 | 14 |
| **AA 12hr** | 12hr | 339 | 405 | 16 |
| **AA 24hr** | 24hr | 345 | 420 | 18 |

### *5.3.2 Interfacial Strength*

To understand the effect of aging on the interlayer strength and ultimately the shear strength of the composite, shear punch testing was performed to obtain load-displacement curves and subsequently shear stress-displacement response using equation (2.10).

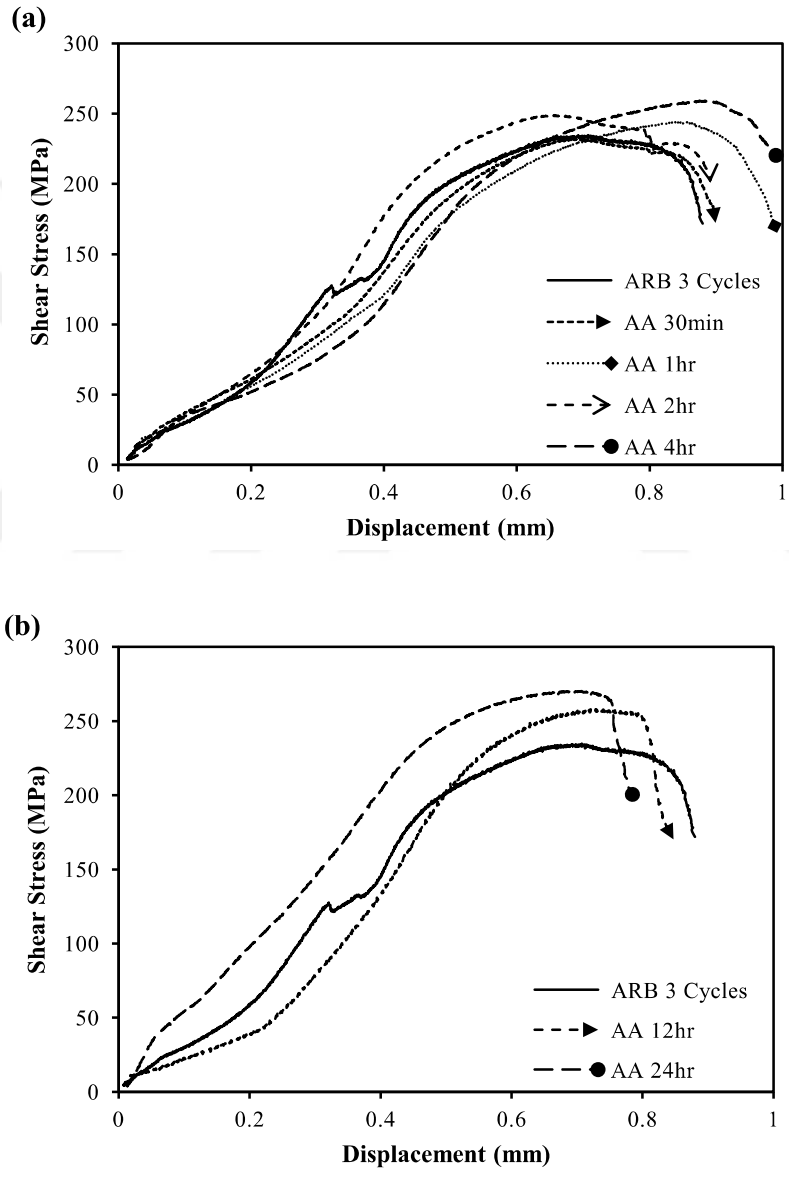



**Figure 5.5** Comparison of bonding strength between three-cycle ARB composite with; (a) short aging, and (b) long aging period.

Figure 5.5 demonstrates the shear strength of the 3 cycle ARB composite along with the response obtained after aging. Aging up to 2h did not affect the shear strength considerably, yet, imposed diffusion led to a slight enhancement of the bond strength (Figure 5.5a) [67]. In contrast, higher aging intervals led to a notable difference in the shear response. The 24h aged sample led to a shear strength over 250MPa with a linear shear stress-displacement response.

The SPT results obtained from aged samples can be correlated with the corresponding uniaxial tensile results through only observation [111]. A similar trend can be observed in terms of tensile and shear stresses by the fluctuation of response with aging time. The increase in ultimate tensile strength (UTS) and ultimate shear strength (USS) is almost identical for high aging durations (12h and 24h).

# 6. NUMERICAL ANALYSIS

## *6.1 Overview*

For modern technology and engineering, it has become quite essential to use computer codes and numerical modeling techniques for the last 25 years. Industries are increasingly utilizing fundamental tools such as finite element method (FEM) and computer-aided engineering (CAE), from research to prototyping. Dynamic procedures with severe nonlinearity were simulated professionally using finite element methods [135].

Numerous studies have been employed using finite element analysis (FEA) for severe nonlinearity processes, including equal-channel angular pressing (ECAP) [136], high-pressure torsion (HPT) [137], warm rolling [135], and few on accumulative roll bonding (ARB) [138, 139]. Effect of roll diameter and friction between rolls on the equivalent plastic strain of rolled sheet was studied by Tadanobu et al. [138]. Fe-code ABAQUS was utilized with a different friction model to simulate thin plates after ARB [137].

The main idea is to prepare a similar model as experiments and validate the numerical analysis results with the experimental ones. Results obtained, in terms of effective strain and stress after the ARB process, were compared. Numerical analysis was performed only on the case study of titanium-IF steel composite.

## *6.2 Modeling*

WORKBENCH LS-DYNA module in ANSYS 18.1 software was used to simulate the ARB process. The finite element (FE) modeling was performed by utilizing LS-DYNA as a solver. Post-processing of the model was done using LS-PRE-POST where the results were extracted for comparison.

### 6.2.1 Geometry

Geometry and meshing play an important part to get optimum results through simulation. Figure 6.1 displays the model implemented for the ARB process on aluminum interlayered Ti-IF steel metallic sheets. Rolling direction (RD) is parallel with X-axis, while sheet thickness, normal direction (ND), along with Y-axis. The value of equivalent strain $\varepsilon_{eq}$ depends upon the mesh size of sheets in the ND ($t_{el}$). By reducing the mesh size in ND, the $\varepsilon_{eq}$ increases and becomes relatively constant when the $t_{el}$ is less than 0.03mm. Moreover, the strain value is about 0.8 at the center regardless of the thickness of the mesh [139, 140].

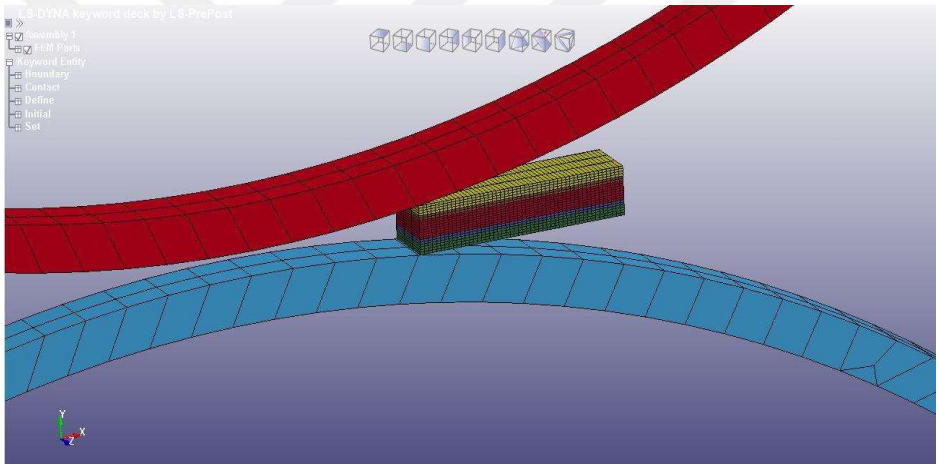



**Figure 6.1** The FE model employed for the ARB of multi-metal composite (1st cycle).

To find the mesh sensitivity of the model, simulation was performed from coarse to fine meshing till response became relatively constant. Table 6.1 represents the meshing elements and their corresponding effective stress (von-Mises) of the model in the first cycle. Finally, the mesh size, 0.13mm and 0.24mm in ND ($t_{el}$) and RD ($L_{el}$), respectively, was chosen for this study. Therefore, the model contains 6561 nodes and 3774 quad elements. The FE meshing of rolls and sheets is demonstrated in Figure 6.2.

**Table 6.1** Different meshing elements and their corresponding stresses of the model for the first cycle.

| Meshing | Elements | Effective stress (v-m) (MPa) |
|---|---|---|
| 1 | 846 | 486 |
| 2 | 2274 | 524 |
| 3 | 3774 | 528 |

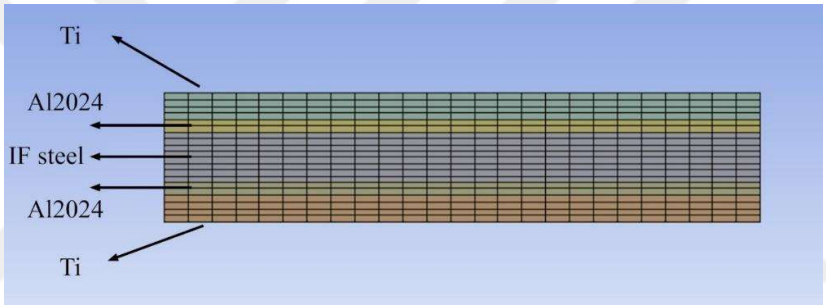



**Figure 6.2** Initial mesh size utilized in the analysis.

### 6.2.2 Assumptions

Following assumptions were considered during the creation of the model.

1. The rolls were rigid bodies, while the plates were flexible.
2. The simulation was performed at room temperature. This is since the individual layers were already bonded in the model, whereas in experiments, high temperatures were applied to enforce bonding between layers during the rolling process.
3. Keyword (Mat018): POWER LAW PLASTICITY was utilized to insert the mechanical properties of sheets in LS-DYNA. Young's modulus of titanium, Al2024, and IF steel were 105GPa, 73GPa, and 107GPa, respectively. While the value of Poisson's ratio was 0.33 at room temperature.

4. The stress-strain relationship ($\sigma = K.\varepsilon^n$) was employed in the analysis, from where values of K and n were calculated. Values of K and n for titanium (679MPa, 0.18), Al2024 (342MPa, 0.25), and IF steel (512MPa, 0.24) were used in the model.
5. Rolling was performed under the unlubricated condition as frictional coefficient was set $\mu = 0.35$ between rolls and sheets.

### 6.2.3 Initial and Boundary Conditions

1. Five sheets were stacked, similar to experiments, with an initial thickness of 2.60mm altogether. Other dimensions of layers were w=3mm and L=12mm, and a 50% reduction ratio per rolling cycle, equal to 0.8 von Mises strain, was provided.
2. The roll diameter was 150mm and they were rotated at 180°/sec.
3. The initial velocity of $10mms^{-1}$ was applied to the sheets.
4. The initial velocity was given in the X direction to the composite sheets, and they were restricted to deform in the Z direction.
5. Rolls were fixed around X and Y direction, but able to rotate freely around Z direction.
6. The temperature was remained fixed till the end of the process.

### 6.2.4 Analysis

In the ARB simulation of the first cycle, a 2.60mm stacked sandwich was rolled with a 50% reduction to provide a 1.30mm composite sheet. Effective plastic strain and effective stress (v-m) were the only two results that were considered when comparing with experimental data, as presented in Figure 6.3 (a, b). After that, two rolled composites were stacked together and rolled back to 1.30mm thickness again (second ARB cycle). Similarly, the process was repeated to get a three-cycle ARB composite.

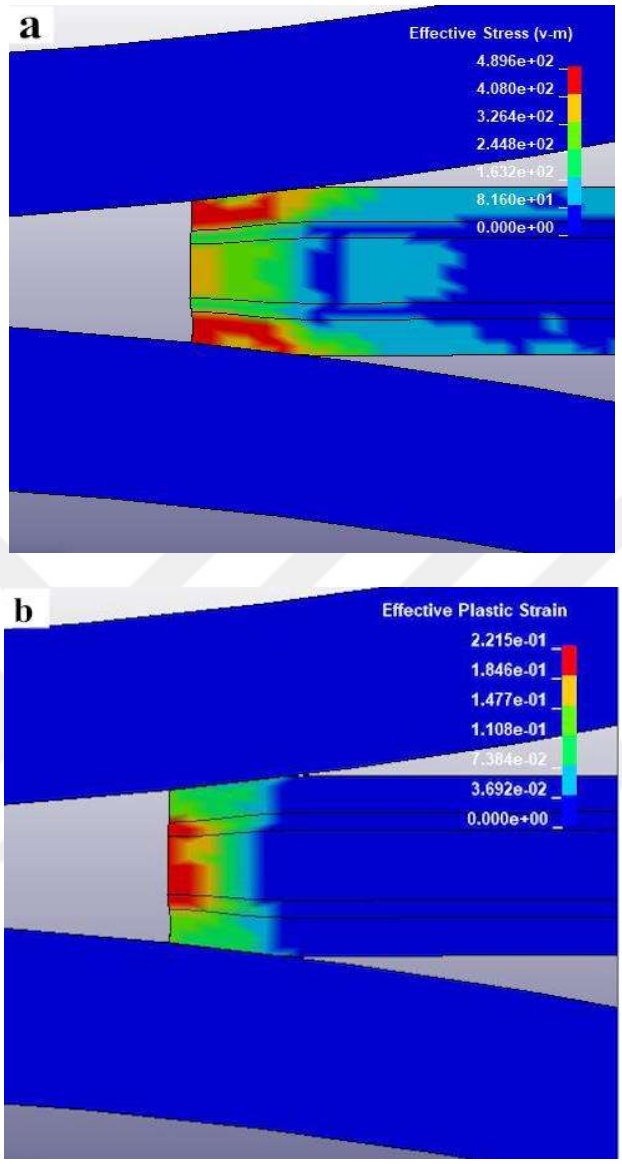



**Figure 6.3** Illustration of the effective (a) (v-m) stress (MPa), and (b) plastic strain during the first rolling step.

Figures 6.4 (a) and (b) demonstrate the existence of effective plastic strain in the layers before the second and third rolling cycle, respectively. The effective plastic strain and effective stress (v-m) obtained in the prior cycle were transferred to the ensuing cycle. Through this transfer, new layers in the next cycle can have the same properties as the plate processed in the previous cycle. In doing so, the gap between simulation results and experimental work becomes closer.

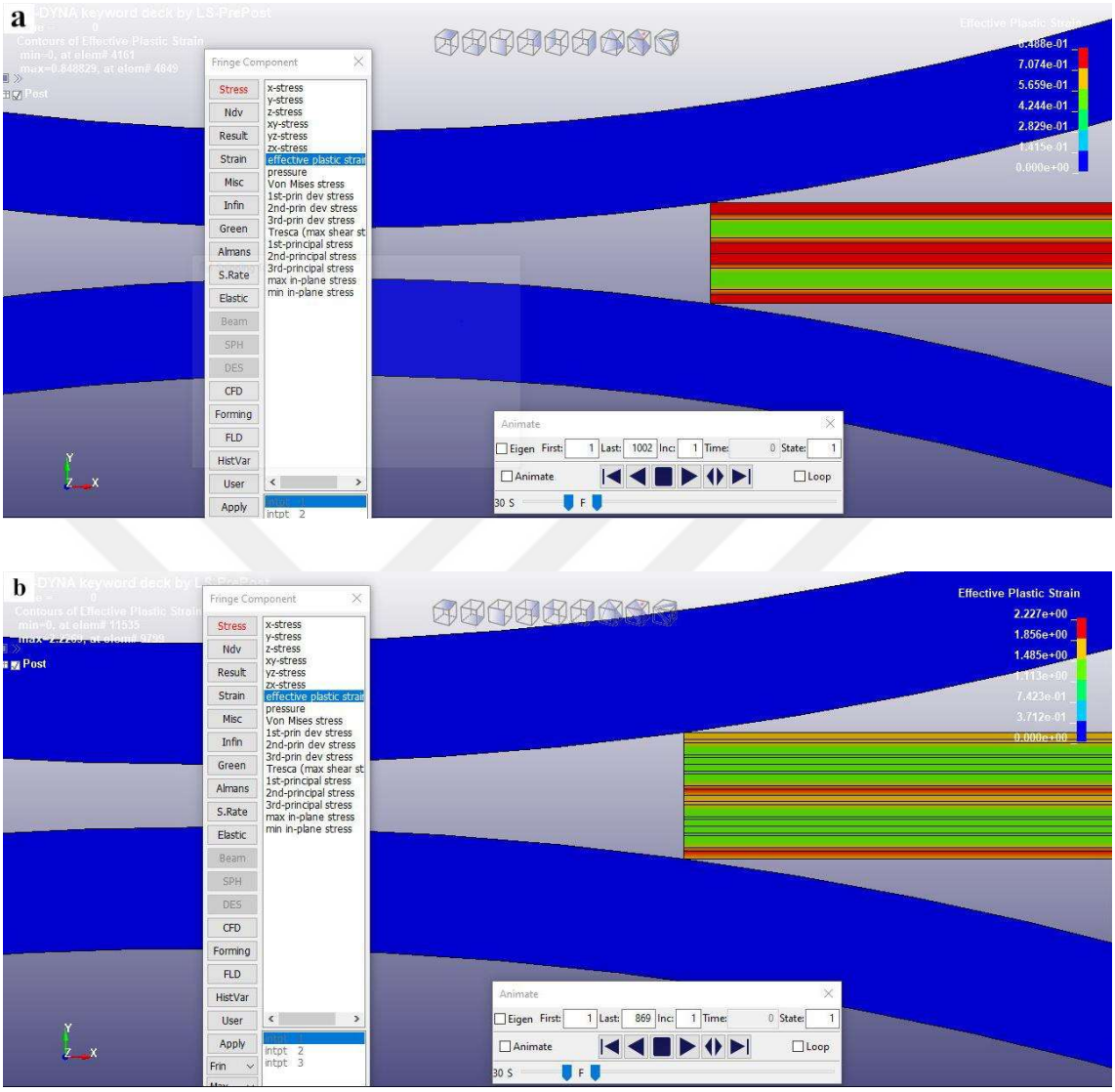



**Figure 6.4** Demonstration of the transferred effective plastic strain of the prior cycle before (a) second, and (b) third cycle rolling process.

## *6.3 Results and Discussion*

Characteristics of the rolled slab, i.e., the effective stress (v-m) and the effective plastic strain, were obtained after three ARB cycles. The resultant slab's thickness in the normal direction (ND) was divided into 10 equal points where effective stress and strain values were obtained, and the average of these values was calculated to get a homogenized value. Similarly, three values were calculated at different positions on the slab's longitudinal direction to give an overall response. Figure 6.5 presents the distribution of the stress value through the thickness of Ti/IF steel composite interlayered with Al2024 only in the first cycle. Expectedly, the value effective stress (v-m) increases by increasing the number of rolling cycles due to the induction of plastic strain after each cycle. The average effective stress levels of about 528MPa, 555MPa, and 609MPa were acquired after the first, second, and third cycles, respectively. Titanium layers were exposed to maximum stress close to the surface. This is the point where high deformation occurred by the effect of frictional shear strain between rolls and sheets during the rolling process [138].

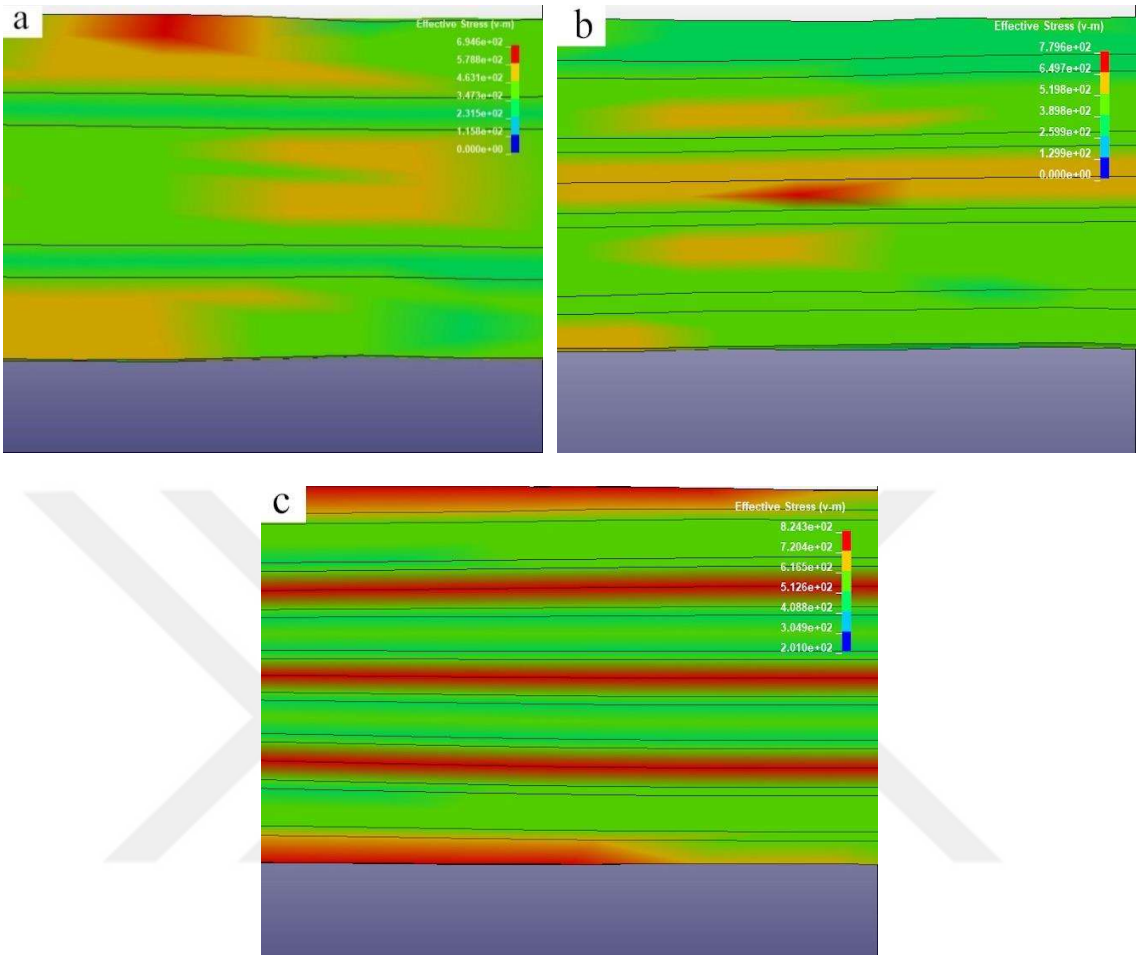



**Figure 6.5** Variation in von Mises stress levels of the layered composite after (a) 1st, (b) 2nd, and (c) 3rd rolling cycle.

To compare the tensile yield stress ($\sigma_{yld}$) and effective stress ($\sigma_{v\text{-}m}$), a mathematical relationship (referred to as von Mises criterion) was used, written in equation 6.1 [141]. The yielding occurs when the equivalent or effective stress reaches to yield strength of the material ($\sigma_{(v\text{-}m)} = \sigma_{(yld)}$), in a simple tension case, or uniaxial stress. Therefore, the von Mises criterion can be simplified as:

$$\sigma_{(v-m)} = \sqrt{\frac{(\sigma_1-\sigma_2)^2+(\sigma_1-\sigma_3)^2+(\sigma_2-\sigma_3)^2}{2}} \tag{6.1}$$

$$\sigma_{(v-m)} = \sigma_{(yld)}$$

Therefore, the tensile yield stress $\sigma_{(yld)}$ which was acquired through uniaxial tensile testing in the experiments was compared with the calculated effective stress $\sigma_{(v\text{-}m)}$ by numerical analysis. Figure 6.6 and Table 6.1 presents the measured result from experiments and simulations of Ti/IF steel composite after the first, second, and third ARB cycles. The experimental and numerical results are in close agreement, as they have an acceptable gap between them.

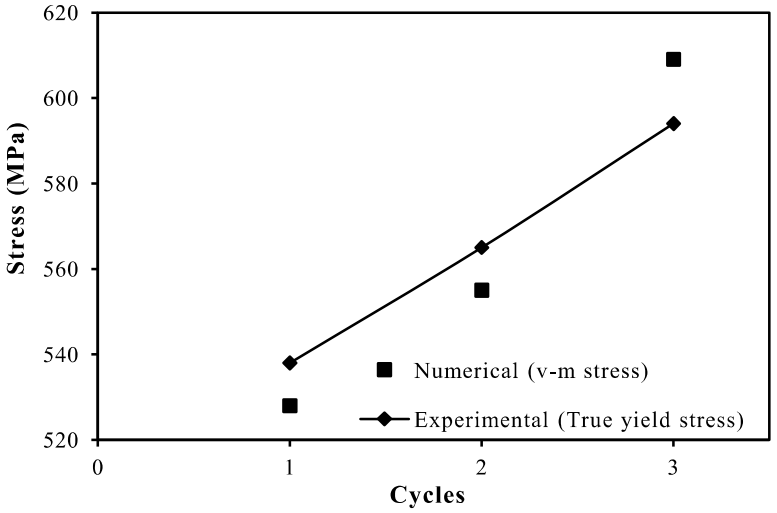



**Figure 6.6** Comparison between stresses gathered through simulations and experiments as a function of the number of cycles.

**Table 6.2** Observed tensile yield strength (true), effective stress, and corresponding error of rolled composite after each cycle.

| Rolling cycle | Experimental stress $\sigma_{(yld)}$ (MPa) | Numerical stress $\sigma_{(v\text{-}m)}$ (MPa) | Error (%) |
|---|---|---|---|
| 1 | 538 | 528 | 1.86 |
| 2 | 565 | 555 | 1.77 |
| 3 | 594 | 609 | 2.52 |

Figure 6.7 shows the distribution of plastic strain through the plate thickness under frictional conditions (frictional coefficient μ = 0.35). After the first cycle, the distribution of strain around the center of the thickness is 0.8, which explains the absence of shear strain and corresponds to a 0.8N von Mises strain value. Maximum deformation occurs on aluminum layers, as they lie at 0.3mm and 1mm thickness of plate where strain values are highest. Apart from aluminum layers, strain is higher closer to the surface layers due to redundant shear strain [61]. For the ensuing cycles, the ε value rises substantially at similar layers due to the occurrence of strain accumulation. The peaks develop homogeneity after the third rolling cycle. On average, strain increases linearly with the increase in rolling cycles (N) [139].

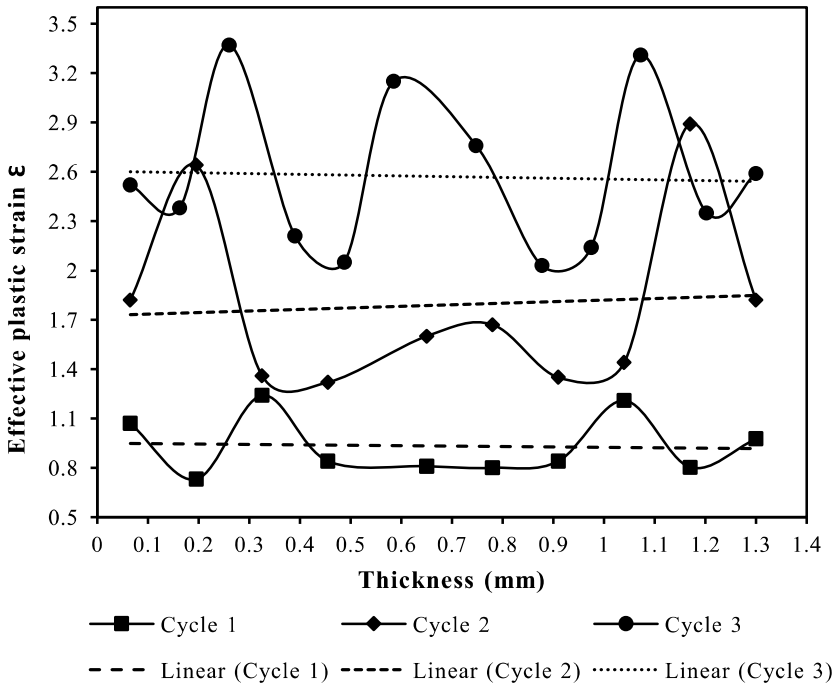



**Figure 6.7** Variation in strain along the layered composite slab thickness in Ti-IF steel ARBed composite after each cycle.

The slopes of linear lines of each cycle are dependent on the behavior of peaks from either side of the center of thickness. Generally, the trend of peaks is usually higher at the surfaces (start and end of thickness). For ensuing cycle, peaks are higher at surfaces and center,

as repetition of rolling cycle occurs. Based upon this, architecture of layers can be changed to obtained composite having mechanical properties.

Figure 6.8 compares the values of plastic strain in the experiment and numerical analysis. The strain was presumed in experiments as a 50% thickness reduction that corresponds to 0.8 after the first ARB cycle. It increased double with each number of cycles. Numerical results establish a close agreement with presumed strain values and curves start to converge as the number of rolling cycles increases. Numerical plastic strain values are 0.9, 1.8, 2.6 for the first, second, and third cycles, respectively.

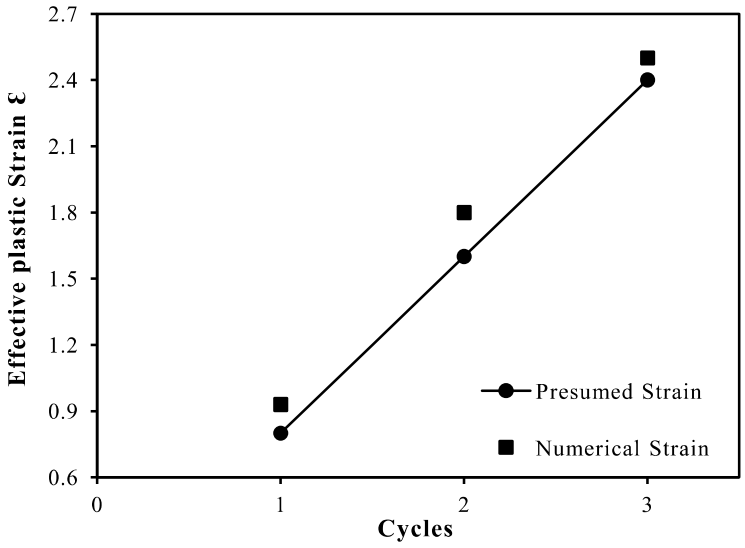



**Figure 6.8** Comparison between applied strain in experiments versus the strain acquired through simulations as a function of the number of cycles.

# 7. CONCLUSION

Accumulative roll bonding (ARB) has been demonstrated as a useful method for manufacturing various composites through this work. Multi-layered composites were successfully fabricated using titanium and IF steel interlayered with aluminum alloy 2024, and IF steel with aluminum alloy 2024 by ARB technique. The key results after the ARB method and further processing are listed below:

The ARB between titanium and steel (IF steel) has never been conducted in the literature. Although aging has been performed aging on the ARB composites, it has never been accomplished on dissimilar ARBed composites. Generally, the strength of all the composites was increased by the increase in the number of ARB cycles due to work hardening and grain refinement. Though, composite became brittle after ARB which was then regained after applying post-ARB heat treatment.

**Titanium-IF steel composites:**

1. Multi-metal composites were successfully produced in both cases of Ti-Al2024-IF steel and Ti-IF steel with layers structure up to 23 and 20, respectively. The final cycle made interface layers indistinctive, and necking initiated after the completion of the process. Fine refinement down to <5μm was achieved in different layers.
2. An increase in hardness levels was apparent and improvement was noticed up to 1.4, 2.6, and 3.0 times for titanium, IF steel, and Al2024, respectively. The rate of increase was higher after the first ARB cycle that became steady afterward, as previous studies suggested.
3. Severe plastic deformation (SPD) through ARB, induced work hardening and grain refinement. This led to a consequential tensile strength exceeding 675MPa which, like

hardness, was higher than parent metals. Strength was increased by the expanse of ductility which was reduced significantly below 5% for every case of composites.

4. Composites under uniaxial shear loading were examined and increasing bond strength was demonstrated with increasing cycles. Interlayer bonding of composites was tested using a shear punch test (SPT) that provides a maximum shear strength of 435MPa upon completion of the process.
5. Overall, the Ti-IF steel composite rolled at 400°C gave the best result from this study.
6. Titanium-IF steel composite was numerically analyzed using ANSYS 18.1 (LS-DYNA module), and findings suggested a very close agreement with experimental results for applied strain and acquired yield strength of the composite.

**Aluminum (Al2024)-IF steel composite:**

This study includes the fabrication of Al2024-IF steel composite after three ARB cycles with a total of 8 layers. The final composite was subsequently post-ARB heat treated to initiate precipitate hardening inside aluminum layers. Summary of the results are listed below:

1. High strength composite along with lowered ductility was achieved after 3 ARB cycles. A reduction in grain size was accomplished by SPD.
2. Post-ARB heat treatment was applied on the final composite that revealed the partial coarsening of the average grain size in both aluminum and IF steel layers through optical micrographs.
3. Enhancement in ductility without losing much strength levels was caused by the concurrent recovery and occurrence of precipitation hardening in composite layers after a longer aging time.
4. Ductility and ultimate tensile strength (UTS) were reached to 18% and 420MPa, respectively after completion of aging at 150°C/24h.

5. Post-ARB heat treatment assisted in attaining better interlayer bonding in a three-cycle ARB composite. Shear strength was increased with the increase in aging time, and a maximum of 270MPa was accomplished after 150°C/24h aging.

# 8. FUTURE WORKS

Despite several efforts that have been done to find the best possible multi-layered composite of titanium and IF steel interlayered with aluminum in the current research, further processing can be done related to this. There are some approaches for future research.

Investigation on corrosion behavior of multi-layered titanium-IF steel composite can be another way to observe the behavior of composite. As titanium has good corrosion resistance, it would be interesting to see the changes induced by the IF steel on the corrosion resistance of the composite. Another subject of attention is to apply precipitation hardening through several heat treatment approaches.

By this study, experimental results were validated through a numerical model. It would be a new way to identify the best layered configuration based on the equivalent von Mises stress, using the model, and validate these results through experiments.

# REFERENCES

[1] E.A. Starke, J.T. Staleyt, Application of modern aluminum alloy to aircraft, Prog. Aerosp. Sci. 32 (1996) 131–172. doi:10.1016/0376-0421(95)00004-6.

[2] S. V. A. Ana, M. Reihanian, and B. Lotfi, "Accumulative roll bonding (ARB) of the composite coated strips to fabricate multi-component Al-based metal matrix composites," Mater. Sci. Eng. A, vol. 647, no. October, pp. 303–312, 2015, doi: 10.1016/j.msea.2015.09.006.

[3] Rajan TPD, Pillai RM, Pai BC. Reinforcement coatings and interfaces in aluminium metal matrix composites. J Mater Sci 1998;33:3491–503. https://doi.org/10.1023/A:1004674822751.

[4] Kok M. Production and mechanical properties of Al2O3 particle-reinforced 2024 aluminium alloy composites. J Mater Process Technol 2005;161:381–7. https:// doi.org/10.1016/j.jmatprotec.2004.07.068.

[5] Ramanathan Arunachalam, Pradeep Kumar Krishnan, Rajaraman Muraliraja, A review on the production of metal matrix composites through stir casting – Furnace design, properties, challenges, and research opportunities, Journal of Manufacturing Processes 42 (2019) 213–245.

[6] M. Kawasaki, Processing of ultrafine-grained materials through the application of severe plastic deformation, Metall. Mater. Trans. A Phys. Metall. Mater. Sci. 42 (2011) 3035–3045. doi:10.1007/s11661-010-0501-2.

[7] M. Ahmadkhanbeigi, O. Shapourgan, G. Faraji, Microstructure and Mechanical Properties of Al Tube Processed by Friction Stir Tube Back Extrusion (FSTBE), Trans. Indian Inst. Met. 70 (2017) 1849–1856. doi:10.1007/s12666-016-0987-4.

[8] Justin L. Milne, Fadi Abu-Farha, Cristina Bunget, Thomas Kurfess, Vincent H. Hammond, Grain refinement and mechanical properties of CP-Ti processed by warm accumulative roll bonding, Materials Science&EngineeringA561(2013)109–117.

[9] A. Azushima, R. Kopp, A. Korhonen, D.Y. Yang, F. Micari, G.D. Lahoti, P. Groche, J. Yanagimoto, N. Tsuji, A. Rosochowski, A. Yanagida, Severe plastic deformation (SPD) processes for metals, CIRP Ann. - Manuf. Technol. 57 (2008) 716–735. doi:10.1016/j.cirp.2008.09.005.

[10] A.P. Zhilyaev, T.G. Langdon, Using high-pressure torsion for metal processing: Fundamentals and applications, Prog. Mater. Sci. 53 (2008) 893–979. doi:10.1016/j.pmatsci.2008.03.002.

[11] T.G. Langdon, Twenty-five years of ultrafine-grained materials: Achieving exceptional properties through grain refinement, Acta Mater. 61 (2013) 7035–7059. doi:10.1016/j.actamat.2013.08.018.

[12] R. S. Mishra, M. W. Mahoney, S. X. McFadden, N. a. Mara, A. K. Mukherjee, High strain rate superplasticity in a friction stir processed 7075 Al alloy, Scr. Mater. 42 (1999) 163–168. doi:10.1016/S1359-6462(99)00329-2.

[13] S. Mizunuma, Large Straining Behavior and Microstructure Refinement of Several Metals by Torsion Extrusion Process, Mater. Sci. Forum. 503–504 (2009) 185–192. doi:10.4028/www.scientific.net/msf.503-504.185.

[14] Y. Saito, N. Tsuji, H. Utsunomiya, T. Sakai, R. Hong, Ultra-fine grained bulk aluminum produced by accumulative roll-bonding process, Scr. Mater. 40 (1999) 795–800.

[15] Y. Saito, H. Utsunomiya, N. Tsuji, T. Sakai, Novel ultra-high straining process for bulk materials development of the accumulative roll-bonding (ARB) process, Acta Mater. 47 (1999) 579–583. doi:10.1016/S1359-6454(98)00365-6.

[16] R.M.C. William F. Hosford, Metal Forming: Mechanics and Metallurgy, 4th Edition, 2011.

[17] I. Topi, Ultrafine-grained Metal Sheets produced using the Accumulative Roll Bonding Process for Light-Weight Structures, (2008).

[18] S. Dziallach, W. Bleck, and M. Köhler, "Roll-Bonded Titanium/Stainless-Steel Couples. Part 3: Adhesion Properties," Adv. Eng. Mater., vol. 12, no. 9, pp. 848–854, Sep. 2010, doi: https://doi.org/10.1002/adem.201000133.

[19] T. Hausöl, H.W. Höppel, M. Göken, Microstructure and mechanical properties of accumulative roll bonded aluminium alloy AA5754, J. Phys. Conf. Ser. 240 (2010) 012128. doi:10.1088/1742-6596/240/1/012128.

[20] Luo, J.G.; Aco_, V.L. Using cold roll bonding and annealing to process Ti/Al multi-Layered composites from elemental foils. Mater. Sci. Eng. 2004, 379, 164–172.

[21] Kwan, C.;Wang, Z.; Kang, S.B. Mechanical behavior and microstructural evolution upon annealing of the accumulative roll-bonding (ARB) processed Al alloy 1100. Mater. Sci. Eng. 2008, 480, 148–159.

[22] Moza_ari, A.; Hosseini, M.; Manesh, H.D. Al/Ni metal intermetallic composite produced by accumulative roll bonding and reaction annealing. J. Alloys Compd. 2011, 509, 9938–9945.

[23] Takata, N.; Yamada, K.; Ikeda, K.I.; Yoshida, F.; Nakashima, H.; Tsuji, N. Change in microstructure and texture during annealing of pure copper heavily deformed by accumulative roll bonding. Mater. Trans. 2007, 48, 2043–2048.

[24] Roostaei, A.A.; Zarei-Hanzaki, A.; Abedi, H.; Rokni, M. An investigation into the mechanical behavior and microstructural evolution of the accumulative roll bonded AZ31 Mg alloy upon annealing. Mater. Des. 2011, 32, 2963–2968.

[25] Talebian, M.; Alizadeh, M. Manufacturing Al/steel multilayered composite by accumulative roll bonding and the effects of subsequent annealing on the microstructural and mechanical characteristics. Mater. Sci. Eng. 2014, 590, 186–193.

[26] Kwan, C.; Wang, Z. Microstructure evolution upon annealing of accumulative roll bonding (ARB) 1100 Al sheet materials: Evolution of interface microstructures. J. Mater. Sci. Lett. 2008, 43, 5045–5051.

[27] Yoda, R.; Shibata, K.; Morimitsu, T.; Terada, D.; Tsuji, N. Formability of ultrafine-Grained Interstitial-Free steel fabricated by accumulative roll-Bonding and subsequent annealing. Scr. Mater. 2011, 65, 175–178.

[28] F. Kümmel, H.W. Höppel, Layer architecture and fatigue life of ultrafine-grained laminated metal composites consisting of different aluminum alloys Author' s Accepted Manuscript, Mater. Sci. Eng. A. (2017). doi:10.1016/j.msea.2017.06.105.

[29] N. Tsuji, Y. Saito, S.H. Lee, Y. Minamino, ARB (accumulative roll-bonding) and other new techniques to produce bulk ultrafine grained materials, Adv. Eng. Mater. 5 (2003) 338–344. doi:10.1002/adem.200310077.

[30] N. Tsuji, Y. Ito, Y. Saito, Y. Minamino, Strength and ductility of ultrafine grained aluminum and iron produced by ARB and annealing, Scr. Mater. 47 (2002) 893–899. doi:10.1016/S1359-6462(02)00282-8.

[31] Y.S. N. Tsuji, K. Shiotsuki, Mater. Trans._Superplasticity of Ultra-Fine Grained Al-Mg Alloy Produced by Accumulative Roll-Bonding.Mater. Trans. JIM 1999, 40, 765, (1999) 765.

[32] N. Tsuji, K. Shiotsuki, H. Utsunomiya, Y. Saito, Low Temperature Superplasticity of Ultra-Fine Grained 5083 Aluminium Alloy Produced by Accumulative Roll-Bonding, Mater. Sci. Forum. 304–306 (2009) 73–78. doi:10.4028/www.scienti\fic.net/msf.304-306.73.

[33] X. Huang, N. Tsuji, N. Hansen, Y. Minamino, Microstructural evolution during accumulative roll-bonding of commercial purity aluminum, Mater. Sci. Eng. A. 340 (2003) 265–271. doi:10.1016/S0921-5093(02)00182-X.

[34] Vaidyanath, L.; Nicholas, M.; Milner, D. Pressure welding by rolling. Bri. Weld. J. 1959, 6, 13–28.

[35] Mohamed, H.;Washburn, J. Mechanism of solid state pressure welding. Weld. J. 1975, 8, 302–310.

[36] F. Erdmann-Jesnitzer, Aluminum 33, 730 (1957).

[37] Parks, J.M. Recrystallization welding. Weld. J. 1953, 209–222.

[38] Semenov, A. The phenomenon of seizure and its investigation. Wear 1961, 4, 1–9.

[39] Pan, D.; Gao, K.; Yu, J. Cold roll bonding of bimetallic sheets and strips. Mater. Sci. Technol. 1989, 5, 934–939.

[40] Cantalejos, N. Morphology of the Interface of Roll-Bonded Aluminum. J. Inst. Met. 1972, 100, 20–23.

[41] Seyed Mahmoud Ghalehbandi, Massoud Malaki, and Manoj Gupta, Accumulative Roll Bonding—A Review.

[42] I. K. Kim and S. I. Hong, “Effect of heat treatment on the bending behavior of tri-layered Cu/Al/Cu composite plates,” Mater. Des., vol. 47, pp. 590–598, 2013, doi: 10.1016/j.matdes.2012.12.070.

[43] H. R. Akramifard, H. Mirzadeh, and M. H. Parsa, “Cladding of aluminum on AISI 304L stainless steel by cold roll bonding: Mechanism, microstructure, and mechanical properties,” Mater. Sci. Eng. A, vol. 613, pp. 232–239, 2014, doi: 10.1016/j.msea.2014.06.109.

[44] X. Huang, N. Tsuji, N. Hansen, and Y. Minamino, “Microstructural evolution during accumulative roll-bonding of commercial purity aluminum,” *Mater. Sci. Eng. A*, vol. 340, no. 1–2, pp. 265–271, 2003, doi: 10.1016/S0921-5093(02)00182-X.

[45] M. Mokhles, M. Hosseini, H. Danesh-Manesh, and S. M. Zebarjad, “Structure and mechanical properties of Ni/Ti multilayered composites produced by accumulative roll-bonding process,” *J. Compos. Mater.*, vol. 54, no. 8, pp. 1119–1126, 2020, doi: 10.1177/0021998319874391.

[46] M. Hosseini and H. Danesh Manesh, “Bond strength optimization of Ti/Cu/Ti clad composites produced by roll-bonding,” *Mater. Des.*, vol. 81, no. December, pp. 122–132, 2015, doi: 10.1016/j.matdes.2015.05.010.

[47] Clemensen, C.; Juelstorp, O.; Bay, N. Cold welding. Part 3: Influence surface preparation on bond strength. Met. Constr. 1986, 18, 625–629.

[48] Jamaati, R.; Toroghinejad, M.R. Manufacturing of high-Strength aluminum/alumina composite by accumulative roll bonding. Mater. Sci. Eng. 2010, 527, 4146–4151.

[49] Mehr, V.Y.; Toroghinejad, M.R.; Rezaeian, A. The e_ects of oxide film and annealing treatment on the bond strength of Al–Cu strips in cold roll bonding process. Mater. Des. 2014, 53, 174–181.

[50] Jamaati, R.; Toroghinejad, M.R. The role of surface preparation parameters on cold roll bonding of aluminum strips. J. Mater. Eng. Perform. 2011, 20, 191–197.

[51] Nicholas, M.; Milner, D. Pressure welding by rolling at elevated temperatures. Br. Weld. J 1961, 8, 375–383.

[52] Hosseini, M.; Manesh, H.D. Bond strength optimization of Ti/Cu/Ti clad composites produced by roll-Bonding. Mater. Des. 2015, 81, 122–132.

[53] Ma, M.; Huo, P.; Liu,W.;Wang, G.;Wang, D. Microstructure and mechanical properties of Al/Ti/Al laminated composites prepared by roll bonding. Mater. Sci. Eng. 2015, 636, 301–310.

[54] Tsuji, N.; Saito, Y.; Utsunomiya, H.; Tanigawa, S. Ultra-Fine grained bulk steel produced by accumulative roll-Bonding (ARB) process. Scr. Mater. 1999, 40, 795–800.

[55] M. Slámová, P. Homola, M. Karlík, Thermal stability of twin-roll cast Al-Fe-Mn-Si sheets accumulative roll bonded at different temperatures, Mater. Sci. Eng. A. 462 (2007) 106–110. doi:10.1016/j.msea.2006.03.148.

[56] P. Homola, M. Slámová, M. Karlík, J. Čížek, I. Procházka, Effect of the Temperature of Accumulative Roll Bonding on the Microstructure and Properties of Twin-Roll Cast AA8006 Alloy, Mater. Sci. Forum. 503–504 (2006) 281–286. doi:10.4028/www.scientific.net/MSF.503-504.281.

[57] H. Yan, J.G. Lenard, A study of warm and cold roll-bonding of an aluminium alloy, Mater. Sci. Eng. A. 385 (2004) 419–428. doi:10.1016/j.msea.2004.07.018.

[58] Zhan, M.Y.; Li, Y.Y.; Chen, W.P. Improving mechanical properties of Mg-Al-Zn alloy sheets through accumulative roll-Bonding. Trans. Nonferrous Metals Soc. China 2008, 18, 309–314.

[59] Jamaati, R.; Toroghinejad, M.R. E_ect of friction, annealing conditions and hardness on the bond strength of Al/Al strips produced by cold roll bonding process. Mater. Des. 2010, 31, 4508–4513.

[60] Miyajima, Y.; Uchiyama, M.; Adachi, H.; Fujii, T.; Onaka, S.; Kato, M. E_ect of Roll-Bonding and Subsequent Annealing on Microstructure Evolution of Accumulative Roll Bonded Pure Copper. Mater. Trans. 2016, 57, 1411–1417.

[61] N. Kamikawa, T. Sakai, and N. Tsuji, “Effect of redundant shear strain on microstructure and texture evolution during accumulative roll-bonding in ultralow carbon IF steel,” *Acta Mater.*, vol. 55, no. 17, pp. 5873–5888, 2007, doi: 10.1016/j.actamat.2007.07.002.

[62] S. Haribabu, W.S. Che, B. Srinivas, D. Venkateswarulu, S. Alapati, T. Ramachandraiah, M. Cheepu, S. Karna, Fabrication and Analysis of Accumulative Roll Bonding Process between Magnesium and Aluminum Multi-Layers, Appl. Mech. Mater. 877 (2018) 183–189. doi:10.4028/www.scientific.net/amm.877.183.

[63] Jang, Y.; Kim, S.; Han, S.; Lim, C.; Goto, M. Tensile behavior of commercially pure copper sheet fabricated by 2-And 3-Layered accumulative roll bonding (ARB) process. Metals Mater. Int. 2008, 14, 171.

[64] G. Krallics, J.G. Lenard, An examination of the accumulative roll-bonding process, J. Mater. Process. Technol. 152 (2004) 154–161. doi: 10.1016/j.jmatprotec.2004.03.015.

[65] Kent, D.; Xiao,W.;Wang, G.; Yu, Z.; Dargusch, M. Thermal stability of an ultrafine grain β-Ti alloy. Mater. Sci. Eng. 2012, 556, 582–587.

[66] Gazder, A.A.; Hazra, S.S.; Pereloma, E.V. Annealing behaviour and mechanical properties of severely deformed interstitial free steel. Mater. Sci. Eng. 2011, 530, 492–503.

[67] Sheng, L.; Yang, F.; Xi, T.; Lai, C.; Ye, H. Influence of heat treatment on interface of Cu/Al bimetal composite fabricated by cold rolling. Compos. Part B 2011, 42, 1468–1473.

[68] H.W. Wagener, J. Haats, Pressure welding of corrosion resistant metals by cold extrusion, J. Mater. Process. Tech. 45 (1994) 275–280. doi:10.1016/0924-0136(94)90352-2.

[69] L. Su, C. Lu, Microstructure and mechanical properties of AA5005 / AA6061 laminated composite processed by accumulative roll bonding, 45 (2014) 515–522.

[70] J.E. Hatch, Aluminum Properties and Physical Metallurgy, ASM Int. (1984) 424. doi:10.1361/appm1984p001.

[71] A.H. Ghobadlou, high temperature mechanical characteristics of friction stir processed high temperature mechanical characteristics of friction stir processed, (2018).

[72] M. Mahendra Boopathi, K.P. Arulshri, N. Iyandurai, Evaluation of mechanical properties of Aluminium alloy 2024 reinforced with silicon carbide and fly ash hybrid metal matrix composites, Am. J. Appl. Sci. 10 (2013) 219–229. doi:10.3844/ajassp.2013.219.229.

[73] A. Shahsavari, F. Karimzadeh, A. Rezaeian, H. Heydari, Significant Increase in Tensile Strength and Hardness in 2024 Aluminum Alloy by Cryogenic Rolling, Procedia Mater. Sci. 11 (2015) 84–88. doi:10.1016/j.mspro.2015.11.111.

[74] M. Naseri, M. Reihanian, E. Borhani, A new strategy to simultaneous increase in the strength and ductility of AA2024 alloy via accumulative roll bonding (ARB), Mater. Sci. Eng. A. 656 (2016) 12–20. doi:10.1016/j.msea.2016.01.020.

[75] R. Zheng, T. Bhattacharjee, A. Shibata, N. Tsuji, C. Ma, Effect of Accumulative Roll Bonding (ARB) and Subsequent Aging on Microstructure and Mechanical Properties of 2024 Al Alloy, Mater. Trans. 57 (2016) 1462–1470. doi:10.2320/matertrans.MH201512.

[76] M. Alvand, M. Naseri, E. Borhani, H. Abdollah-Pour, Nano/ultrafine grained AA2024 alloy processed by accumulative roll bonding: A study of microstructure, deformation texture

and mechanical properties, J. Alloys Compd. 712 (2017) 517–525. doi:10.1016/j.jallcom.2017.04.117.

[77] B. Sarkar, Anjana Deva, S. Mukhopadhyay, B.K. Jha, D. Mukerjee & A.S. Mathur, Processing and Application of Interstitial Free (IF) Grade Steel: Prospects in SAIL.

[78] M.J. Zehetbauer, R.Z. Valiev, Nanomaterials by Severe Plastic Deformation, 2004. doi:10.1002/3527602461.

[79] S. Tamimi M. Ketabchi N. Parvin, Microstructural evolution and mechanical properties of accumulative roll bonded interstitial free steel, Materials & Design, Volume 30, Issue 7, August 2009, Pages 2556-2562.

[80] Nadim James Hallab, Joshua James Jacobs, in Biomaterials Science (Third Edition), 2013.

[81] J. L. Milner, F. Abu-Farha, C. Bunget, T. Kurfess, and V. H. Hammond, "Grain refinement and mechanical properties of CP-Ti processed by warm accumulative roll bonding," *Mater. Sci. Eng. A*, vol. 561, pp. 109–117, 2013, doi: 10.1016/j.msea.2012.10.081.

[82] A. Fattah-alhosseini, A. Reza Ansari, Y. Mazaheri, M. Karimi, and M. Haghshenas, "An Investigation of mechanical properties in accumulative roll bonded nano-grained pure titanium," *Mater. Sci. Eng. A*, vol. 688, no. February, pp. 218–224, 2017, doi: 10.1016/j.msea.2017.02.013.

[83] H. Sieber, G. Wilde, J.H. Perepezko, Thermally activated amorphous phase formation in cold-rolled multilayers of Al ± Ni, Al ± Ta, Al ± Fe and Zr ± Cu, 252 (1999) 611–615.

[84] J.M. Lee, B.R. Lee, S.B. Kang, Control of layer continuity in metallic multilayers produced by deformation synthesis method, Mater. Sci. Eng. A. 406 (2005) 95–101. doi:10.1016/j.msea.2005.06.030.

[85] G. Min, J.M. Lee, S.B. Kang, H.W. Kim, Evolution of microstructure for multilayered Al/Ni composites by accumulative roll bonding process, Mater. Lett. 60 (2006) 3255–3259. doi:10.1016/j.matlet.2006.03.001.

[86] T.H.E. Perfect, P. For, Bumpers made of clad metals, 2011,http://www.cladit.com/ examples/bumpers.html.the Perfect Partner for Active, (n.d.).

[87] H. Alvandi, K. Farmanesh, Microstructural and Mechanical Properties of Nano/Ultra-fine Structured 7075 Aluminum Alloy by Accumulative Roll-Bonding Process, Procedia Mater. Sci. 11 (2015) 17–23. doi:10.1016/j.mspro.2015.11.020.

[88] O¨ Yazar, T. Ediz, T. Öztürk, Control of macrostructure in deformation processing of metal/metal laminates, Acta Mater. 53 (2005) 375–381. doi:10.1016/j.actamat.2004.09.033.

[89] M. Eizadjou, A. Kazemi Talachi, H. Danesh Manesh, H. Shakur Shahabi, K. Janghorban, Investigation of structure and mechanical properties of multi-layered Al/Cu composite produced by accumulative roll bonding (ARB) process, Compos. Sci. Technol. 68 (2008) 2003–2009. doi:10.1016/j.compscitech.2008.02.029.

[90] M. Tayyebi, B. Eghbali, Study on the microstructure and mechanical properties of multilayer Cu/Ni composite processed by accumulative roll bonding, Mater. Sci. Eng. A. 559 (2013) 759–764. doi:10.1016/j.msea.2012.09.021.

[91] R.S. V. G. Arigela , L. Lienshoeft1, P.Chekhonin, Comparative study of texture evolution in ARB processed AA2014, AA6063 and AA2014/6063 aluminium laminates, Kov. Mater. 53 2015 245–249 DOI 10.4149/Km 2015 4 245. 53 (2015) 1–5. doi:10.4149/km-2015-4-245.

[92] H. Chang, M.Y. Zheng, C. Xu, G.D. Fan, H.G. Brokmeier, K. Wu, Microstructure and mechanical properties of the Mg/Al multilayer fabricated by accumulative roll bonding (ARB) at ambient temperature, Mater. Sci. Eng. A. 543 (2012) 249–256. doi:10.1016/j.msea.2012.02.083.

[93] Y.F. Sun, N. Tsuji, H. Fujii, F.S. Li, Cu/Zr nanoscaled multi-stacks fabricated by accumulative roll bonding, J. Alloys Compd. 504 (2010) 443–447. doi:10.1016/j.jallcom.2010.02.201.

[94] T. Hausöl, H.W. Höppel, M. Göken, Microstructure and Mechanical Properties of Accumulative Roll Bonded AA6014 / AA5754 Aluminium Laminates, 669 (2011) 217–222. doi:10.4028/www.scientific.net/MSF.667-669.217.

[95] S.L. Semiatin, H.R. Piehler, Deformation of sandwich sheet materials in uniaxial tension, Metall. Trans. A. 10 (1979) 85–96. doi:10.1007/BF02686411.

[96] M. Soltan Ali Nezhad, A. Haerian Ardakani, A study of joint quality of aluminum and low carbon steel strips by warm rolling, Mater. Des. 30 (2009) 1103–1109. doi:10.1016/j.matdes.2008.06.042.

[97] B. Alemán, L. Gutiérrez, and J. J. Urcola, “Interface microstructures in diffusion bonding of titanium alloys to stainless and low alloy steels,” *Mater. Sci. Technol.*, vol. 9, no. 8, pp. 633–641, Aug. 1993, doi: 10.1179/mst.1993.9.8.633.

[98] K. Bhanumurthy and G. B. Kale, “Reactive diffusion between titanium and stainless steel,” *J. Mater. Sci. Lett.*, vol. 12, no. 23, pp. 1879–1881, 1993, doi: 10.1007/BF00540018.

[99] J. G. Liu, W. C. Cai, L. Liu, J. T. Han, and J. Liu, “Investigation of interfacial structure and mechanical properties of titanium clad steel sheets prepared by a brazing-rolling process,” *Mater. Sci. Eng. A*, vol. 703, no. June, pp. 386–398, 2017, doi: 10.1016/j.msea.2017.06.095.

[100] M. Kaya, M. Kılıç, Kırık, E. M. Karakurt, and B. Gülenç, “Diffusionsschweißen zwischen einer Ti6Al4V Legierung und interstitiellfreiem Stahl,” *Materwiss. Werksttech.*, vol. 48, no. 7, pp. 661–665, 2017, doi: 10.1002/mawe.201700003.

[101] V. Karthik, P. Visweswaran, A. Vijayraghavan, K. V. Kasiviswanathan, B. Raj, Tensile-shear correlations obtained from shear punch test technique using a modified experimental approach, J. Nucl. Mater. 393 (2009) 425–432. doi:10.1016/j.jnucmat.2009.06.027.

[102] S.M. Kurtz, C.W. Jewett, J.S. Bergström, J.R. Foulds, A.A. Edidin, Miniature specimen shear punch test for UHMWPE used in total joint replacements, Biomaterials. 23 (2002) 1907–1919. doi:10.1016/S0142-9612(01)00316-7.

[103] M. Kuna, M. Abendroth, Identification and validation of ductile damage parameters by the small punch test, 15th Eur. Conf. Fract.‘Advanced Fract. Mech. Life Saf. Assessments.’1(2004)710–725.http://www.gruppofrattura.it/ocs/index.php/esis/ECF15/paper/view/8719/4785.

[104] S. Acharya, K.K. Ray, Assessment of tensile properties of spot welds using shear punch test, Mater. Sci. Eng. A. 565 (2013) 405–413. doi:10.1016/j.msea.2012.12.068.

[105] P. Bahrami, A. Azizi, Investigation of Mechanical Properties for Commercial Purity Titanium Severely Plastic Deformed by Accumulative Roll-bonding Process, J. Mod. Process. Manuf. Prod. 6 (2017) 37–49.

[106] S. Acharya, K.K. Ray, Assessment of tensile properties of spot welds using shear punch test, Mater. Sci. Eng. A. 565 (2013) 405–413. doi:10.1016/j.msea.2012.12.068.

[107] G.R. Stewart, A.M. Elwazri, R. Varano, N. Pokutylowicz, S. Yue, J.J. Jonas, Shear punch testing of welded pipeline steel, Mater. Sci. Eng. A. 420 (2006) 115–121. doi:10.1016/j.msea.2006.01.081.

[108] P. Bahrami, A. Azizi, Investigation of Mechanical Properties for Commercial Purity Titanium Severely Plastic Deformed by Accumulative Roll-bonding Process, J. Mod. Process. Manuf. Prod. 6 (2017) 37–49.

[109] M. Zabihi, M.R. Toroghinejad, A. Shafyei, Evaluating the mechanical behavior of hot rolled Al/alumina composite strips using shear punch test, Mater. Sci. Eng. A. 618 (2014) 490–495. doi:10.1016/j.msea.2014.09.037.

[110] Avram A. Edidin, UHMWPE Biomaterials Handbook (Third Edition), 2016

[111] E. Lucon, Comprehensive Materials Processing, 2014

[112] D. H. Jawad, A. Hosseinzadeh, and G. G. Yapici, "On the mechanical behavior of accumulative roll bonded lightweight composite," *Mater. Res. Express*, vol. 6, no. 9, 2019, doi: 10.1088/2053-1591/ab2d93.

[113] N. Tsuji, S. Okuno, Y. Koizumi, and Y. Minamino, "Toughness of ultrafine grained ferritic steels fabricated by ARB and annealing process," *Mater. Trans.*, vol. 45, no. 7, pp. 2272–2281, 2004, doi: 10.2320/matertrans.45.2272.

[114] A. Lervik, C.D. Marioara, M. Kadanik, J.C. Walmsley, B. Milkereit, R. Holmestad, Precipitation in an extruded AA7003 aluminium alloy: Observations of 6xxx-type hardening phases, Materials and Design 186 (2020) 108204.

[115] TAHIR Ahmad, MUHAMMAD Kamran, MUHAMMAD Faizan, RAFIQ Ahmad, BAMBANG Ariwahjoedi, FARAZ Hussain, FAHAD Riaz, Studying the Effect of Precipitation Hardening on 6061 Aluminum Alloy Weldments, Advanced Materials Research Vol. 1133 (2016) pp 300-304.

[116] M. Greger, L. Kander, V. Snasel, and M. Cerny, "Microstructure evolution of pure titanium during ECAP," *Mater. Des.*, vol. 18, no. July 2015, pp. 1–8, 2011, [Online].

[117] D. Kent, G. Wang, Z. Yu, X. Ma, and M. Dargusch, "Strength enhancement of a biomedical titanium alloy through a modified accumulative roll bonding technique," *J. Mech. Behav. Biomed. Mater.*, vol. 4, no. 3, pp. 405–416, 2011, doi: 10.1016/j.jmbbm.2010.11.013.

[118] J. G. Liu, W. C. Cai, L. Liu, J. T. Han, and J. Liu, "Investigation of interfacial structure and mechanical properties of titanium clad steel sheets prepared by a brazing-rolling process," *Mater. Sci. Eng. A*, vol. 703, no. June, pp. 386–398, 2017, doi: 10.1016/j.msea.2017.06.095.

[119] Z. Noohi, M. R. Toroghinejad, M. A. Golozar, and P. Cavaliere, "Evaluation of aluminium/alumina/titanium composites produced by continual annealing and roll-bonding process," *Mater. Sci. Technol. (United Kingdom)*, vol. 35, no. 13, pp. 1614–1623, 2019, doi: 10.1080/02670836.2019.1635308.

[120] M. Naseri, A. Hassani, and M. Tajally, “An alternative method for manufacturing Al/B4C/SiC hybrid composite strips by cross accumulative roll bonding (CARB) process,” *Ceram. Int.*, vol. 41, no. 10, pp. 13461–13469, 2015, doi: 10.1016/j.ceramint.2015.07.137.

[121] D. Yang, P. Cizek, P. Hodgson, and C. Wen, “Ultrafine equiaxed-grain Ti/Al composite produced by accumulative roll bonding,” *Scr. Mater.*, vol. 62, no. 5, pp. 321–324, 2010, doi: 10.1016/j.scriptamat.2009.11.036.

[122] J. Romberg *et al.*, “Ti/Al multi-layered sheets: Accumulative roll bonding (Part A),” *Metals (Basel).*, vol. 6, no. 2, pp. 1–14, 2016, doi: 10.3390/met6020030.

[123] A. Tohidi, M. Ketabchi, and A. Hasannia, “Nanograined Ti-Nb microalloy steel achieved by Accumulative Roll Bonding (ARB) process,” *Mater. Sci. Eng. A*, vol. 577, pp. 43–47, 2013, doi: 10.1016/j.msea.2013.04.025.

[124] S. H. Lee, Y. Saito, T. Sakai, and H. Utsunomiya, “Microstructures and mechanical properties of 6061 aluminum alloy processed by accumulative roll-bonding,” *Mater. Sci. Eng. A*, vol. 325, no. 1, pp. 228–235, 2002, doi: https://doi.org/10.1016/S0921-5093(01)01416-2.

[125] A. Fattah-alhosseini, M. K. Keshavarz, Y. Mazaheri, A. Reza Ansari, and M. Karimi, “Strengthening mechanisms of nano-grained commercial pure titanium processed by accumulative roll bonding,” *Mater. Sci. Eng. A*, vol. 693, no. December 2016, pp. 164–169, 2017, doi: 10.1016/j.msea.2017.03.070.

[126] H. R. Akramifard, H. Mirzadeh, and M. H. Parsa, “Cladding of aluminum on AISI 304L stainless steel by cold roll bonding: Mechanism, microstructure, and mechanical properties,” *Mater. Sci. Eng. A*, vol. 613, pp. 232–239, 2014, doi: 10.1016/j.msea.2014.06.109.

[127] N. Zhang, W. Wang, X. Cao, and J. Wu, “The effect of annealing on the interface microstructure and mechanical characteristics of AZ31B/AA6061 composite plates fabricated by explosive welding,” *Mater. Des.*, vol. 65, pp. 1100–1109, 2015, doi: https://doi.org/10.1016/j.matdes.2014.08.025.

[128] A. Lervik, C. D. Marioara, M. Kadanik, J. C. Walmsley, B. Milkereit, and R. Holmestad, “Precipitation in an extruded AA7003 aluminium alloy: Observations of 6xxx-type hardening phases,” *Mater. Des.*, vol. 186, p. 108204, 2020, doi: 10.1016/j.matdes.2019.108204.

[129] Y. K. Kim, P. W. Shin, and S. I. Hong, “Effect of Heat Treatment on the Mechanical Properties and Interface Structure of 3-ply Ti/Cu/Ti Clad Composite,” *Adv. Mater. Res.*, vol. 1102, pp. 51–54, 2015, doi: 10.4028/www.scientific.net/AMR.1102.51.

[130] N. Tsuji, Y. Ito, Y. Saito, Y. Minamino, Strength and ductility of ultrafine grained aluminum and iron produced by ARB and annealing, Scr. Mater. 47 (2002) 893–899. doi:10.1016/S1359-6462(02)00282-8.

[131] E. Borhani, H. Jafarian, D. Terada, H. Adachi, N. Tsuji, Microstructural evolution during ARB process of Al-0.2 mass% Sc alloy containing $Al_3Sc$ precipitates in starting structures, Mater. Trans. 53 (2012) 72-80.

[132] C. Zhu, L. Sun, W. Gao, G. Li, and J. Cui, “The effect of temperature on microstructure and mechanical properties of Al/Mg lap joints manufactured by magnetic pulse welding,” J. Mater. Res. Technol., vol. 8, no. 3, pp. 3270–3280, 2019, doi: 10.1016/j.jmrt.2019.05.017.

[133] A.J. Kulkarni, K. Krishnamurthy, S.P. Deshmuk and R.S. Mishra, Effect of Particle Size Distribution on Strength of Precipitation-hardened Alloys, J. Mater. Res. 19(9) (2004) 2765-2773.

[134] R.N. Lumley, I.J. Polmear and A.J. Morton, Control of Secondary Precipitation to Improve the Performance of Aluminium Alloys, Forum of Materials Science 396-402 (2002) 893-898.

[135] L. Fratini, M. Merklein, W. Boehm, D. Campanella, Modelling Aspects in Accumulative Roll Bonding Process by Explicit Finite Element Analysis, Key Eng. Mater. 549 (2013) 452–459. doi:10.4028/www.scientific.net/KEM.549.452.

[136] H.S. Kim, P. Quang, M.H. Seo, S.I. Hong, K.H. Baik, H.R. Lee, D.M. Nghiep, Process Modelling of Equal Channel Angular Pressing for Ultrafine Grained Materials, Mater. Trans. 45 (2004) 2172–2176. doi:10.2320/matertrans.45.2172.

[137] S.C. Yoon, Z. Horita, H.S. Kim, Finite element analysis of plastic deformation behavior during high pressure torsion processing, J. Mater. Process. Technol. 201 (2008) 32–36. doi:10.1016/j.jmatprotec.2007.11.204.

[138] T. Inoue, N. Tsuji, Quantification of strain in accumulative roll-bonding under unlubricated condition by finite element analysis, Comput. Mater. Sci. 46 (2009) 261–266. doi:10.1016/j.commatsci.2009.03.005.

[139] T. Inoue, A. Yanagida, J. Yanagimoto, Finite element simulation of accumulative roll-bonding process, Mater. Lett. 106 (2013) 37–40. doi:10.1016/j.matlet.2013.04.093.

[140] M. Science, x Strain variations on rolling condition in accumulative roll-bonding by finite element analysis, (2010) 589–611.

[141] Richard G. Budynas, J. Keith Nisbett, Design Engineering Mechanical, 2006.